Institute of Paper Science and Technology

ACOUSTIC EMISSIONS AND DAMAGE CONSTITUTIVE CHARACTERISTICS OF PAPER

Project 3571

Final Report

to the

PAPER PROPERTIES AND USES
PROJECT ADVISORY COMMITTEE

July 1992

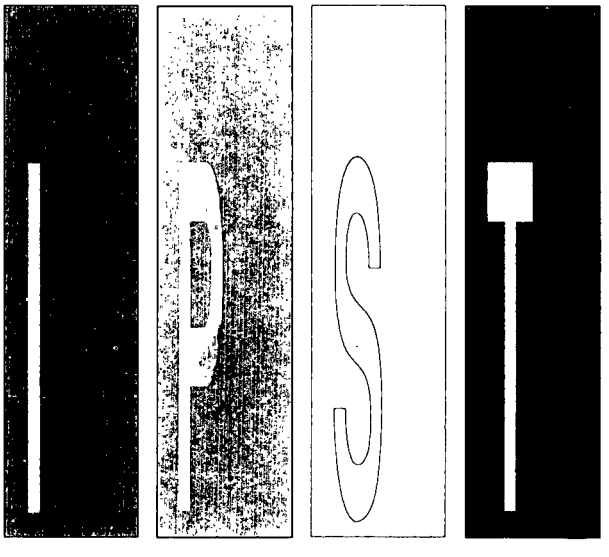

Atlanta, Georgia

NOTICE & DISCLAIMER

The Institute of Paper Science and Technology (IPST) has provided a high standard of professional service and has put forth its best efforts within the time and funds available for this project. The information and conclusions are advisory and are intended only for internal use by any company who may receive this report. Each company must decide for itself the best approach to solving any problems it may have and how, or whether, this reported information should be considered in its approach.

IPST does not recommend particular products, procedures, materials, or service. These are included only in the interest of completeness within a laboratory context and budgetary constraint. Actual products, procedures, materials, and services used may differ and are peculiar to the operations of each company.

In no event shall IPST or its employees and agents have any obligation or liability for damages including, but not limited to, consequential damages arising out of or in connection with any company's use of or inability to use the reported information. IPST provides no warranty or guaranty of results.

INSTITUTE OF PAPER SCIENCE AND TECHNOLOGY

Atlanta, Georgia

ACOUSTIC EMISSIONS AND DAMAGE CONSTITUTIVE CHARACTERISTICS OF PAPER

Project 3571

Final Report

A Progress Report

to the

PAPER PROPERTIES AND USES
PROJECT ADVISORY COMMITTEE

By

Mohsen Paul Sarfarazi

July 1992

SUMMARY

During the last year, we focussed on the problem of damage and failure of paper under the influence of tensile stresses. Of interest was to study the non-linear constitutive behavior of paper when it was subjected to progressively damaging uniaxial tensile stresses. The objective was to characterize and measure damage through a well-established non-destructive experimental technique. We chose the acoustic emission measurement technique. This method is based upon the fundamental idea that when the paper sample is damaged, a transient wave is emitted upon rapid release of strain energy from the microstructure. The apparatus set-up was such that a resonant-type transducer was attached to the paper sample through a compression mount. The transducer contained a ceramic plate which was very sensitive to the acoustic emission of ultrasonic wave. Medium samples of a variety of pulp types (NSSC, Caustic Carbonate, Green Liquor, Recycled) and various moisture contents were progressively damaged through continuous tensile straining using an Instron Machine at various crosshead speeds. Samples were tested both in MD and CD. The principle of operation of the testing equipment was that first the signal from the transducer was preamplified and directed to an acoustic emission data analyzer. The signal was then filtered through a high-pass filter with a low frequency cutoff in order to eliminate noise. The counts, amplitude, energy, and various other standard acoustic emission measurements were recorded. The list of gathered data also included stress, stretch, elastic modulus, TEA, and other mechanical

parameters as recorded by the Instron Machine. It was found that the acoustic emission technique characterized damage in paper materials rather well. Many interesting conclusions emerged from these studies which include:

(1) The amplitude of the acoustic emission signal's largest excursion is a very important parameter which directly gives an indication of the type of damage deformation that is taking place in the paper material.

(2) The amplitude of 96 db may be considered as the "acoustic signature" for the propagation of a self-similar crack in the paper web. The propagation of the crack is due to the continuous cutting of the fibers in the network.

(3) At least three distinct regimes of amplitude may be identified:

(I) Below 35 db: This may be due to microstructural events (e.g. dislocation motion, other shear mechanisms, moving and breaking of the fibrils, cavitational processes, etc.). It is believed that these emissions are manifestations of the plastic behavior of the paper material. One practical example for this would be the relief of residual stresses in the network.

(II) Between 35 db and 45 db: This is may be due to some mesostructural processes such as fiber debonding.

(III) Between 45 db and the second principal amplitude (roughly 65 to 70 db): This may be due to breakage of some individual fibers. These occur less abundantly than the hits described previously.

(4) The area under the cumulative hit distribution curve may be considered as a parameter which is indicative of the "failure toughness" of the paper material. Note that the term "failure" is not necessarily restricted to brittle fracture.

(5) The total number of hits (as well as counts) decreases as the loading rate is increased.

(6) The severity of the principal hit (as reflected by the magnitudes of principal counts, energy, and duration) decreases as the loading rate is increased.

(7) Loading rate does not affect the principal amplitude.

(8) The area under the cumulative hit distribution curve decreases as the loading rate is increased. The material behaves in a less compliant, more brittle manner.

(9) The principal effect of loading rate on the acoustic emission behavior is that it changes the frequency of its occurrence in terms of the loading interval of emission. At low loading rates there is a distinction between a "low emission" and "frequent emission" states. As the loading rate is increased, emission

becomes more sporadic until there is no distinction between the low emission and the frequent emission stages. However, the loading interval in which sporadic emissions occur becomes progressively shorter as the loading is increased. As the loading rate approaches an optimally fast speed, there is the evidence that the number of emissions at a particular load level becomes increasingly higher.

(10) The total number of hits (as well as counts) decreases as the relative humidity increases.

(11) The severity of the principal hit (as reflected by the magnitudes of principal counts, energy, and duration) decreases as the relative humidity is increased.

(12) Relative humidity does not affect the principal amplitude except at very high levels of humidities. It is believed that at such humidities the fibrillar structure of the paper changes. As a result, the paper material deforms under different mechanisms, and the principal amplitude drops to a lower level which is reflective of a more plastic deformational behavior.

(13) The area under the cumulative hit distribution curve decreases as the relative humidity is increased. The material behaves in a more compliant, plastic manner.

(14) The principal effects of high loading rate and high humidities are to accelerate the paper material toward failure. However, in

each case, a totally different mechanism is in effect. In the former case, failure occurs due to brittle fracture, while in the latter case, ductile mechanisms such as shear localization are responsible for failure.

(15) Finally, the location of the sensor has a strong effect on the magnitude of the acoustic emission. Generally, the acoustic emission waves dissipate in the paper material as the waves travel through the material.

TABLE OF CONTENTS

1. INTRODUCTION

It is well-known that the fibrous structure of paper/board damages during the converting and manufacturing processes. This damage causes a considerable reduction in the tensile and compressive strengths of the paper product both in MD and CD directions. The reductions in the tensile and compressive strengths are due to the evolutions of diversified micromechanisms of damage (e.g., debonding, delamination, fiber microbuckling, fiber fracture, etc.), which occur as a result of various types of stresses inflicted on the medium during the converting/manufacturing processes. A number of fundamental problems are indigenous to the problem of paper damage during the converting/manufacturing processes. These include:

1. Damage and failure of a fibrous network structure under direct tension.

2. Problem of microbuckling of individual fibers under compression.

3. Shear delamination of paperboard and related laminates.

The primary objective of this manuscript is to report on the constitutive behavior as well as the acoustic emissions/damage characteristics of paper when it is subjected to a progressively damaging uniaxial tensile loading at various rates of loading and

humidity conditions. Only commercial paper will be considered. In particular, the emphasis will be on the corrugating paper (or more specifically green liquor), which is the basic component for manufacturing corrugating board.

Because of the new nature of the applicability of the acoustic emissions studies in paper materials, it seems appropriate to first present an overview of this technique as is commonly utilized in other fields of materials science and engineering. To the best of the author's knowledge, only very few studies have ever been conducted on the acoustic emissions characteristics of paper materials [1-4]. In general, the application of the acoustic emissions technique to paper materials is in its infancy. The primary objective of this study is, therefore, to explore the acoustic emissions characteristics of paper materials. With this intent, attempts will be made to categorize certain unified and reproducible behavior and to establish guidelines for further research in this field. Of particular interest will be to try and establish a link between the acoustic emissions characteristics and the constitutive/fracture behavior of paper materials.

2. AN OVERVIEW OF THE ACOUSTIC EMISSIONS TECHNIQUE

2.1 Introduction

Most materials emit sound (or stress waves) when they are deformed. Acoustic emission is the term applied to the "low-level sound waves" emitted by a material when it is deformed [5-6]. Acoustic emissions are generated by the irreversible, heterogeneous alterations of interatomic spacings that constitute inelastic deformation. They are generated only when some abrupt and permanent change takes place somewhere in the material. The classical sources of acoustic emissions are defect-related deformational processes such as crack nucleation/growth and plastic deformation. Examples of the mechanisms that produce acoustic emissions in metals include: the movement and multiplication of dislocations, slip, twinning, fracture and debonding of precipitates or inclusions, corrosion processes; microcrack formation and growth, crack jumps, and frictional processes during crack opening and closure.

When a material fractures or deforms inelastically, there is a sudden movement at the defect source which produces a stress wave at the source. The resulting stress wave propagates through the solid due to the energy released during the deformational process. The amount of acoustic energy released depends primarily on the size and the speed of the local deformational process. The source of the acoustic emissions energy is the stress wave generated in the material [7]. Without stress, there are no emissions. The

acoustic emissions produced by the stress-induced deformation of a material are also highly dependent on the stress history of the material (see the section entitled "The Kaiser and Felicity Effects"). The relations between load, time, and acoustic emissions depend on the material and the type of deformational process causing the acoustic emissions. For example, brittle materials respond almost instantaneously to applied stress by emitting and then quickly stabilizing. On the other hand, viscoelastic materials such as resin-matrix composites take some time to stabilize after the load is applied. In materials involving hydrogen-induced cracking, a constant load often produces progressive damage and continual acoustic emissions to failure, and therefore, the material may never stabilize.

2.2 Factors Affecting Acoustic Emissions

Some materials produce acoustic emissions copiously when deformed; others are "quiet" by comparison. There are many factors that affect the acoustic emissions response from a material [8]. For example, the crystalline structure (or generally the microstructure) plays an important role in the acoustic emissions behavior. The signal amplitude level recorded from materials with distinct crystalline structures could vary by an order of magnitude in some cases. Generally, one could determine whether a material will be "noisy" or "quiet" from its crystalline structure. HCP materials are noisier than FCC materials (which are more

isotropic). HCP materials are also noisier and have higher-amplitude acoustic emissions signals than BCC materials (which twin only above certain temperatures). In general, the more anisotropic the crystalline structure, the higher the amplitude of the acoustic emissions signal. Also, the presence or lack of homogeneity drastically affects the acoustic emissions response. The acoustic emissions response of a material when tested in tension is completely different than the same material containing a sharp crack. Furthermore, the geometry and size of the crack determines the degree of brittleness and, thus, the acoustic emissivity of the solid. Monolithic and composite materials exhibit a different acoustic emissions response. For example, graphite epoxy is of an order of magnitude noisier than mild steel. Generally, brittleness, heterogeneity, and anisotropy are three major factors that effect high acoustic emissivity. On the other hand, ductile, homogeneous, and isotropic deformational mechanisms (such as microvoid coalescence in certain metals) cause low emissivity.

Apart from ductility, homogeneity, and isotropy, another factor that can affect the acoustic emissivity is the geometry. More specifically, the acoustic emissions response of a thin section is different than a thick section. Higher amplitude acoustic signals are often obtained from thicker specimens. The state of stress also greatly influences acoustic emissivity. Many materials studies involve the development of a test approach in the laboratory environment in which specimens are subjected to a simple uniaxial

stress in a particular direction. However, materials in industrial service are often subjected to complex biaxial and triaxial stress fields. In such cases, the acoustic emissions from the laboratory tests may not simply be considered as a model to represent the acoustic emissions from the materials utilized in the field. A triaxial state of stress, as it is found in the vicinity of a sharp crack, accentuates acoustic emissions. In thicker cracked solids, the triaxial stresses are often higher in magnitude which lead to plain strain stabilities and a greater likelihood of cleavage brittle type fracture near the center of the specimen. It should be emphasized that extrapolation of thin section acoustic data to determine thick section response is as inaccurate as extrapolating thin section (plain stress) fracture toughness data from thick section (plain strain) specimens. Another factor that affects acoustic emissivity is the strain-rate which, in turn, is greatly influenced by the rate of loading. High strength materials are also known to produce a larger number of acoustic emissions.

If the material condition changes by radiation damage, heat treatment, or mechanical processing, the acoustic emissivity changes. In metals, the amplitude of the acoustic signal increases at lower temperatures, primarily due to a change from a ductile to cleavage (or brittle) mode of response. Changes in the mechanical history or heat treatment that may be reflected by reduced grain size, higher dislocation density, or more random crystalline orientation cause lower acoustic emissivity.

To summarize the effect of various factors on acoustic emissions detectability, it may be considered that the following phenomenon are synonymous with high acoustic emissivity: damage of flawed materials, crack propagation, low-temperature deformation and fracture, brittle fracture, anisotropy, heterogeneity, high strength, high strain-rate (or rate of loading), or more specifically, in the case of crystalline solids or metals: cleavage fracture, twinning, large grain size, martensitic transformation, and cast structure.

2.3 The Nature of the Acoustic Emissions Wave

When a material deforms inelastically, the elastic energy absorbed within the material is liberated. If the nature of the deformation is such that a rapid movement occurs at the defect sources, the amount of the elastic energy liberated is significant and causes acoustic waves to be emitted at the source. The acoustic waves radiated from defect sources propagate in all directions. These waves often exhibit a strong directionality which depends on the nature of the material and the source process. The original wave released at a particular acoustic emissions source has a typical form as the one illustrated in Fig. 1. The displacement waveform is basically a step-like function and corresponds to the irreversible and permanent deformational movement that has occurred at the source. The corresponding velocity or the stress wave has a pulse-like form (Fig. 1). The width (duration) and the height (amplitude)

of the stress waveform very much depend on the dynamics of the source process.

Source processes such as microcrack jumps or inclusion fractures generate stress waves of very short durations often lasting a fraction of microseconds or at most a few microseconds. The amplitude (and, consequently, the energy) of the stress pulse generated at a defect source can vary drastically depending on the nature of the defect and the dynamics of the source process. For example, the movement of a single dislocation produces a stress wave which is of such a small amplitude that it cannot be easily detected [9-11]. In the absence of general yielding, slow and continuous processes such as microvoid coalescence (ductile tearing) and active path corrosion are not detectable. On the other hand, due to the stress concentrations in their vicinity, cracks and other defects emit during a monotonically rising load, while the unflawed material elsewhere is still silent [12-15]. Microscopically rapid mechanisms such as brittle intergranular fracture and transgranular cleavage are readily detectable even when the crack front is advancing only one grain at a time at subcritical stress levels [16-17]. Acoustic emissions from crack initiation and growth have been extensively studied in the literature. One can easily distinguish between the acoustic emissions signals from the growth of the plastic zone at the crack tip and the acoustic emissions signals from the movement of the crack front itself. Growth of the plastic zone typically produces

many emissions of low amplitude, while the amplitudes of the acoustic signals emanating from the advancement of the crack front are considerably larger.

The form of the original wave pulse which is emitted at the acoustic source changes drastically as the wave propagates through the medium material. There are several important aspects of the elastodynamics of the wave propagation process which need to be considered [18]. Some of these include attenuation and wave velocity. Attenuation is the loss of signal amplitude due to material damping as well as geometric factors as the wave travels through the material. Attenuation is a very important factor that governs detectability of the waveform at a distance. In an acoustic emissions testing it is often necessary to perform attenuation trial measurements in order to determine permissible sensor positions and spacings. Wave velocity is an important factor for consideration when the acoustic emissions technique is to be used to determine the locations of the source defects. By measuring the arrival times of the acoustic wave at several sensors and recording the wave velocity, the precise location of a source may be readily calculated. The attainable accuracy is governed by the wave propagation processes and depends on such factors as geometry and medium properties. Another important aspect of the wave propagation process is the effects of multiple paths and multiple wave modes by which the waves travel from the source to the sensor.

During an acoustic emissions testing, the transducer senses a large number of transient signals. A typical acoustic emissions signal emanating from a single, discrete deformation event is shown in Fig. 2. This signal is referred to as a burst signal. A burst-type signal has a fast rise time and a slower decay. These signals vary widely in shape, size, and rate of occurrence, depending on the microstructure of the material and test conditions. The electrical signal at the sensor output is the product of the ringing of the resonant transducer. It is evident that there is a drastic difference between the original waveform (Fig. 1) and this observed signal at the sensor. In addition to the wave propagation factors discussed earlier (particularly the problem associated with multiple paths and multiple modes of the acoustic waves), the transformation of the acoustic signal is further compounded by the response of the sensor.

When there is a high rate of occurrence, the individual burst signals combine to form a continuous signal. Continuous emissions is commonly observed during plastic deformation of steel, aluminum alloys, and many other metals, and has been extensively studied in the past, and many detailed findings have also been related to dislocation activity, microstructure, and materials properties [19]. The signal generated by the formation and movement of a single dislocation is often of such an insignificant intensity that it cannot be detected. However, when millions of dislocations are forming and moving, the individual signals overlap and superimpose

in such a way as to give a detectable result. The overall result is a continuous excitation of the material and the sensor which becomes detectable as soon as the voltage of the produced signal becomes comparable with the background noise. The higher is the strain-rate, the larger is the signal. The primary difference between the continuous emissions and the burst-type emissions discussed earlier is that in the former case the individual original signals emanating from various source emissions are not discernible. Fig. 3 illustrates a typical continuous emissions, which is commonly experienced during tensile testing of unflawed ductile specimens. Generally, continuous emissions refers to low level, high signal density output. The peak in the acoustic emissions rate occurs near the yield stress of the material. Continuous emissions is highly strain-sensitive, and under the condition of very slow strain-rates can totally disappear. Continuous emissions is best measured using energy rate measuring circuitry.

There are basically two fundamental approaches in the acoustic emissions signal analysis. In the first approach, the researcher determines the original source waveform by using a broadband sensor and performing a detailed analysis of the early part of the received signal. This methodology, which is referred to as the source function analysis, is very complex and time consuming. In performing source function analysis, only a single waveform may be processed at a time. The problem of determination of the source

pulse from the resulting movement at the point of detection has been extensively studied during the past two decades [20-23]. There are many inherent theoretical, computational, and experimental difficulties associated with determination of the source pulse from the signal recorded at a remote sensor. The resulting waveform associated with the vertical surface movement of a point in a semi-infinite solid due to the abrupt application of a vertical force in another point of the same body is highly complex. The waveform is even more complex when a finite plate is considered [24]. This is primarily due to the fact that the motion at the point of detection is strongly dependent on the ratio of source distance to plate thickness. The problem becomes even more complicated when the horizontal as well as the vertical components of the motion are considered. Other aspects of the elastodynamics of the wave propagation process such as multiple wave paths and wave modes, wave reflection, and attenuation introduce further complexities. In addition to the aspects of wave propagation in the material, the transformation of an acoustic waveform is further compounded by the response of the sensor.

The study of the transformation of the acoustic waveform from its original pulse shape to the final form detected at a sensor is of rudimentary importance both to the acoustic emissions researcher and the non-destructive evaluation inspector. Instead, most materials researchers as well as non-destructive evaluation inspectors utilize the overall statistical features of the acoustic

emissions activity, which are indifferent to the exact details of each source event. In this (second) approach, the materials scientist or the NDT inspector uses narrowband sensors and electronic equipment. Although by using this approach only a few features of the received signal are measured, it is possible to process hundreds of signals at a time.

2.4 The Acoustic Emissions Equipment Required for Material Testing

The most important device used during an acoustic emissions testing is a resonant sensor which is used to pick up the acoustic signal. The key element of an acoustic emissions sensor is a piezoelectric crystal (transducer) that is used to convert movement into an electrical voltage. The smallest signal that can be detected is about 10 microvolts at the transducer output, which corresponds to a surface displacement of about 1×10^{-6} inches for a high sensitivity sensor. When a stress wave impinges on the face of an acoustic sensor, the resonant sensor becomes excited by a broadband transient pulse, rings like a bell at its own natural frequencies, and a small electric signal is generated by the transducer. By carefully selecting the resonant frequency of the sensor, one can monitor the operating frequency. When the monitoring frequency is very low, there are increasing problems with mechanical background noise. At high frequencies, on the other hand, the wave attenuates (damps out) very rapidly, and the detection range of the sensor diminishes. Choice of the operating frequency is, therefore, a

trade-off between noise and high detection range. Low frequencies are often used in cases when either the detection range is at a premium (e.g., pipelines) or when the material is highly attenuating (e.g., rocks and soils). On the other hand, high frequencies are used in applications when the background noise is unusually high (e.g., steam lines in electricity-generating stations). In materials application (including paper), the acoustic emissions testing is often well performed with sensors that are resonant at about 150 KHz.

The small signal produced by the transducer needs to be amplified to produce a higher, more usable voltage. This is usually accomplished by placing a preamplifier close to (or even inside) the sensor in order to minimize pickup of electromagnetic interference. The gain of the preamplifier is typically 100 (40 db). The preamplifier typically contains a high-pass or bandpass filter to eliminate the mechanical and acoustic noise that prevails at low frequencies. The bandpass filter often has a frequency range of 100-300 KHz, which encompasses the 150 KHz resonant frequency of the most commonly used filters. Because of the large dynamic range of the preamplifier, the signal may be driven over a long cable. Therefore, the main signal processing equipment could be placed hundreds of feet from the testpiece if necessary.

After sensing and preamplification, the signal from the preamplifier is then diverted to the main signal processing

equipment where it is further amplified and filtered. Next, the signal is detected using a comparator circuit. The comparator circuit generates a digital output pulse whenever the acoustic emissions signal exceeds a fixed threshold. Threshold is the key variable that determines test sensitivity. The threshold level is usually set by the operator. It can also be controlled by adjusting the amplifier gain. The acoustic emissions signal processing equipment vary widely in form. Some are designed to function automatically in automated production environments. Some are designed for use by technicians and non-destructive testing inspectors performing routine testings. Of interest to materials researchers are those which are designed to perform comprehensive data acquisition and extensive data analysis. Such equipment are often computer-based systems.

Each acoustic emissions signal that crosses the threshold is recorded as a hit. The digital description of each hit (usually between 20 and 40 bytes) is generated by the front-end software and is then passed in sequence with other hit descriptions to the computer system. The computer system is used for acoustic data storage, analysis, display, and replay for post-test analysis. The task of data processing is shared by many microprocessors. The front-end microprocessor rapidly stores the descriptions of many hundred hit signals in its buffer, pending further processing. The highest priority of the microprocessors is to read the results of each signal measurement as soon as the measurement process is

complete, so that the measurement circuitry could be reset to the next event. A software-based, hit-driven acoustic emissions system can distinguish among many different signal features of burst-type acoustic emissions, which can be very useful to a materials researcher.

2.5 Basic Signal Measurement Parameters Used in Acoustic Emissions

There are basically five parameters that have been widely accepted in the acoustic emissions field. These are counts, amplitude, duration, energy, and rise time. Other less frequently used parameters are counts to peak, average frequency, spectral moment, and true energy. Along with these signal parameters, the hit-driven data stored in the computer also include external variables such as the time of detection, the current value of the applied load, the cycle count (fatigue tests), and the current level of background noise. Following is a more detailed description of the most commonly used acoustic emissions parameters.

Counts (or ringdown counts) -- The oldest and the simplest way to quantify the acoustic emissions activity is to count the threshold-crossing pulses generated by the comparator (Fig. 4). Counts depend on the magnitude of the source event. They also strongly depend on the acoustic properties and the reverberant nature of the material specimen and the sensor.

Amplitude -- Amplitude is the highest voltage attained by an acoustic emissions signal (Fig. 5). It is perhaps the most important parameter because it directly determines the detectability of the acoustic emissions event. Amplitude is directly related to the magnitude of the source event. Among all the other acoustic emissions parameters mentioned earlier, amplitude is the best one suited for developing statistical information in the form of distribution function [25]. Such data are very useful for distinguishing among different deformational mechanisms and for observing the changes in the acoustic emissions intensity as the test proceeds.

Energy -- More commonly known as MARSE. This is the measured area under the rectified signal envelope (Fig. 5). Analogous to counts this quantity represents a measure of the acoustic energy signal magnitude. Although the required circuitry for measuring MARSE is relatively complex, this quantity is preferred over counts because it is sensitive to both amplitude and duration. It is also less sensitive to operating frequency and threshold setting. Of all the acoustic emissions parameters mentioned earlier, MARSE is the best suited for specifying the overall cumulative acoustic emissions activity.

Duration -- This is the time elapsed from the first threshold crossing to the last, and is commonly measured in microseconds (Fig. 5). Analogous to counts, this parameter measures the source

magnitude. It is also dependent on such factors as the structural acoustics and the reverberant nature of the sensor and the specimen. It is particularly useful for noise filtering and other kinds of signal qualification. A good application of duration is in composite materials, specifically for characterizing certain long-duration source processes such as delamination [26].

Rise Time -- This is the elapsed time from the first threshold crossing to the signal peak (Fig. 5). This parameter is often useful in problems involving time-dependent processes such as dynamic loading or vibration of structures. It is also sometimes utilized for different types of signal qualification and noise rejection.

Counts to Peak -- This is the number of threshold crossings from the first threshold to the signal peak. This parameter is often used in conjunction with the rise time.

A software-based, hit-driven acoustic emissions system can often produce many types of graphic displays. Also, the results can be refined, filtered, and replayed in a post-test analysis. Broadly speaking, the following types of acoustic emissions displays may be generated:

(1) Distribution Plots -- These show statistical properties of the emissions in the form of histograms or distribution functions.

There are two types of distribution plots: cumulative and differential.

The cumulative form is a convenient display for reading off the total acoustic emissions quantity. It may be constructed either in the max-min (decreasing) form or the min-max (increasing) form. On the other hand, the differential form is useful for illustrating the changes in the acoustic emissions activity. The distribution plots of various acoustic emissions parameters against amplitude are of particular interest.

(2) History Plots -- These illustrate the course of the experimentation from start to finish. Two types of history plots are of interest: load-based history plots and time-based history plots. Either kind may be constructed in cumulative form or differential form. A history plot of acoustic emissions data versus load is a particularly useful display because it illustrates the state of damage in the material at various stages of loading. It is also the best way to display the Kaiser and the Felicity effects.

(3) Point Plots -- These plots show the correlation between different acoustic emissions parameters. Point plots of various acoustic parameters versus amplitude are of particular interest in noise filtering and signal qualification. In this case each hit is shown as one point on the plot, and its position shows information about the size and the shape of the waveform. Usually, these plots (constructed for signals that originate from impulsive sources)

contain a main band which consists of the actual deformational records and the noise record which falls either above or below this band. For example, noise signals from electromagnetic interference which are not prolonged by acoustic reverberation fall below the band, while noise signals from friction and leaks which originate from a non-impulsive source fall above the main band.

(4) Location Displays -- These show the position of the acoustic emissions source. This display is basically a map of the structure (or the material). The computed location of each emissions event is shown as a single point in the appropriate position. Sensor locations are often shown as large dots, thus providing a frame of reference. The structurally significant defects may be easily identified as clusters of points, which correspond to the most active sources.

2.6 The Felicity and Kaiser Effects

The acoustic emissions produced by the stress-induced deformation of materials is highly dependent on the stress history of the structure. Acoustic emissions testing is often conducted under a monotonically increasing load. On the other hand, when a material is subjected to repeated loadings, it is often found that the first application of the loading generates more emissions than any subsequent loading. When subjected to repeated loading, if the response of the material is such that the material does not produce

any acoustic emission until the previous maximum load is exceeded, the material is said to obey the Kaiser Effect. This behavior was first reported by Kaiser in 1950 [27]. It was first shown by Dunegan [28] that for materials that obey the Kaiser effect, emissions on a repeat loading below the prior maximum indicates that structural damage occurred between the first loading and the repeat loading. When a structure (or material) begins to emit on repeat loading at load levels that are less than the prior maximum loading, it is said to obey the Felicity Effect. A parameter is often defined, known as the Felicity Ratio, as the ratio of the load at which emissions begins on repeat loading to the previous maximum load. Therefore, it could be said that a material which obeys the Kaiser effect has a Felicity ratio of one or greater. On the other hand, materials that obey the Felicity effect must have Felicity ratios of less than 1.0. The best way to illustrate the Kaiser and Felicity effects is through a cumulative load history plot of acoustic emissions data as is shown in Fig. 6. The portion AB-BC-CB of the graph illustrates the Kaiser effect. During AB, the material is in emissions until it reaches the point B. During the portion BC, the material is being unloaded, and no further emissions takes place. As the load is again increased from C, no emission takes place until the load level increases to the previous maximum level at B. Portion BD-DE-EF-FG illustrates the Felicity effect. Portion BD is the loading phase, while the material is being unloaded with no further emissions during DE. As the load is again increased in the material starting from E, this time

emissions begin to occur starting at F, which corresponds to a lower load level than D. The ratio F/D represents the Felicity ratio.

The Felicity ratio may be used to assess the structural integrity of a material. For materials that obey the Felicity effect, often systematic decreases occur in the material as the material approaches failure [29]. For example, for fiber reinforced plastic (FRP) pressure vessels or tanks, a Felicity ratio of 0.95 is cause for rejection [30]. In acoustic emissions monitoring of certain materials and structures, it is sometimes a matter of common practice to totally ignore the emissions from first loading and instead concentrate on the acoustic emissions characteristics at subsequent loading. The rationale for this approach is that often the acoustic emissions on the first loading is the result of the local plastic deformation of the material, and it is often not until repeat loading that the structurally significant defects begin to emit. Another example in which the structurally significant defects begin to emit is the case of emissions at constant loading portion GH of Fig. 6. On the other hand, emissions related to stabilization of the material, such as relief of residual stresses, tend not to recur when the material is loaded again.

2.7 Applications of the Acoustic Emissions Technique

Because the acoustic emissions response of a material depends on its microstructure and the deformational mode, different materials often exhibit diverse acoustic emissions behavior. The acoustic emissions technique is often utilized as a powerful non-destructive evaluation tool for studying deformation and fracture. It gives an immediate indication of the response of a material under stress. It is also intimately related to strength, damage, and failure. The acoustic emissions technique is a particularly useful tool for studying material response when it is utilized in conjunction with other diagnostic techniques such as optical/laser or scanning electron microscopy, ultrasonics, fracture mechanics techniques (e.g., crack opening displacement measurements), and constitutive (stress-strain) measurements. It should be emphasized that the acoustic emissions method differs from most other non-destructive techniques in two respects: first, in the case of acoustic emissions, the signal originates from the material itself and does not come from an external exciting source (as, for example, is the case in ultrasonic measurement). Second, the acoustic emissions technique detects movement, while most other techniques detect existing geometrical discontinuities. Note no one non-destructive evaluation technique can ever provide the whole solution. Instead, it is often essential to use a combination of techniques to study the response of a particular material thoroughly. Due to the aforementioned unique features of the acoustic emissions technique,

it is a particularly useful method when used in conjunction with other non-destructive techniques.

Acoustic emissions inspection gives valuable information about the performance of a structure under load. It is particularly appropriate for inspecting large structures in which the whole volume of the structure may be non-destructively examined in a single loading operation without scanning the structure for defects. With appropriate positioning of a suitable number of sensors (typically 1-6 m apart), the defective areas within the structure may be readily identified. Other non-destructive techniques can then be used to determine the precise nature of the emitting defects. Often large cost savings are realized when the acoustic emissions method is first utilized for source location, and then the test is conclusively followed up with other NDT inspection techniques. These cost-effective results are particularly significant when inspecting large structures. In structural testing the acoustic emissions technique has been used on pressure vessels and storage tanks [31], pipelines and piping [32], aircraft and space vehicles [33], electric utility plants [33], bridges [33], railroad tank cars [34], bucket trucks [33], and many other equipment. Typical uses include detection of cracks and material embrittlement [17], weld defects [35], corrosion [36-38], and wear [39]. By using an appropriate acoustic emissions equipment one can also detect such other processes as solidification, friction, impact, flow, and phase transformations.

3. EXPERIMENTAL DETAILS AND EQUIPMENT SETUP

Samples of corrugating paper were prepared in MD and CD by cutting into a width of 0.6 in. and a gauge length of 8 in. using a conventional cutter. The average thickness of the paper samples was measured to be approximately 0.01 in. These samples were then placed between the upper and lower jaws of an Instron machine using a specially designed clamp system. Two clamps were used to keep the paper sample in a vertical posture. One clamp was attached to the load cell at the upper jaw. The other clamp was housed on the Instron frame body below the load cell. The clamp consisted of a slot in which an end of a paper sample could slide and reside. Through application of a small compressive force across each clamp, it was possible to hold the paper sample in place. This compressive force was applied to each clamp by a torque-rod assembly. Care was taken (through reinforcing the ends of the samples by additional paper, as well as not excessively compressing the clamp ends) as to not damage the paper samples locally. A 150 KHz transducer was then mounted at the central area of the specimen through a compression mount using a specially designed clamp. This clamp consisted of a soft spring which could stretch slightly as to just mount the transducer on the paper sample without exerting any damaging compressive force to the paper sample. The reason for directly mounting the transducer to the sample was that it was intended to capture the acoustic emissions waves (emanating due to the deformation of the paper sample) as closely as possible. Also,

application of a waveguide was avoided in order to eliminate any problems associated with the wave propagation in the waveguide. No fluid couplant was used between the paper sample and the face of the transducer because it was believed that the fluid couplant would change the properties of the paper samples. The Instron crosshead was then made to move as to take the slack from the paper sample so that the sample could be positioned in a vertical position. The offset associated with positioning of the crosshead was eliminated from consideration. The transducer was wired to a preamplifier located at its vicinity as an attempt to minimize electromagnetic interference. The preamplifier was connected to a computer-based acoustic emissions signal processor and data analyzer (Physical Acoustic Corporation's LOCAN AT). A series of experiments were performed on a variety of paper samples conditioned at various relative humidities. Tests were conducted under uniaxial tensile loading at different values of crosshead speeds. The results of these experimentations will be reported under two categories:

(1) Those conducted on samples conditioned similarly (50% RH) and tested at various crosshead speeds (0.05, 0.5, 5.0, and 10 in/min),

(2) Those conducted on samples conditioned differently (30%, 50%, 70%, and 90% RH) and tested at the same crosshead speed (0.5 in/min), and for MD direction only. Additionally, two sets of special tests were performed in an attempt to investigate:

(a) The effect of initial imperfection,

(b) The impact of sensor location,

as well as reaffirm some of the conclusions of the first and second sets of results. These will be discussed later.

4. THE EFFECT OF LOADING RATE ON THE CONSTITUTIVE AND ACOUSTIC EMISSIONS CHARACTERISTICS

4.1 Introduction

Experiments were conducted on numerous samples of corrugating paper as diversified as green liquor, caustic carbonate, NSSC, and recycled. These experiments were carried out at crosshead speeds of 0.05, 0.5, 5.0, and 10 in/min. A total of 10 samples was tested in each case in order to evaluate repeatability. The range of the crosshead speed chosen represents a complete interval at which the acoustic emissions response of the paper medium could be adequately studied. It was found that at crosshead speeds of larger than 10 in/min (e.g., 50 in/min) the time of test was so short that the sample fractured almost immediately upon loading. Therefore, it was not possible to gather acoustic emissions data prior to the fracture load. It seems that at such rates of loading the mechanism of progressive damage is not likely to occur. Furthermore, as it

will become clearer later on, it was experienced that such tests do not render any significantly different body of acoustic data other than the fact that in such cases considerably larger numbers of similar acoustic hits are produced.

4.2 Discussion of the Mechanical (Constitutive) Data

It was found that of the four types of the corrugating mediums considered green liquor gave the most reproducible results. In fact, for all the samples of green liquor tested under the same condition (same orientation, crosshead speed, and relative humidity), it was possible to construct a single master constitutive curve by simply translating the origins of the stress-strain curve. This is to say that the elastic moduli (slope of the stress-strain curve) would be the same provided an initial offset (stress-strain) value was used. This way, the termination point (failure stress or strain) would be different, but all the constitutive curves would have the same shape and would lie on one another. It was, therefore, decided that green liquor would provide the best pulp type for studying the damage constitutive behavior because all samples would have the same stress-strain curve. The actual records of the constitutive curves for green liquor when tested at various crosshead speeds are shown in Fig. 7. This figure illustrates that the higher is the crosshead speed, the more linear is the constitutive behavior. Also, it is evident that the material has a higher stiffness (constitutive slope) when it is tested at

larger crosshead speeds. Fig. 8 graphically illustrates the effect of crosshead speed on Young's modulus for the green liquor medium considered. The higher elastic moduli of the green liquor medium when tested at higher loading rates is due to the inhibition of an otherwise compliant deformational mechanism. In other words, since loading is applied at high speeds, there is relatively not sufficient time for the stresses to distribute through the material to adequately deform (stretch) the network structure. Note that the apparent increase in the stiffness at higher crosshead speeds becomes more significant as the speed is increased beyond 5 in/min, i.e., at significantly high crosshead speeds. This is to say that the effect of crosshead speed on stiffness increases unproportionally as the crosshead speed is increased. The tensile strength of the material also increases as the crosshead speed is increased. However, when compared with the effect of crosshead speed on stiffness, the difference in tensile strength is comparatively much smaller. The effect of crosshead speed on tensile strength of green liquor medium is graphically illustrated in Fig. 9. It is evident that the effect of speed on tensile strength is more significant at low speeds, while it is minimal at speeds of greater than 5 in/min. It may be speculated that at low speeds non-elastic deformational processes occur more abundantly. This leads to the damage of the fibrous network structure which, in turn, reduces the overall tensile strength of the material. As we will see later, this conjecture could be easily verified from the results of the acoustic emissions studies. The effect of crosshead

speed on stretch has been illustrated in Fig. 10. Basically, as the crosshead speed is increased, the material behaves in a less compliant manner, thus reducing its overall stretch. This effect is particularly more pronounced at speeds larger than 5 in/min, which is consistent with the result of stiffness described earlier. Note that these conclusions are very much in accord with the mechanics of all deformable solids. Namely, if a material is less compliant and cannot readily deform, it resists the applied loads effectively thus raising its strength. At the same time, such a material often has a high stiffness and hardness associated with it, and behaves in a more brittle manner. Fig. 7 indicates that as the speed of testing is increased the constitutive curve more closely resembles that of a brittle material behaving in a linear elastic manner. It is logical to speculate that the fracture of such a specimen occurs as a result of a perhaps single localized event, e.g., through a self-similar crack propagation scheme. Therefore, if the loading is applied at such a fast speed (that it could be considered as almost instantaneous), it is expected that the paper sample would behave in a completely brittle manner (like glass), and the stress-strain curve becomes completely linear. The theories of linear fracture mechanics and, in particular, the Griffith's theory of fracture would then completely apply. The Tensile Energy Absorption (TEA) of green liquor at various crosshead speeds is graphically illustrated in Fig. 11, which suggests that no conclusive deductions may be made with regard to the relations between TEA and loading rate or fracture.

4.3 Discussion of the Acoustic Emissions Data

4.3.1 Amplitude Distribution Data

Amplitude is a very important parameter that directly determines the detectibility of the acoustic emissions event because it is directly related to the magnitude of the source event. Of all the conventionally measured acoustic parameters discussed earlier, it is the one best suited for developing statistical information in the form of distribution function [25]. Such distribution plots may be constructed either in the cumulative or the differential form. The differential form of the distribution function plot shows how many hits (or any other measure of the acoustic emissions data) are generated at a particular amplitude level. This type of distribution plot is often useful for distinguishing among different deformation mechanisms and for observing changes in the acoustic emissions intensity as the test proceeds. The cumulative form indicates how many hits (or any other measure of the acoustic emissions data) exceeded a given amplitude level. The cumulative form of the distribution function may be constructed from a maximum-minimum histogram record of the actual acoustic emissions data. This type of distribution plot is useful for quantitative modelling and for assessing how the detectability of the acoustic emissions will be affected by changes in the test sensitivity.

Fig. 12 illustrates a typical cumulative distribution histogram of an actual hit data which was collected during the MD uniaxial testing of a green liquor specimen at conditions of room temperature, 50% relative humidity, and crosshead speed of 0.05 in/min. All of the samples tested exhibited a similar trend. The ordinate of the plot at point 1 represents the total number of hits that was recorded during the uniaxial tensile testing of this particular sample. The abscissa of point 4 signifies the highest signal amplitude that was measured during the experimentation, which was considerably larger than any other acoustic hit recorded. It is of interest to note that only one such hit was seen during the entire testing of the sample. This hit always occurred either at or close to the maximum fracture load of the specimen. The cumulative hit distribution record also shows that the distribution function has a point of inflection. Alternatively, when the differential distribution of hits at various amplitudes is considered (Fig. 13), it is observed that this point of inflection corresponds to the point of maxima on the differential distribution curve (shown here as a histogram). This point is believed to be the incipient point that would separate two entirely different types of acoustic records, each belonging to a different class of deformation mechanism. It is possible to distinguish among three different regimes of amplitude (Fig. 12):

(1) The low-amplitude acoustic hit regime: This is the portion of the graph between points 1 and 2, which is probably associated with

the structural events that occur on the microscale. This regime of acoustic data has entirely different characteristics than the rest of the data.

(2) The intermediate-amplitude acoustic hit regime: This refers to the acoustic body of data between points 2 and 3 on the cumulative hit distribution curve. It is believed that mesostructural events such as single fiber fracture and fiber debonding occur during this regime.

(3) The "silent" regime: This is the interval between points 3 and 4 at which no acoustic activity occurs.

(4) "The Principal Hit": This refers to the hit with the largest amplitude (point 4). This is undoubtedly associated with a macroscopic event which causes the final fracture of the specimen. It is believed that the mechanism which is responsible for the generation of the principal hit and the final fracture is that of the massive fracture (or cutting) of the fibers in the web, which gives rise to a self-similar macroscopic crack propagation across the fibrous network structure.

Apart from the principal hit defined above, there are often one or two hits at amplitudes considerably lower than the principal hit (e.g., 70 db), but larger than the rest of the hit data (point 3). Such hits may be referred to as the "Second Principal Hits." The

second principal hits are associated with the mechanisms (possibly on the mesoscale) that are responsible for initiating the macroscopic fracture process. In other words, when such events occur, the damage process becomes unstable thus giving rise to macroscopic crack propagation.

Fig. 14 summarizes the amplitude of the principal hit for the samples of green liquor when tested in MD, at normal conditions (room temperature, relative humidity of 50%), and under a monotonically increasing uniaxial tensile loading. It is interesting to note that the amplitude of the principal hit is almost always the same for all the samples tested at various speeds. This corresponds to an average of about 96 db. In fact, the results of the tests conducted on the paper samples of other pulp types (recycled, caustic carbonate, NSSC) also indicated that the value of the principal hit is about 96 db. The amplitude of 96 db may be considered as the "acoustic signature" for the fracture of corrugating paper when it is stressed uniaxially under tension in the MD direction. It is believed that this amplitude level corresponds to a macroscopic event in which a self-similar crack is propagating in the paper material.

The amplitude of the second principal hit(s) for the green liquor medium tested under the aforementioned testing conditions has been shown in Fig. 15. From this figure, it may be deduced that the amplitude of the second principal hit decreases slightly as the

crosshead speed is increased. Fig. 16 summarizes the amplitude data at the point of inflection of the hit distribution curve. It is interesting to note that for all the samples tested the point of inflection is constant and corresponds to a value of 35 db. It may be therefore concluded that the interval II in Figure 12 decreases as the loading is carried out at higher speeds. The data corresponding to the ordinate (cumulative hit) of the point of inflection of the cumulative hit distribution curve have been graphically illustrated in Fig. 17. It may be seen that the cumulative hit at the point of inflection of the hit distribution curve also decreases as the crosshead speed is increased. Therefore, it may be concluded that the shaded area A under the right half portion of the cumulative hit distribution curve (Fig. 12) decreases as the crosshead speed increases. It was previously elaborated that the primary effect of the loading rate on the constitutive behavior of the material is that it decreases the ductility (or toughness) of the paper material. It is, therefore, proposed that the area A under the hit distribution curve (on the right-hand side of its point of inflection) may be considered as a measure or indication for ductility or toughness of the paper material. This definition is particularly appropriate when it is considered that the hits in the interval II are related with the mesostructural events which eventually lead the specimen to instability and final fracture. The effect of crosshead speed on the total number of acoustic emissions hits is shown in Fig. 18. It is evident that the number of hits increases as the test is

conducted more slowly. This is to say that at lower crosshead speeds more deformational events are occurring on the microscale, which increase the overall stretch of the fibrous network structure.

A typical point plot of counts versus amplitude is shown in Fig. 19. Each hit is shown as one point on the plot. The ordinate of each point shows the actual counts which gives information about the size and the shape of the waveform. This type of plot is used for data quality evaluation, and specifically for identifying the commonly encountered unwanted noise [40]. Fig. 19 shows that the acoustic signals emanating from the impulsive defect sources form a diagonal band which run across the plot. There are also some isolated hit records which fall either above or below this band. These are products of extraneous noise that are sometimes picked up by the sensor [40]. It is possible to distinguish between at least two types of extraneous noise. Some signals fall below the main band because they are not prolonged by acoustic reverberation. The common source of these noise signals is from electromagnetic interference. Some signals are above the main band because the source process is extended in time, and it is not of an impulsive origin. These noise signals are most likely due to friction. It is evident that apart from the few isolated and noise-related hit records the acoustic data fit into a well-definable function. It is also possible to distinguish among four different amplitude regimes:

(1) Regime I at which the magnitude of the amplitude is below that corresponding to the point of inflection of the cumulative hit distribution curve (35 db). During this regime the total number of counts does not change with the amplitude.

(2) Regime II at which the number of counts changes monotonically nonlinear with the amplitude.

(3) Regime III at which the number of counts varies linearly with the amplitude.

(4) Regime IV at which no acoustic activities occur.

These classifications are consistent with those introduced for the hit data. Regimes I and IV are exactly the same as before. Regime II in the cumulative hit distribution data has now been divided into two separate regimes here, which correspond to a body of hit data at which the count increases monotonically with the amplitude, once nonlinearly, and once linearly, respectively.

Distribution functions using other signal measurement parameters can also be useful in studying the acoustic emissions behavior. A typical record of the cumulative counts distribution versus amplitude is shown in Fig. 20. The shape of the distribution curve is very similar to that observed for the hit data. All samples exhibited a point of inflection at about 45 db. The corresponding

plot of the differential distribution record is shown in Fig. 21. It is seen that significant changes in the cumulative counts data are obtained only at amplitudes above 35 db. There is a major jump in the cumulative counts level at the principal hit (amplitude of about 96 db). This jump accounts for a good portion of the overall cumulative counts level (about 20-50%). There is also a relatively large contribution of the counts level to the overall cumulative counts at 45 db. The effect of crosshead speed on the cumulative counts is illustrated in Fig. 22. As the crosshead speed is increased the overall cumulative counts are reduced. This is consistent with the cumulative hit data.

4.3.2 Other Distributions

A similar cumulative distribution curve may be obtained for energy as is shown in Fig. 23. It is evident that a significant amount of acoustic energy comes from the principal hit. Sometimes this is larger than the total energy dissipated by all the other events. The ratio of the energy at the principal hit to that of the total cumulative energy changes drastically from sample to sample (47-93%). A typical histogram plot of energy versus amplitude is shown in Fig. 24. It is, again, possible to distinguish among three different regimes for amplitude:

(1) Regime I, at amplitudes less than 35 db: The energy does not change with amplitude significantly, and there is no clear pattern

for which the relation between energy and amplitude may be described.

(2) Regime II, at amplitudes between 35 db and that corresponding to the second principal hit: The energy monotonically increases with amplitude.

(3) Regime III, at amplitudes between the second principal hit and the principal hit: Here, no acoustic activity occurs.

The effect of crosshead speed on the cumulative energy is illustrated in Fig. 25. It is evident that the cumulative energy decreases as the crosshead speed is increased.

A typical cumulative distribution plot of duration versus amplitude is shown in Fig. 26. This figure indicates that a considerably large portion of the overall duration comes from the principal hit. It is again possible to distinguish among the same three regimes of amplitude:

Regime I, <35 db: Duration changes only slightly with amplitude and without any clear pattern.

Regime II, 35 db to second principal hit amplitude: Duration increases monotonically with amplitude.

Regime III, second principal hit amplitude up to 96 db: No acoustic activities occur.

The results of the experiments discussed so far emphasize the importance of the concept of the "principal hit" in determining the fracture or failure of a paper material. More broadly speaking, the principal hit may be defined as the single acoustic event which is responsible for a considerably large portion of the overall acoustic energy dissipated. It is also the hit at which all other acoustic parameters (amplitude, counts, duration) are considerably larger than any other hit. Fig. 27 illustrates the correlation between the principal hit load and the maximum load at which the samples were seen to physically fracture. It is evident that for most practical purposes the principal hit load and the fracture load are the same. The peculiarity or discrepancy occurs only in a very small number of samples in which the principal hit load is only slightly lower than the fracture load. Such a discrepancy is more related to the exact scheme in which fracture propagates across the specimen. If the fracture does not propagate across the web with a sufficiently high speed, the specimen is not yet separated into two pieces, and there is still time for the material away from the fracture line to withstand additional loads. The material still deforms slightly, while the main crack is propagating in the web. As a result, the maximum load the paper material can resist is slightly higher than the principal hit load. The exact details of the crack propagation process and certain

peculiarities are, however, not very important because in most cases it is seen that a self-similar brittle fracture governs. It may be considered that the load at which the principal hit is obtained truly reflects the ultimate load capacity of the paper material. Once this load is reached, the material is totally unstable, and it is only a matter of time in which the specimen separates into pieces. The effect of crosshead speed on the principal hit load for the samples considered before is shown in Fig. 28. The results indicate that the principal hit load increases slightly as the crosshead speed increases. This trend is consistent with the results of the tensile strength discussed earlier. The effect of crosshead speed on the principal hit data (energy, counts, duration) is shown in Figs. 29-31. Basically, as the crosshead speed is increased, the severity of the principal hit decreases. This is indicative of a less compliant, more brittle behavior, as was discussed earlier. Therefore, the results of the acoustic emissions experiments are consistent with the constitutive behavior discussed earlier.

4.3.3 Load History Data

A history plot of acoustic data versus load is the most fundamental plot that directly relates cause to effect. It is particularly useful for characterizing the damageabilty of a material. A material which is extensively defective and highly prone to damage accumulation begins to emit at low loads. On the contrary, a

material with good structural integrity gives less emissions at all load levels [41]. Fig. 32 shows a typical load history plot of hit data for a green liquor specimen when tested under normal conditions at a crosshead speed of 0.05 in/min. This plot is in the min-max cumulative form, which is convenient for reading off the total emissions quantity at any given load level. It is seen that the acoustic emissions activities initiate at a relatively low load level (although above the elastic limit), but initially, there are relatively very few acoustic activities. It is possible to categorize the following sequence of events:

(1) Acoustic emissions activities (the damage process) initiate at point 1.

(2) In the load interval from point 1 to point 2, there is sporadic and very little accumulation of acoustic activities (i.e., damage progresses very slowly). This regime of loading may be referred to as the initial or low damage state.

(3) In the load interval from point 2 to point 3, there is a progressive accumulation of acoustic activities. This regime of loading may be referred to as the progressive damage state.

(4) At point 3 there is a significant jump in the total acoustic hits. This regime of loading may be referred to as the intense damage state which leads to fracture.

A differential load history plot of a hit data is shown in Fig. 33. This plot specifies the number of hits that the material emitted at a particular loading level. This plot re-emphasizes the fact that the frequency of the acoustic activities increases with loading. Initially, in the slow damage regime, the acoustic activities occur sporadically. Later, in the progressive damage stage, the frequency of acoustic activities increases drastically. It is also evident that the differential number of hits at a particular load level does not necessarily increase with loading. However, the number of differential hits at the fracture load is the highest and is considerably larger than the number of hits obtained at any other load level. The majority (two-thirds) of the samples tested exhibited the behavior shown in Figs. 32 and 33. For the remaining samples, the initial or slow damage stage was totally absent. For these samples, the acoustic activities began at a considerably higher load, which was comparable with the load level at point 2 in the previous case (see Fig. 34). It is believed that due to the absence of certain types of initial defects the acoustic activity (or damage) was delayed until higher loads were reached, and then, at such levels new defects were created, and other less critical defects began to propagate.

The load history aspect of acoustic emissions behavior was also studied with reference to other acoustic parameters such as the counts, energy, and duration. It was found that for all the different acoustic parameters considered the trend is similar to

that of the hit data discussed earlier. It was generally possible to distinguish between the "initial" and the "progressive" damage stages. Definitions of the initial and progressive damage stages and their onset loads, however, very much depend on which acoustic emissions parameter is used. Generally, hit gives the largest progressive damage interval, while the progressive damage interval associated with energy is the smallest. Counts and duration fall in between, with counts giving a relatively shorter interval for the progressive damage stage. A typical value for the incipient point at which progressive damage starts is 90% of the maximum loading for the energy case and 70% for the case of hit data.

As far as the load history is concerned, the crosshead speed has a pronounced effect on the acoustic activities only at higher speeds. In fact, it was experienced that when tested at a crosshead speed of 0.5 in/min and under the same testing conditions, green liquor exhibits a similar trend to the one discussed before. However, when the speed of the testing is increased to 5.0 in/min, there is the evidence that the acoustic activities occur more sporadically (see Fig. 35). It is no longer possible to distinguish between the initial and progressive damage stages as was pointed out earlier. The acoustic emissions hits now occur at relatively large discrete load intervals. The number of these discrete load intervals is much smaller than when tested at lower speeds. It is interesting to note that for all the samples tested the load interval at which the acoustic activities occur becomes progressively shorter as the

loading is increased. There is also a tendency toward obtaining a larger number of acoustic hits as the loading is increased (see Fig. 36). When the crosshead speed is increased to 10 in/min, damage is even more sporadic Fig. 37). The number of load intervals at which acoustic emissions hits occur becomes even smaller. The number of hits at a given load level (differential hits) monotonically increases with the loading.

5. THE EFFECT OF RELATIVE HUMIDITY

5.1 Introduction

Samples of corrugating paper were conditioned at normal room temperature (72^0 F) and relative humidities of 30%, 50%, 70%, and 90%, respectively. They were kept in the conditioning chamber until they could be tested by an Instron Machine. Just prior to the time of testing, they were stored and carried in plastic bags to the testing lab. Tests were conducted under uniaxial tensile loading at a crosshead speed of 0.5 in/min. It was intended that the time of the test should be short enough as to minimize moisture losses by the specimens during tensile testing. At the same time it was planned to test the samples at such a speed as to ensure that a relatively abundant record of acoustic emissions data could be generated. Experiments were conducted on a variety of corrugating papers in MD direction. The results of these experiments which

were performed on green liquor will be analyzed and presented in this manuscript.

5.2 Discussion of the Constitutive Data

Typical stress-strain curves for green liquor at various conditions of relative humidities are shown in Fig. 38. A similar shape is obtained for the stress-strain curve at all humidity conditions, which follows the classic linear-nonlinear trend. Although the elastic limits for the conditions of 30, 50, and 70% relative humidity are comparable (elastic limit only reduces slightly with increasing the relative humidity), the behavior for the 90% RH is remarkably different. For the 90% RH condition, the elastic limit is considerably less. There is also a large drop in the ultimate tensile strength. Fig. 39 summarizes the effect of relative humidity on average tensile strength for all the samples tested. Similar results are obtained for the elastic modulus (Fig. 40). The extensive reduction in the values of tensile strength and the elastic modulus for the 90% relative humidity condition is due to the softening of the lignin and hemicellulose components of the fibers in the paper which gives rise to a plasticizing effect [42-43]. The effect of relative humidity (or moisture content) on stretch has been illustrated in Fig. 41. It is evident that the stretch decreases as the relative humidity (or moisture content) is increased in the sheet. It is also of interest to note that at lower values of relative humidity (30, 50% RH) the stretch is

almost constant. The increase in stretch is approximately proportional to the moisture content (or relative humidity) at relative humidity levels above the room condition (50% RH). Therefore, although very high moisture contents (e.g., those corresponding to 90% RH) have drastic effects on the elastic limit and the ultimate tensile strength of the paper, the effect on the stretch is not comparable.

5.3 Discussion of the Acoustic Emissions Data

5.3.1 Amplitude Distribution Data

All of the tested samples conditioned at various relative humidities exhibited the same trend for the cumulative distribution function of hit with respect to the amplitude. One such typical plot is shown in Fig. 42. These plots exhibited a point of inflection at 35 db. This behavior is similar to the one experienced for the experiments involving different crosshead speeds. It is believed that hits with the maximum amplitudes above and below the 35 db threshold describe different acoustic emissions events, perhaps originating from entirely different deformation mechanisms. A similar type of classification for the hit record may be introduced as the one suggested for the crosshead speed experiments. Namely, at least three different regimes of amplitude may be distinguished:

(1) Regime I: low amplitude regime (<35 db).

(2) Regime II: intermediate amplitude regime (between 35 db and the second principal amplitude).

(3) Regime III: The no-hit regime (between the second principal and the principal amplitude).

A glance at a typical hit record for the condition of relative humidity of 30% will show that the regime II may be further divided into two separate regimes: the low hit regime and the higher hit regime. This distinction is possible at the amplitude level of about 45 db. These results suggest that different types of deformational processes are in effect at above and below the maximum amplitude level of 45 db. The effect of relative humidity on the magnitude of the principal amplitude has been shown in Fig. 43. It is of interest to note that the principal amplitude is basically constant for the paper provided the relative humidity is not extensive (e.g., 90%). It is believed that at such high levels of relative humidities water interacts with the fiber components drastically thus changing the overall microstructure of the fibrous system. The deformational process and, particularly, the fracture mechanism become entirely different. This gives rise to the generation of a completely different signal of a notably lower intensity at the source. Fig. 44 illustrates the effect of relative humidity on total cumulative hit for the aforementioned paper

samples tested. It is evident that the overall cumulative hit is decreased as the relative humidity is increased. This is due to the softening of the paper at higher moisture contents. There is also a drastic drop in the cumulative hit at a relative humidity of 90%. These results suggest that there is a significant difference in the progressive deformational process of paper at a relative humidity of 90%. It may also be deduced that the cumulative hit at the point of inflection decreases with increasing the relative humidity. On the other hand, the maximum amplitude of the second principal hit is, on average, somewhat similar at all relative humidities. Therefore, it may be concluded that the area A under the cumulative hit distribution curve decreases as the relative humidity increases. This result is analogous to the one found for the crosshead experiments. In other words, the principal effect of crosshead speed and relative humidity are that these factors both reduce the overall acoustic emissions activities. It is proposed here that these factors both reduce the toughness of the material through different mechanisms. The crosshead speed reduces the toughness of the paper material through stiffening and brittlizing. The relative humidity diminishes toughness by softening and plasticizing.

5.3.2 Other Distributions

Again, similar distribution curves may be constructed to illustrate the relation between counts (or energy, or duration) and maximum

amplitude. It is found that for all the samples tested, and any of the acoustic emissions parameters considered, all curves have a similar shape as the hit data. Furthermore, significant changes in the cumulative values of counts, energy, and duration are found only at maximum amplitude levels of above 35 db. Figs. 45-46 illustrate the effect of relative humidity on total cumulative counts and energy, respectively. It may be concluded that the cumulative counts and energy decrease as the relative humidity is increased. The impact of moisture content on the magnitudes of principal hit counts, energy, and duration may be deduced from Figs. 47-49. It is evident that all of these acoustic emissions parameters decrease as the moisture content in the sheet increases. Particularly, notable reductions in these parameters are seen at the relative humidity level of 90%. The effect of relative humidity on the principal hit load is shown in Fig. 50. It is of interest to emphasize the reduction in the hit load as a result of the increase in the relative humidity. It is particularly interesting to note the relative reduction in the principal hit load at the relative humidity of 90%. Again, it seems appropriate to conclude that in this case the paper material is failing by an entirely different mechanism. Note that although increasing the crosshead speed enhances the ultimate tensile strength, the principal effect of increasing the moisture content is that it decreases the tensile strength. These results are, however, consistent with the behavior of all solid materials. Namely, stiffening (or brittlizing) always increases the ultimate strength, while plasticizing (or softening)

reduces the ultimate strength. The principal difference between the two is that stiffening (e.g., through increasing the load rate) causes the material behavior to divert toward a more brittle behavior, while softening (as in the case of humidifying) instigate a more ductile behavior. As a result, in the first case the material fails by a fracture process, possibly through self-similar crack propagation. On the other hand, plasticizing causes ductile failure through perhaps void coalescence, shear localization, or other pertinent mechanisms. It is not surprising to find that increasing crosshead speed leads to decreased stretch, while raising the humidity level gives rise to considerably higher (plastic) strains at failure.

5.3.3 Load History Data

A typical load history plot of cumulative hit data for a green liquor specimen when tested under uniaxial tension and at a crosshead speed of 0.5 in/min and relative humidity of 30% is shown in Fig. 51. It is seen that at least three distinct load regions can be identified. In the first region, which may be considered as the low hit (or initial damage) load regime, the total cumulative hit is either almost constant or changes very slightly with the load. In the second regime, which may be referred to as the progressive damage regime, there are considerably more acoustic emissions activities. This regime is the progressive damage regime, as was pointed out earlier. One may yet define a third load regime,

which is either at or very close to the maximum load, at which the acoustic activities (or damage) become highly intense. The plot shown here is typical for all the samples tested. Fig. 52 shows a typical load history plot of the cumulative hit for a sample of green liquor at the relative humidity condition of 90%. Again, a similar behavior is seen as that of 30% RH, but this time the progressive damage stage is much shorter, i.e., most of the acoustic emissions occur at magnitudes closer to the final load.

6. FURTHER REMARKS ON THE ACOUSTIC EMISSIONS CHARACTERISTICS OF CORRUGATING PAPER

In order to better comprehend the acoustic emissions behavior and the fracture characteristics of corrugating paper, the following experiments were conducted. Specimens of green liquor corrugating paper were prepared under the normal lab conditions (temperature of 73^0 F and at a relative humidity of 50%). The size of the specimens was the same as that indicated previously. Two small horizontal incisions were introduced along the horizontal center line of the specimens starting from the outer edges of the specimens. Care was taken as to make the geometric configuration of these incisions as unified as possible. The objective of this kind of sample preparation was to ensure that samples will fracture along the horizontal center line of the paper when tested under uniaxial tensile loading (applied perpendicular to the line of incision).

Two sets of experiments were then performed at the crosshead speed of 0.05 in/min. In the first set of experiments, the transducer was mounted at the center of the tensile specimens (CUT1 experiments). In the second set of experiments, the transducer was mounted on the top of the sample, close to the upper jaw of the Instron Machine (CUT2 experiments). The objectives of these experimentation were:

(1) To compare the results of the tests performed on the CUT2 specimen with those of the uncut specimens considered earlier. During the experimentation on the uncut specimens, the transducer was always mounted at the center line of the specimens. It was also observed that most of the uncut specimens separated at comparable positions close to the upper jaw. The results of these experiments (with adequate filtration of those cases that fractured at other locations) will be compared to those of the CUT2 experiments.

(2) To compare the results of the CUT1 and CUT2 experiments in order to understand the effect of transducer location on the acoustic emissions signal pickup. This should give some indication about the mechanism of acoustic emissions wave propagation in paper.

6.1 Comparison of the CUT2 and Uncut Experiments

The stress-strain curves for typical cut and uncut samples are shown in Fig. 53. Comparisons of the salient characteristics of the

constitutive curve (namely, the Young's modulus for stiffness, ultimate tensile strength, stretch, TEA, and the elastic/proportional limit) are also given in Figs. 54-58. From these data it may be concluded that:

(1) The stiffness is increased when the incision is introduced in the specimen. This result is inconsistent with the result obtained with other materials. In other conventional materials, the introduction of cracks to the specimen usually leads to stiffness reduction.

(2) The ultimate tensile strength of the paper with the incision is considerably lower. This is very much in accord with the behavior of cracked solids. The introduction of cracks reduces the overall strength of the solid.

(3) The stretch is much lower for the cut specimen. This result can be readily explained by the fact that the introduction of the incisions at the edges is expected to give rise to localized fracture events. In other words, when the cracks are introduced to the paper material, a great deal of energy of the external loading is expended in extending the incisions as opposed to randomly or uniformly deforming the sheet.

(4) The tensile energy absorption (TEA) is much less for the cut specimen. This is as expected because much less energy is required

to fracture a specimen with a crack than a specimen without a crack.

(5) The nonlinear portion of the constitutive curve is longer for the specimen with incisions. This is also in accord with the characteristics of brittle solids which behave in a more linear elastic manner. In other words, in the case of cracked solids, most of the dissipative energy is used locally to extend the crack (localized damage) rather than introducing new deformational mechanisms throughout the specimen (distributed damage).

Fig. 59 shows a cumulative hit distribution curve for a typical CUT2 sample. The shape of the distribution curve is the same as one for uncut samples discussed earlier. For all the samples tested, the distribution curve shows a point of inflection at the maximum amplitude level of 35 db. As was mentioned earlier, the 35 db amplitude marks the incipient point between two distinct types of acoustic emissions (or deformational) behavior. It may also be deduced that in the 35-45 db interval there are relatively higher jumps in the cumulative hit level (the high hit regime) than in the interval between 45 db and the second principal hit amplitude (the low hit regime). The high hit regime and the low hit regime are representatives of two distinct acoustic emissions (or deformational) behaviors. Fig. 60 compares the maximum amplitude at the principal hit for the CUT2 and the uncut specimens. It is interesting to note that for the CUT2 specimens the principal

amplitude is also about 96 db. The mechanism of fracture for the cut specimens is well defined. It occurs due to propagation of a single self-similar crack in the specimen due to the fibers cutting across the web. It may, therefore, be concluded that the 96 db amplitude is the acoustic emissions signature for the propagation of a macroscopic crack across a paper specimen, which occurs as a result of massive cutting of the cellulosic fibers across the paper web. The results of the cumulative hit for the uncut and CUT2 specimens are summarized in Fig. 61, which show that a drastic reduction occurs in the total cumulative hit level when incisions are introduced at the edges of the specimens. A similar result is obtained for the cumulative count (Fig. 62). The cumulative hit at the point of inflection is also reduced drastically for the CUT2 specimens when compared with the uncut samples. It was also found that, on average, the magnitude of the maximum amplitude at the second principal hit diminishes when incisions are introduced to the samples. Therefore, the area A under the cumulative hit distribution is much lower in the case of the CUT2 specimens. This result confirms the conclusion that the area A is representative of the overall toughness of the specimen because a cracked solid has a lower toughness than that of a solid with a crack. The results of the principal hit data for the uncut and the CUT2 specimens are summarized in Figs. 63-65. It may be seen that principal count, energy, as well as duration are decreased when incisions are introduced to the paper samples. It is evident that in the absence of the incisions more effort is needed in the form of dissipative

damage deformation to nucleate a crack, which under the influence of the external load could subsequently propagate across the web.

6.2 Remarks Regarding the Role of the Sensor Position

In this section the results of the CUT1 and CUT2 experiments will be compared in an attempt to determine whether the position of the sensor has any impact on the acoustic emissions data. Fig. 66 compares and summarizes the results of the principal amplitude for the CUT1 and CUT2 experiments. Again, it is found that for all the samples tested, and in both cases, the principal amplitude occurs at about 96 db. Therefore, the value of the principal amplitude is indifferent to the position of the sensor. These results reaffirm the conclusion that the maximum amplitude is associated with a particular deformation mechanism rather than the conditions of testing. The results of the total cumulative hits and cumulative counts are illustrated in Figs. 67-68 for the CUT1 and CUT2 specimens. Both the cumulative hit and the cumulative counts are reduced when the sensor is mounted remotely. The impact of the transducer position is much more serious in the case of cumulative counts. The effect of sensor position on the principal hit data may be deduced from Figs. 69-71. These figures indicate that, on average, the values of the principal hit data could diminish by as much as a factor of 2 when the sensor is mounted remotely. These results are reflective of the fact that the acoustic emissions waves dissipate in the paper medium. This may occur either due to

the damping nature of the paper material, or due to reflection, or possibly due to the particular sample geometry chosen. Whatever is the exact cause or the nature of the dissipative process, it is important to note that the position of the sensor is an important factor in the interpretation of the acoustic emissions data.

7. SUMMARY AND CONCLUSIONS

Many interesting conclusions have emerged from these studies that may be emphasized. These include:

(1) The amplitude of the acoustic emissions signal's largest excursion is a very important parameter which directly gives an indication of the type of the damage deformation that is taking place in the paper material.

(2) The amplitude of 96 db may be considered as the "acoustic signature" for the propagation of a self-similar crack in the corrugating paper. The propagation of the crack is due to the continuous cutting of the fibers in the network.

(3) At least three distinct regimes of amplitude may be identified:

(I) Below 35 db: This may be due to microstructural events (e.g., dislocation motion, other shear mechanisms, moving and breaking of

the fibrils, cavitational processes, etc.). It is believed that these emissions are manifestations of the plastic behavior of the paper material. One practical example for this would be the relief of residual stresses in the network.

(II) Between 35 db and 45 db: This may be due to some mesostructural processes such as fiber debonding.

(III) Between 45 db and the second principal amplitude (roughly 65 to 70 db): This may be due to breakage of some individual fibers. These occur less abundantly than the hits described previously.

(4) The area under the cumulative hit distribution curve may be considered as a parameter which is indicative of the "failure toughness" of the paper material. Note that the term "failure" is not necessarily restricted to brittle fracture.

(5) The total number of hits (as well as counts) decreases as the loading rate is increased.

(6) The severity of the principal hit (as reflected by the magnitudes of principal counts, energy, and duration) decreases as the loading rate is increased.

(7) Loading rate does not affect the principal amplitude.

(8) The area under the cumulative hit distribution curve decreases as the loading rate is increased. The material behaves in a less compliant, more brittle manner.

(9) The principal effect of loading rate on the acoustic emissions behavior is that it changes the frequency of its occurrence in terms of the loading interval of emission. At low loading rates there is a distinction between "low emission" and "frequent emission" states. As the loading rate is increased, emission becomes more sporadic until there is no distinction between the low emission and the frequent emission stages. However, the loading interval in which sporadic emissions occur becomes progressively shorter as the loading is increased. As the loading rate approaches an optimally fast speed, there is the evidence that the number of emissions at a given load becomes increasingly higher.

(10) The total number of hits (as well as counts) decreases as the relative humidity increases.

(11) The severity of the principal hit (as reflected by the magnitudes of principal counts, energy, and duration) decreases as the relative humidity is increased.

(12) Relative humidity does not affect the principal amplitude except at very high levels of humidities. It is believed that at such humidities the fibrillar structure of the paper changes. As a

result, the paper material deforms under different mechanisms, and the principal amplitude drops to a lower level which is reflective of a more plastic deformational behavior.

(13) The area under the cumulative hit distribution curve decreases as the relative humidity is increased. The material behaves in a more compliant, plastic manner.

(14) The principal effects of high loading rate and high humidities are to accelerate the paper material toward failure. However, in each case a totally different mechanism is in effect. In the former case, failure occurs due to brittle fracture, while in the latter ductile mechanisms such as shear localization are responsible for failure.

(15) Finally, the location of the sensor has a strong effect on the magnitude of the acoustic emissions. Generally, the acoustic emissions waves dissipate in the paper material as the waves travel through the material.

8. REFERENCES

1. Corte, H., Kallmes, O., and Jarrot, D., Paper-Maker, Vol. 142, No. 7, p. 61, 1961.

2. Yamauchi, T., Okumura, S., and Murakami, K., "Measurement of Acoustic Emission During the Tensile Straining of Paper," J. Pulp Paper Sci., Vol. 15, No. 1, p. 23, 1989.

3. Yamauchi, T., Okumura, S., and Noguchi, M., "Acoustic Emission as an Aid for Investigating the Deformation and Fracture of Paper," J. Pulp Paper Sci., Vol. 16, No. 2, p. 443, 1990.

4. Yamauchi, T., Murakami, K., "Acoustic and Optical Measurements During the Straining of Paper," Proceedings of the International Paper Physics Conference, 1991.

5. Liptai, R.G., Harris, D.O., and Tatro, C.A., " An Introduction to Acoustic Emission," Acoustic Emission, ASTM STP 505, American Society for Testing and Materials, pp. 3-10, 1972.

6. Liptai, R.G., Harris, D.O., "Acoustic Emission -- An Introductory Review," Materials Research and Standards, MTRSA, Vol. 11, No. 3, pp. 8-10, 1971.

7. Schofield, B.H., "Research on the Sources and Characteristics of Acoustic emissions," Acoustic Emission, ASTM STP 505, American Society for Testing and Materials, pp. 11-19, 1972.

8. Dunegan, H.L., and Green, A.t., "Factors Affecting Acoustic Emissions Response From Materials," Acoustic Emission, ASTM STP

505, American Society for Testing and Materials, pp. 100-113, 1972, Also in Materials Research and Standards, MTRSA, Vol. 11, No. 3, pp. 21-24, 1971.

9. Gillis, P.P, "Dislocation Mechanism as Possible Sources of Acoustic Emission," Materials Research and Standards, MTRSA, Vol. 11, No. 3, pp. 11-16, 1971.

10. Gillis, P.P, "Dislocation Motions and Acoustic Emission," Acoustic Emission, ASTM STP 505, American Society for Testing and Materials, pp. 20-29, 1972.

11. Frederick, J.R., and Felbeck, D.K., "Dislocation Motions as Source of Acoustic Emission," Acoustic Emission, ASTM STP 505, American Society for Testing and Materials, pp. 129-139, 1972.

12. Nakamura, Y., Veach, C.L., and McCauley, B.O., "Amplitude Distribution of Acoustic Emission Signals," Acoustic Emission, ASTM STP 505, American Society for Testing and Materials, pp. 164-186, 1972.

13. Dunegan, H.L., Harris, D.O., and Tatro, C.A., "Fracture Analysis by Use of Acoustic Emission," Engng. Fracture Mech., Vol. 1, No. 1, pp. 105-122, 1968.

14. Palmer, I.G., and Heald, P.T., "The Application of Acoustic

Emission Measurements to Fracture Mechanics," Mater. Sci. Eng., Vol. 11, No. 4, pp. 181-184, 1973.

15. Yuyama, S., Imanaka, T., and Ohtsu, M., "Quantitative Evaluation of Microfracture due to Disbonding by Waveform Analysis of Acoustic Emission," J. Acoust. Soc. Am., Vol. 82, No. 2, pp, 506-512, 1987; Vol. 83, No. 3, pp. 976-983, 1988.

16. Tetelman, A.S., and Chow, R., "Acoustic Emission Testing and Microcracking Processes," Acoustic Emission, ASTM STP 505, American Society for Testing and Materials, pp. 30-40, 1972.

17. Vahaviolos, S.J., "Real Time Detection of Microcracks in Brittle Materials Using Stress Wave Emission (SWE)," IEEE Trans., Vol. PHP-10, No. 3, pp. 152-159, 1974.

18. Pollock, A.A., "Classical Wave Theory in Practical AE Testing," in Progress in Acoustic Emission III, Proceedings of the Eighth International Acoustic Emission Symposium, The Japanese Society of Non- Destructive Inspection, pp. 708-721, 1986.

19. Heiple, C.R., and Carpenter, S.H., "Acoustic Emission Produced by Deformation of Metals and Alloys - a Review," J. Acoust. Emiss., Vol. 6, No. 3, pp.177-204, 1987, Vol. 6, No. 4, pp. 215-237, 1987.

20. Pao, Y.H., "Theory of Acoustic Emission," in Elastic Waves and

Non-Destructive Testing of Materials, AMD-20, American Society of Mechanical Engineers, pp. 107-128, 1978.

21. Enoki, M., Kishi, T., and Kohara, S., "Determination of Microcracking Moment Tensor of Quasi-Cleavage Facet by AE Source Characterization," in Progress in Acoustic Emission III, Proceedings of the Eighth International Acoustic Emission Symposium, The Japanese Society of Non- Destructive Inspection, pp. 763-770.

22. Scruby, C.B., "Quantitative Acoustic Emission Techniques," in Research Techniques in Non-Destructive Testing, Vol. VIII, R.S. Sharpe, Ed., Academic Press, pp. 141-210, 1985.

23. Acoustic Emission Testing, Vol. 5, 2nd ed., Nondestructive Testing Handbook, R.K. Miller and P. McIntire, E.d., American Society for Nondestructive Testing, pp. 64-90, 1987.

24. Fowler, K.A., and Papadakis, E.P., "Observation and Analysis of Simulated Ultrasonic Acoustic Emission Waves in Plates and Complex Structures," Acoustic Emission, ASTM STP 505, American Society for Testing and Materials, pp. 222-237, 1972.

25. Pollock, A.A., "Acoustic Emission Amplitude Distributions," in International Advances in Nondestructive Testing, Vol. 7, Gordon and Breach, pp. 215-239, 1981.

26. Gorman, M.R., and Rytting, T.H., "Long Duration AE Events in Filament Wound Graphite/Epoxy in the 100-300 KHz Band Pass Region," in First International Symposium on Acoustic Emission From Reinforced Composites, the Society of Plastic Industries, 1983.

27. Kaiser, J., Erkenntnisse und Folgerungen aus der Messung von Gerauschen bei Zugbeanspruchung von Metallischen Werkstoffen, Arch. Eisenhuttenwes., Vol. 24, No. 1-2, pp.43-45.

28. Dunegan, H.L., and Tetelman, "Acoustic Emission," Ress. Dev., Vol. 22, No. 5, pp. 20-24, 1971.

29. Acoustic Emission Testing, Vol. 5, 2nd ed., Non-Destructive Testing Handbook, R.K. Miller and P. McIntire, Ed., American Society for Nondestructive Testing, p.426, 1987.

30. "Acoustic Examination of Fiber-Reinforced Plastic Vessels," Boiler and Pressure Vessel Code, Article 11, Subsection A, Section V, American Society of Mechanical Engineers, 1983.

31. Cole, P.T., "Acoustic Emission Technology and Economics Applied to Pressure Vessels and Storage Tanks," in Proceedings of the Fourth European Conference on Destructive Testing, Pergammon Press, London, 1987, p. 2892.

32. Parry, D.L., "Industrial Application of Acoustic Emission

Analysis Technology," in Monitoring Structural Integrity by Acoustic Emission, STP 571, ASTM, pp. 150-183, 1975.

33. Acoustic Emission Testing, Vol. 5, 2nd ed., Non-Destructive Testing Handbook, R.K. Miller and P. McIntire, Ed., American Society for Nondestructive Testing, pp. 226-259, 267-271, 333-3339, 421-424, 434-443.426, 1987.

34. Fowler, T.J., "Recent Developments in Acoustic Emission Testing of Chemical Process Equipment," in Progress in Acoustic Emission IV, Proceedings of the Ninth International Acoustic Emission Symposium, The Japanese Society of Non- Destructive Inspection, pp. 391-404, 1988.

35. Acoustic Emission Testing, Vol. 5, 2nd ed., Non-Destructive Testing Handbook, R.K. Miller and P. McIntire, Ed., American Society for Nondestructive Testing, pp. 213-219, 472-484, 1987.

36. Chaskelis, H.H., Callen, W.H., and Kraft, J.M., "Acoustic Emission from Aqueous Stress Corrosion Cracking in Various Temper of 4340 Steel," NRL Report # 2608, Naval Research Laboratory, 1973.

37. Pollack, A.A., "Acoustic Emission Capabilities and Applications in Monitoring Corrosion," in Corrosion Monitoring in Industrial Plants Using Nondestructive Testing and Electrochemical Methods, STP 908, G.C. Moran and P. Labine, Ed., ASTM, pp. 30-42, 1986.

38. Yuyama, S.H., "Fundamental Aspects of Acoustic Emission Applications to the Problems Caused by Corrosion," in Corrosion Monitoring in Industrial Plants Using Nondestructive Testing and Electrochemical Methods, STP 908, G.C. Moran and P. Labine, Ed., ASTM, pp. 43-47, 1986.

39. McBride, S.L., "Acoustic Emission Measurement on Rubbing Surfaces," in Proceedings of the World Meeting on Acoustic Emission, Charlotte, NC, March 1989.

40. Fowler, T.J., "Experience with Acoustic Emission Monitoring of Chemical Process Industry Vessels," in Progress in Acoustic Emission III, Proceedings of the Eighth International Acoustic Emission Symposium, The Japanese Society of Non- Destructive Inspection, pp. 150-162.

41. Hutton , P.H., and D.L. Parry, "Assessment of Structural Integrity by Acoustic Emission," Materials Research and Standards, MTRSA, Vol. 11, No. 3, pp. 25-32.

42. Sarfarazi, M.P., "The Effects of Temperature and Moisture Content on the Tensile Strength and Stretch Behavior of Corrugating Mediums," To be published in TAPPI.

43. Sarfarazi, M.P., "High Temperature Strength/Runnability," IPST

project 2696-26 final report submitted to the Containerboard and Kraft Paper Group (CKPG) of the American Paper Institute, February 1992.

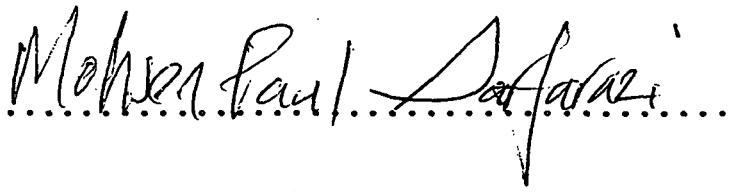

Mohsen Paul Sarfarazi

Assistant Professor

Engineering and Paper Materials Division

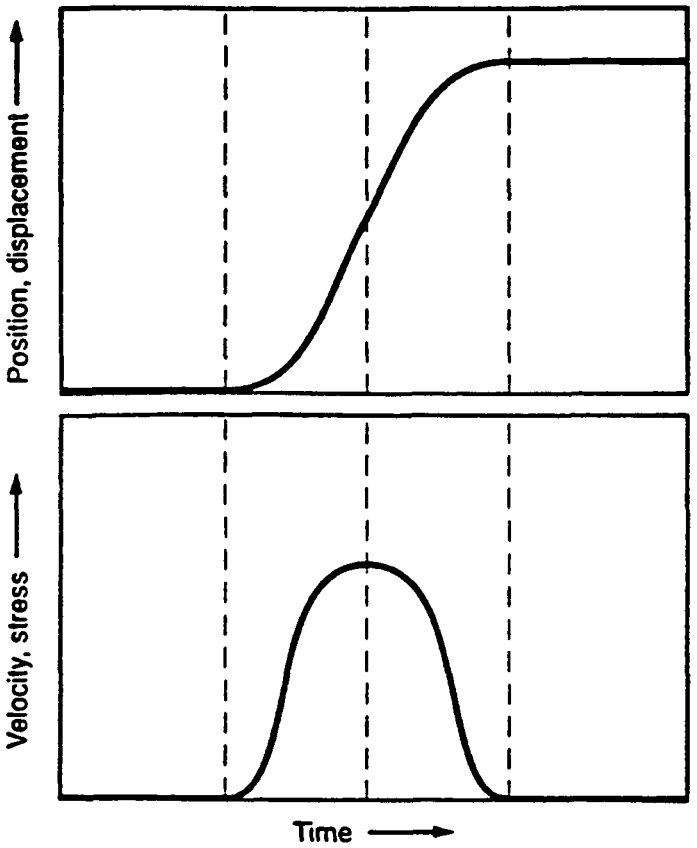

Fig.1 The original acoustic emission waveform released at the source.

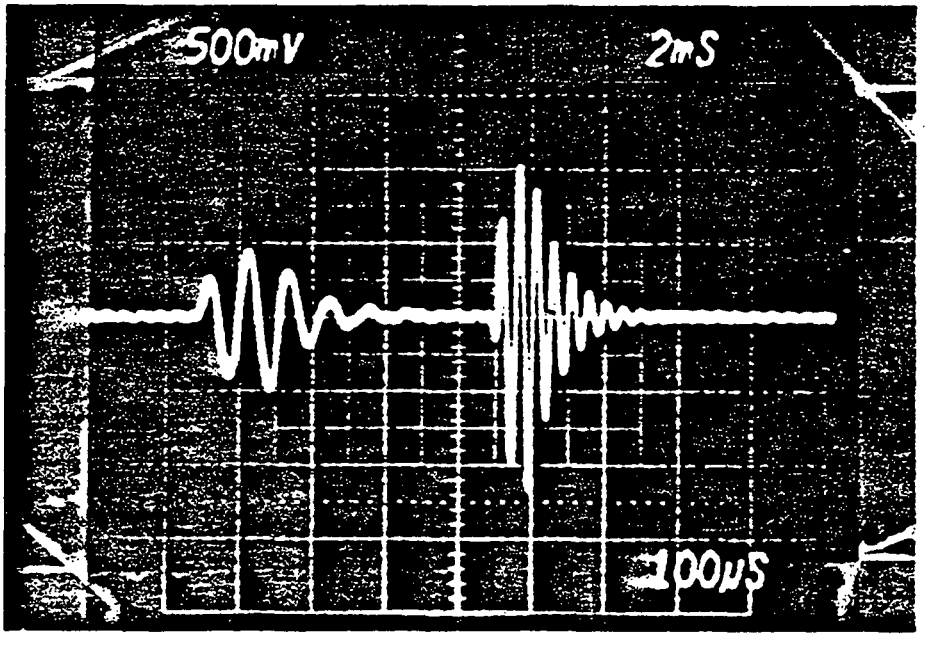

Fig. 2 A typical burst-type acoustic emission waveform originating from a single, discrete deformational event.

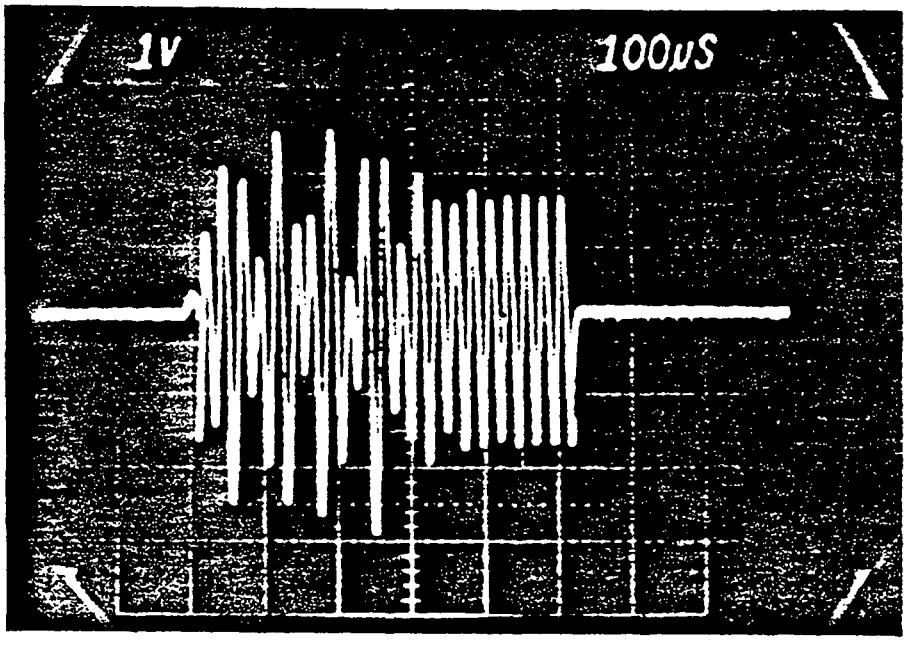

Fig. 3 A typical continuous acoustic emission waveform originating from plastic deformation of metals.

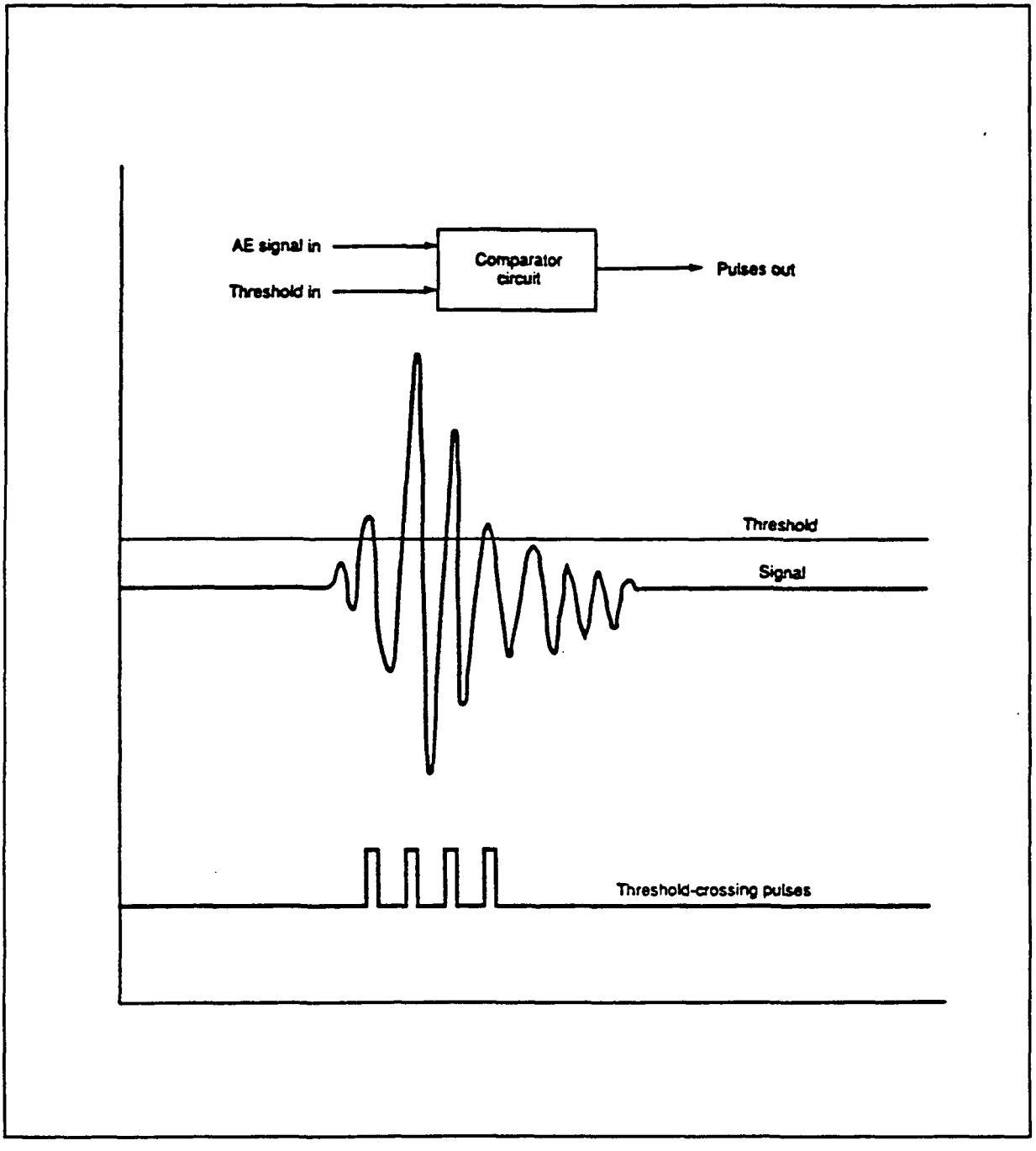

Fig. 4 Illustration of the definition of counts.

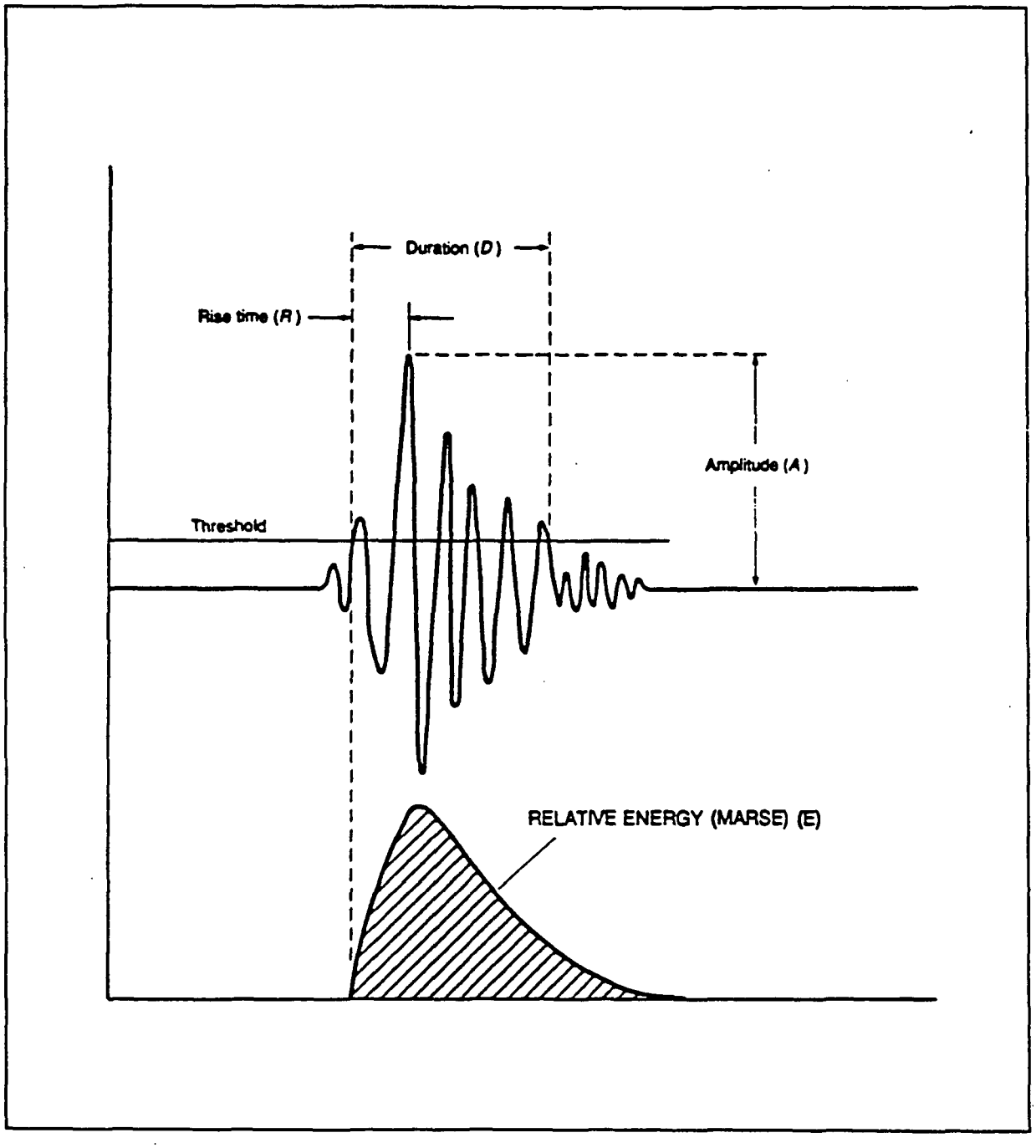

Fig. 5 Illustration of the definitions of amplitude, energy, duration, and rise time.

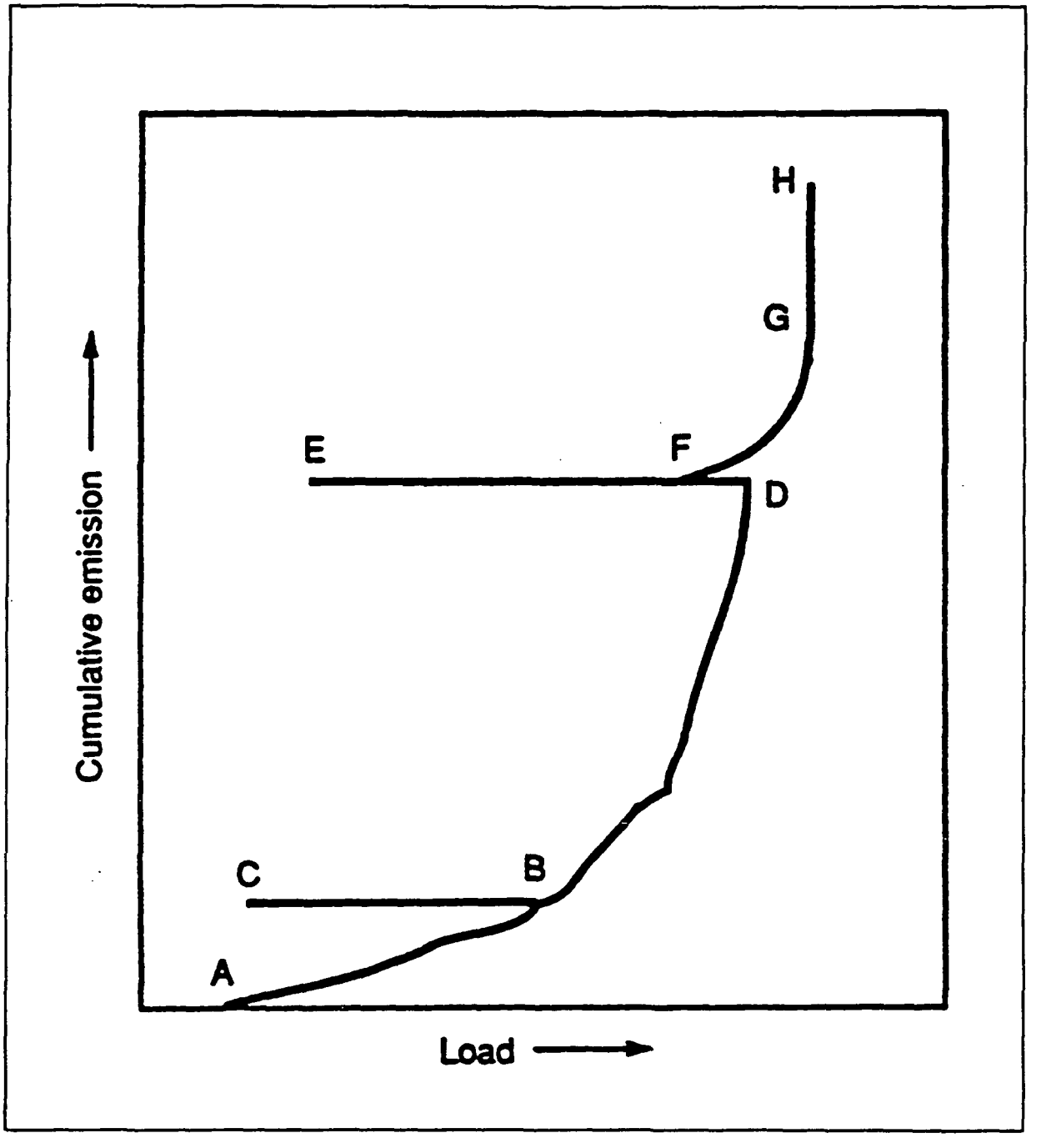

Fig. 6 Illustration of the Kaiser and Felicity effects.

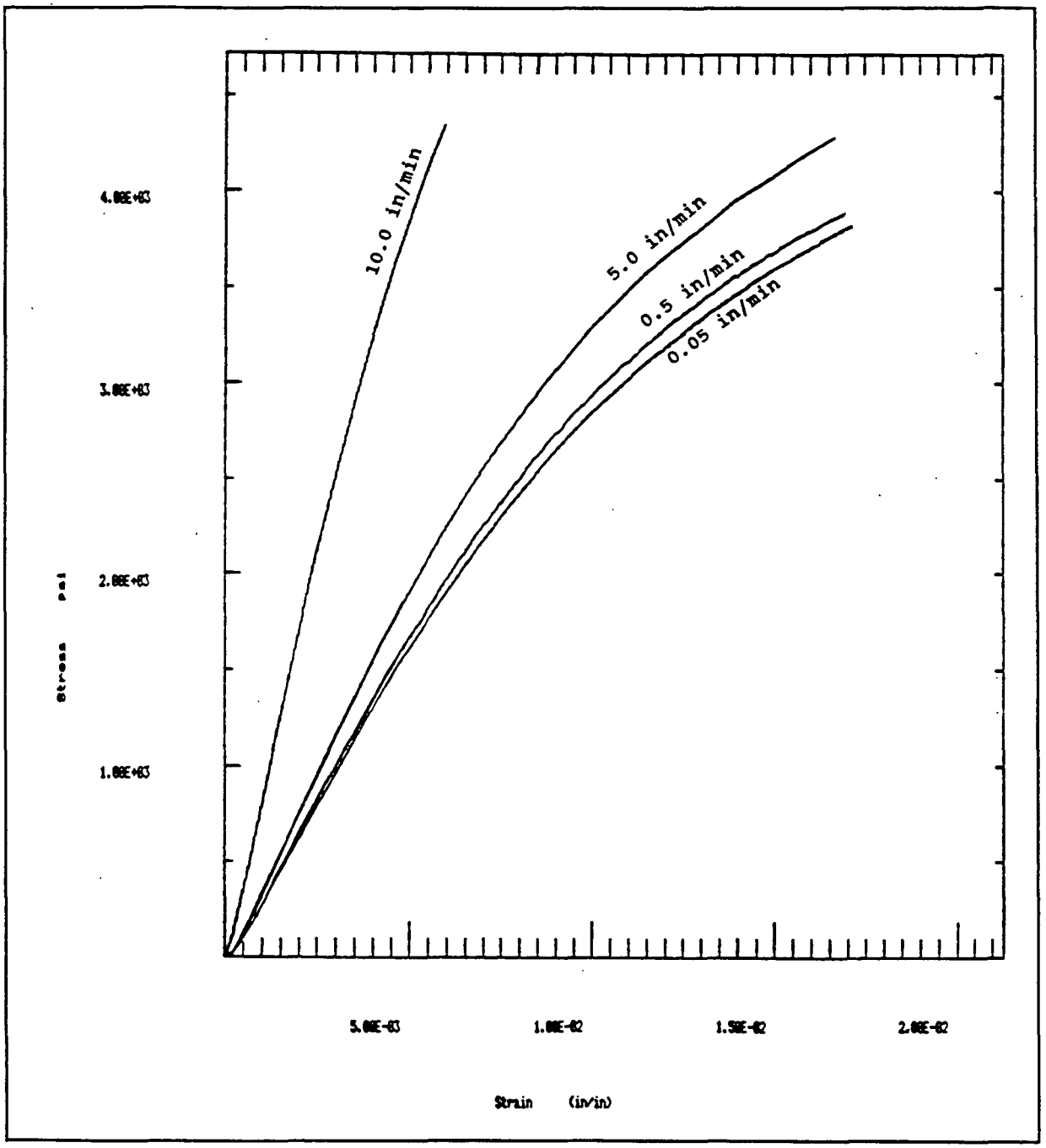

Fig. 7 Constitutive curves for green liquor corrugating paper conditioned at 50% RH, and tested in MD under uniaxial tensile loading at various crosshead speeds.

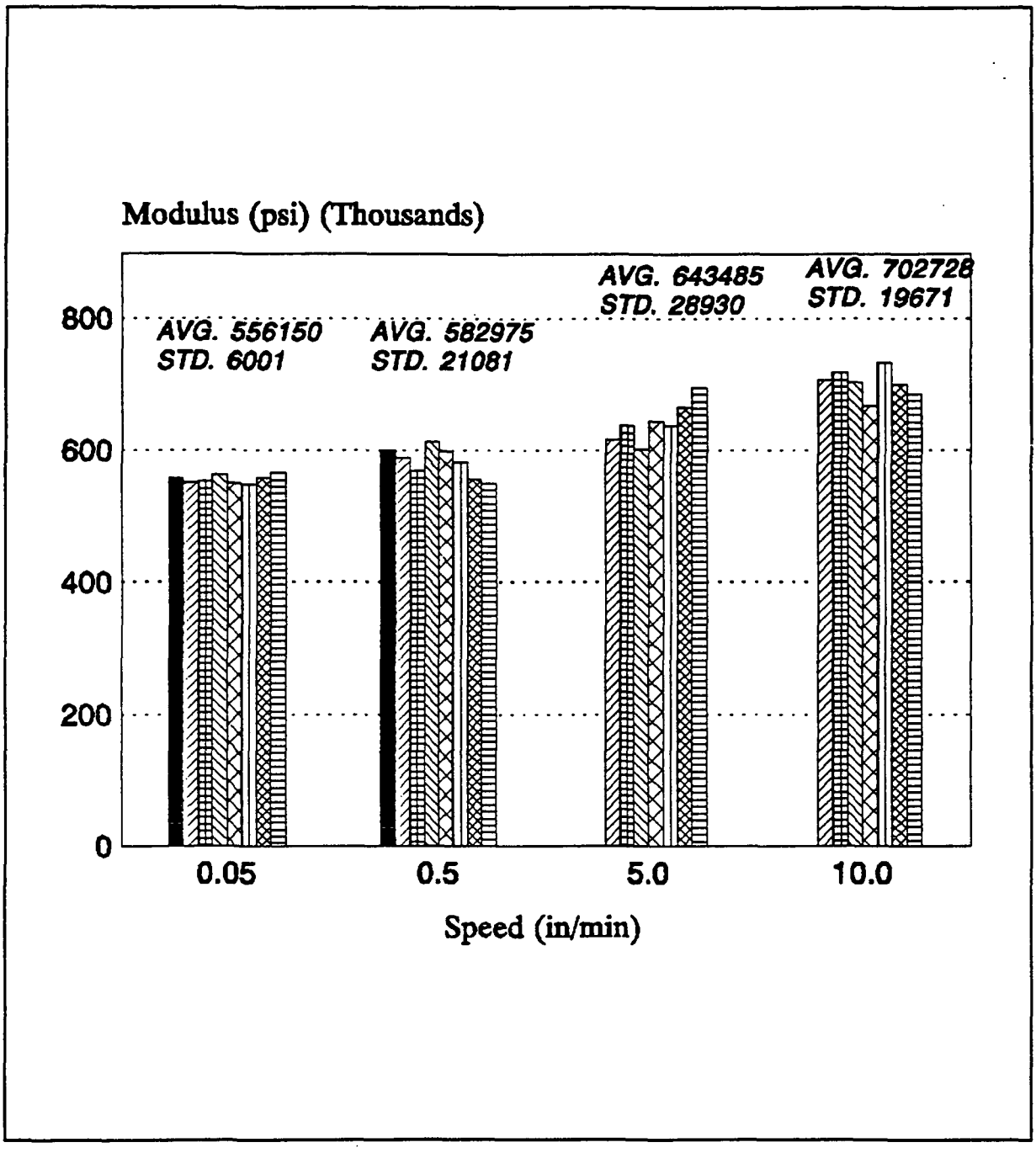

Fig. 8 The effect of crosshead speed on elastic modulus for green liquor corrugating paper conditioned at 50% RH, and tested in MD under uniaxial tensile loading.

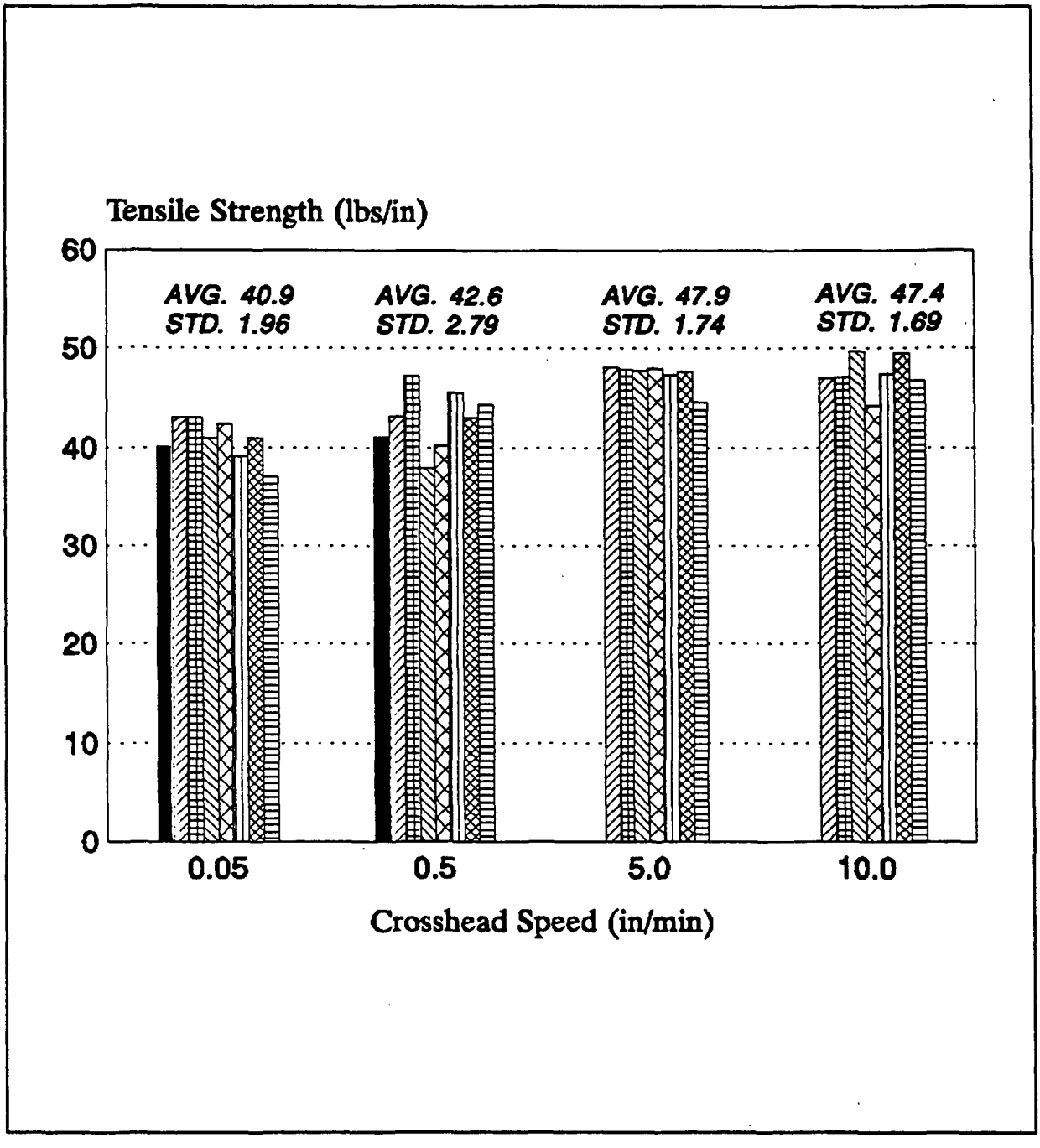

Fig. 9 The effect of crosshead speed on tensile strength for green liquor corrugating paper conditioned at 50% RH, and tested in MD under uniaxial tensile loading.

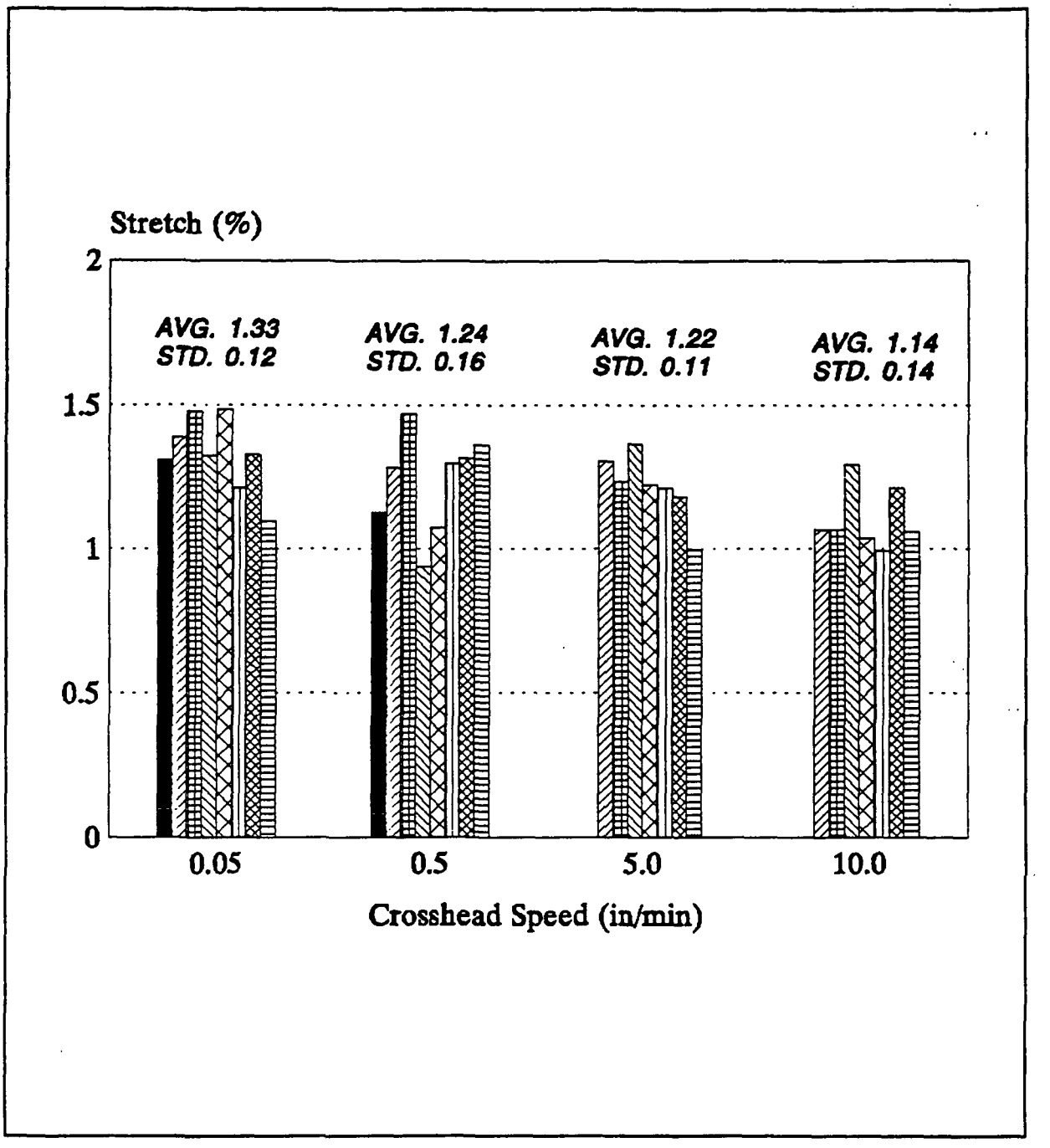

Fig. 10 The effect of crosshead speed on stretch for green liquor corrugating paper conditioned at 50% RH, and tested in MD under uniaxial tensile loading.

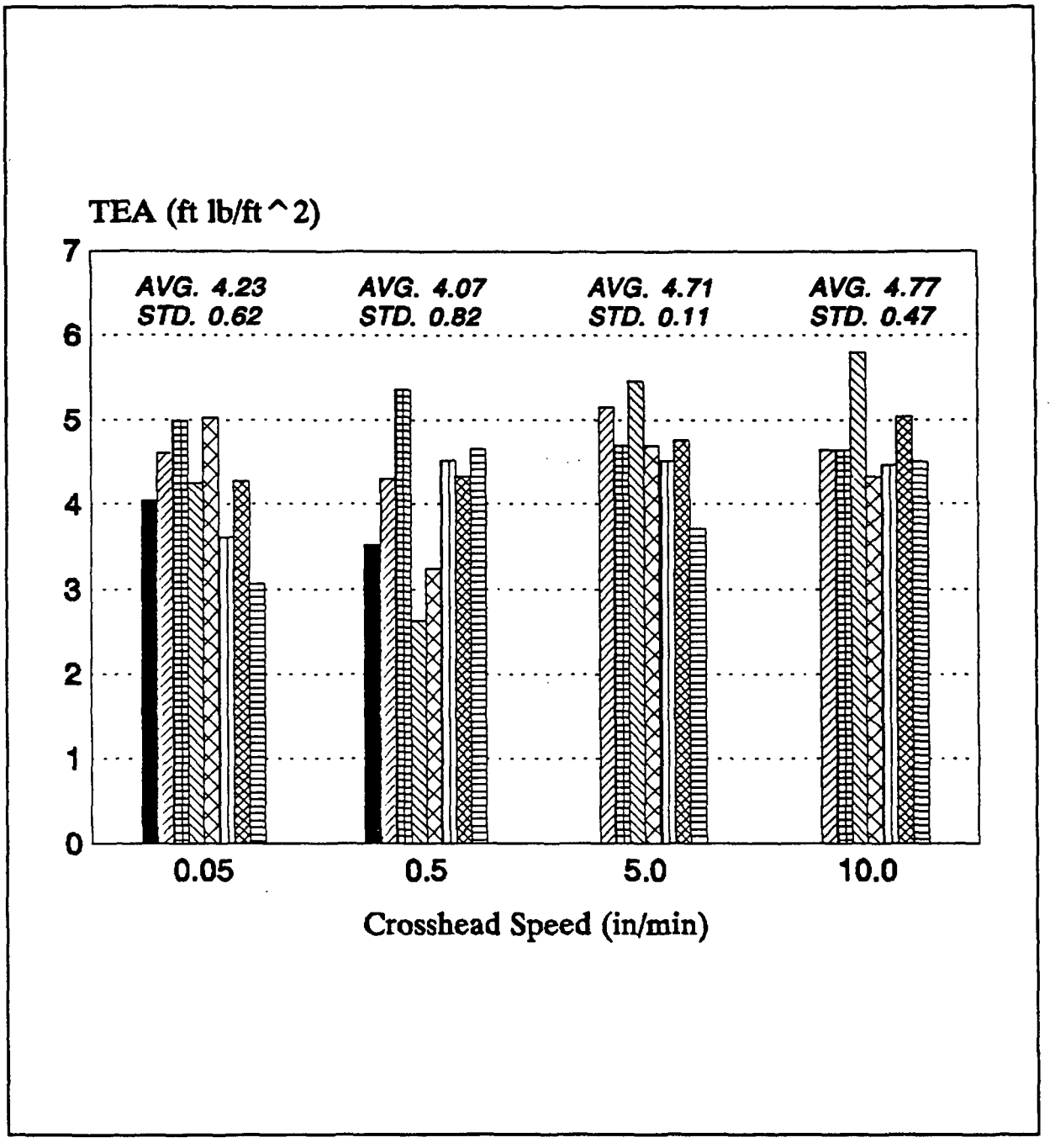

Fig. 11 The effect of crosshead speed on tensile energy absorption (TEA) for green liquor corrugating paper conditioned at 50% RH, and tested in MD under uniaxial tensile loading.

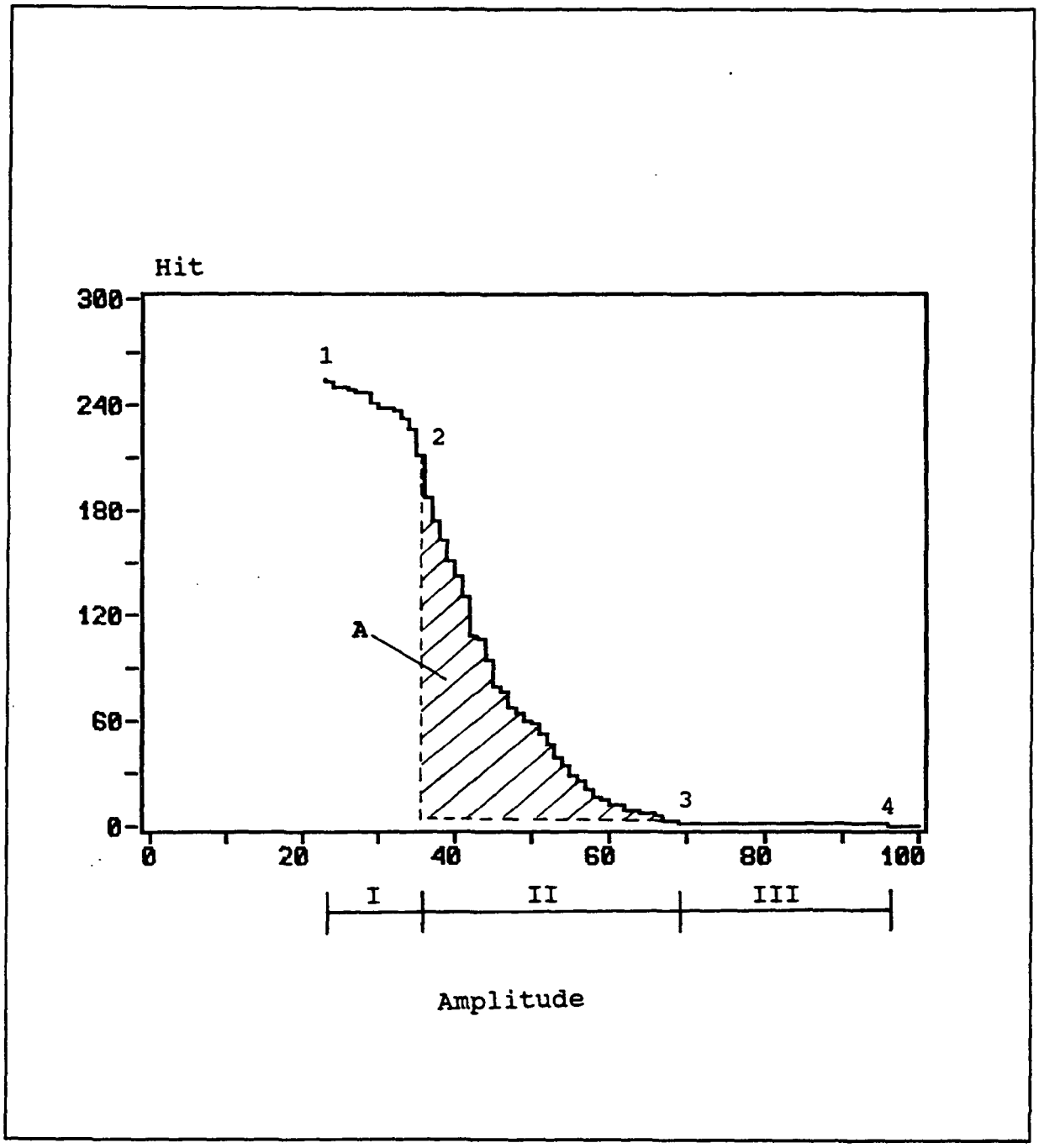

Fig. 12 A typical cumulative distribution plot of hit versus amplitude for green liquor corrugating paper conditioned at 50% RH, and tested in MD under uniaxial tensile loading at crosshead speed of 0.05 in/min.

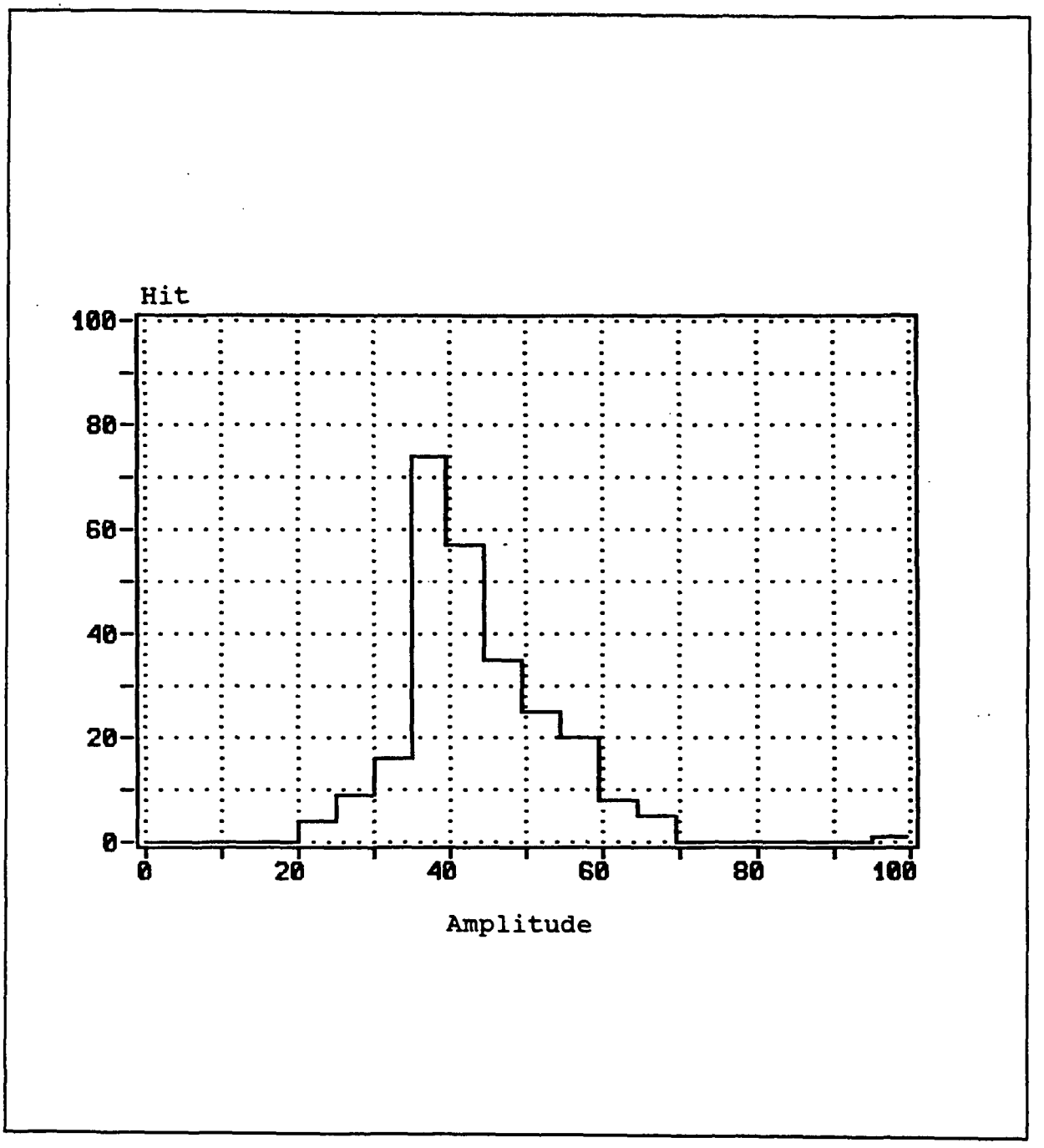

Fig. 13 A typical differential distribution plot of hit versus amplitude for green liquor corrugating paper conditioned at 50% RH, and tested in MD under uniaxial tensile loading at crosshead speed of 0.05 in/min.

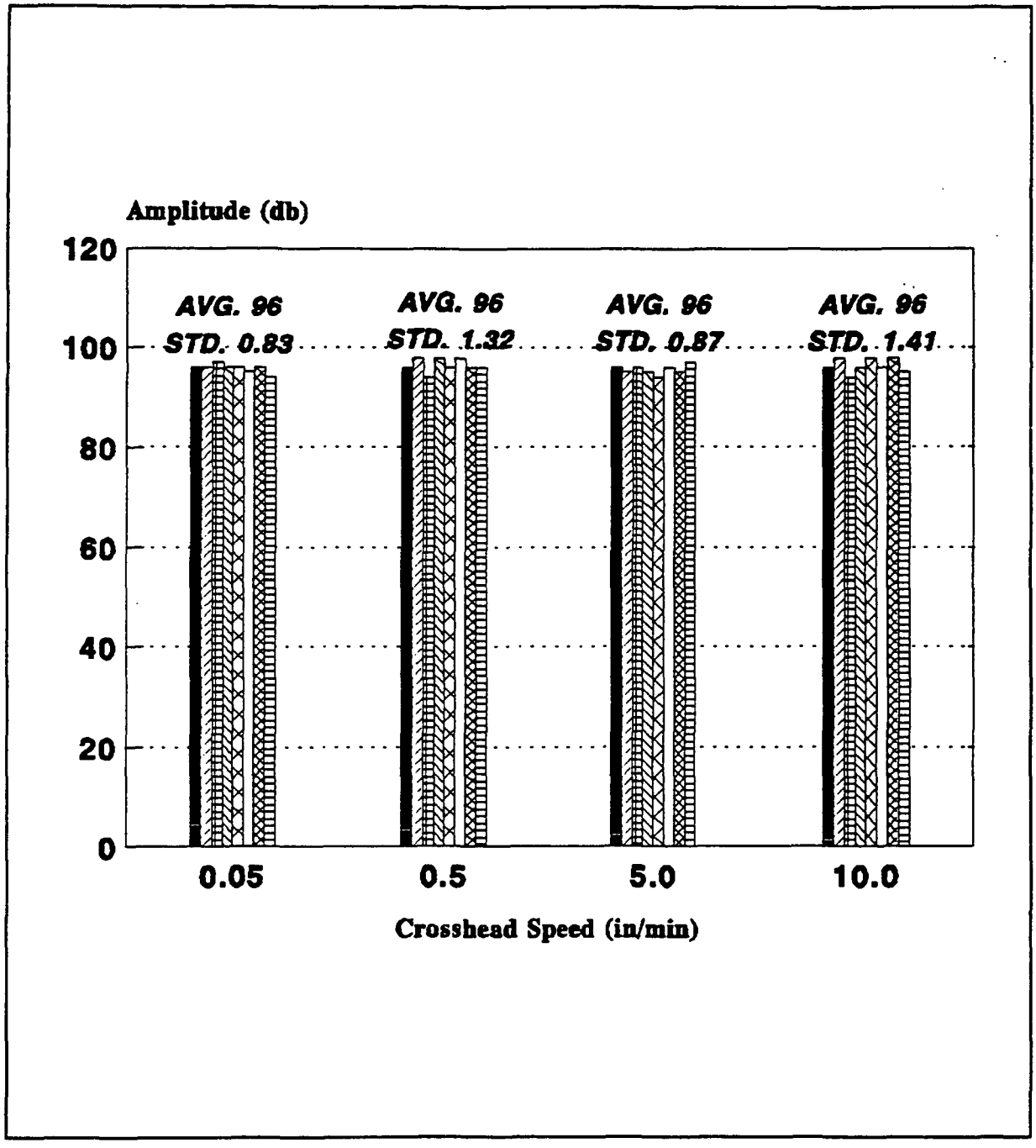

Fig. 14 Summary of the principal hit amplitudes for green liquor corrugating paper conditioned at 50% RH, and tested in MD under uniaxial tensile loading at various crosshead speeds.

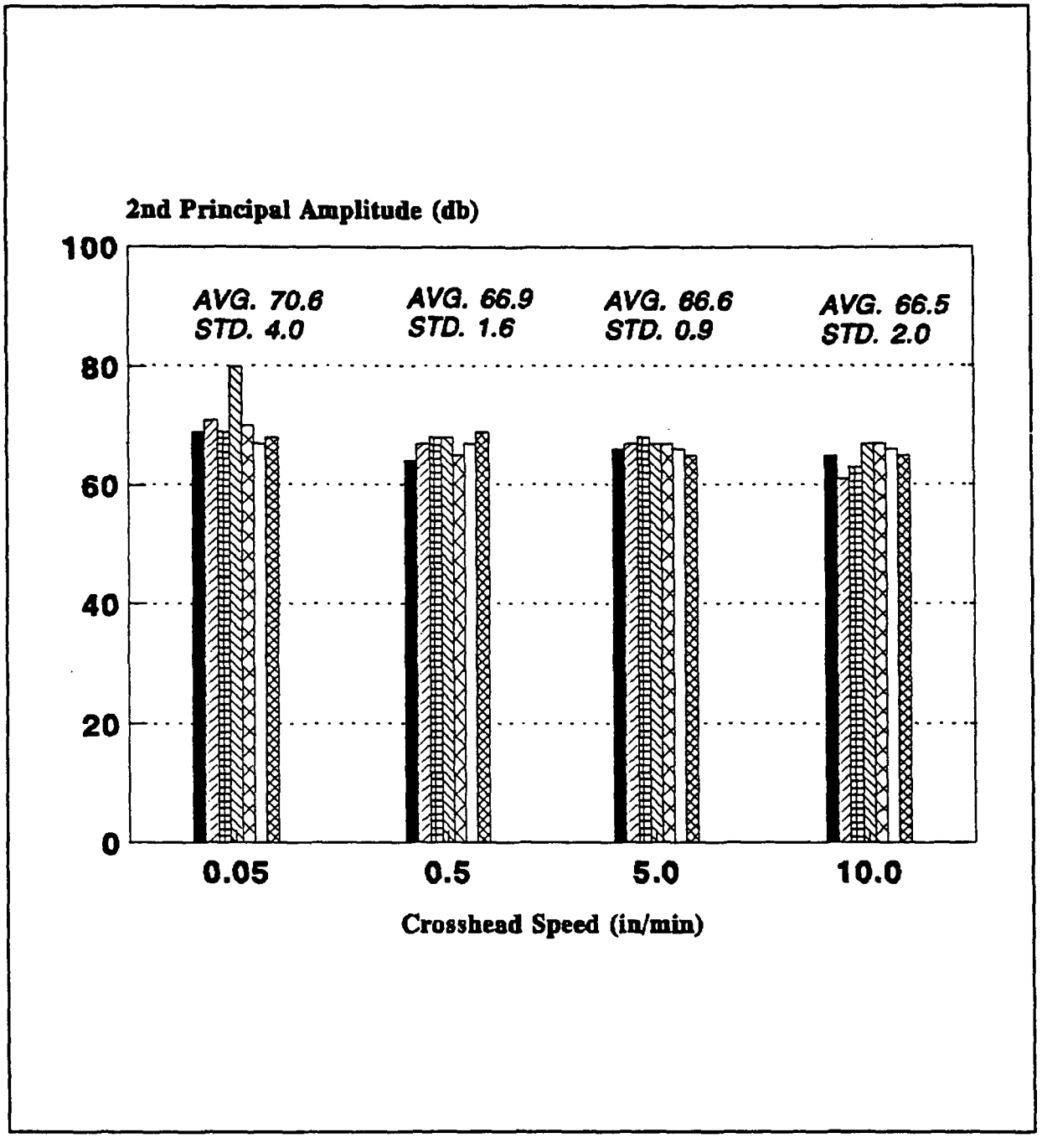

Fig. 15 Amplitude at the second principal hit for green liquor corrugating paper conditioned at 50% RH, and tested in MD under uniaxial tensile loading at various crosshead speeds.

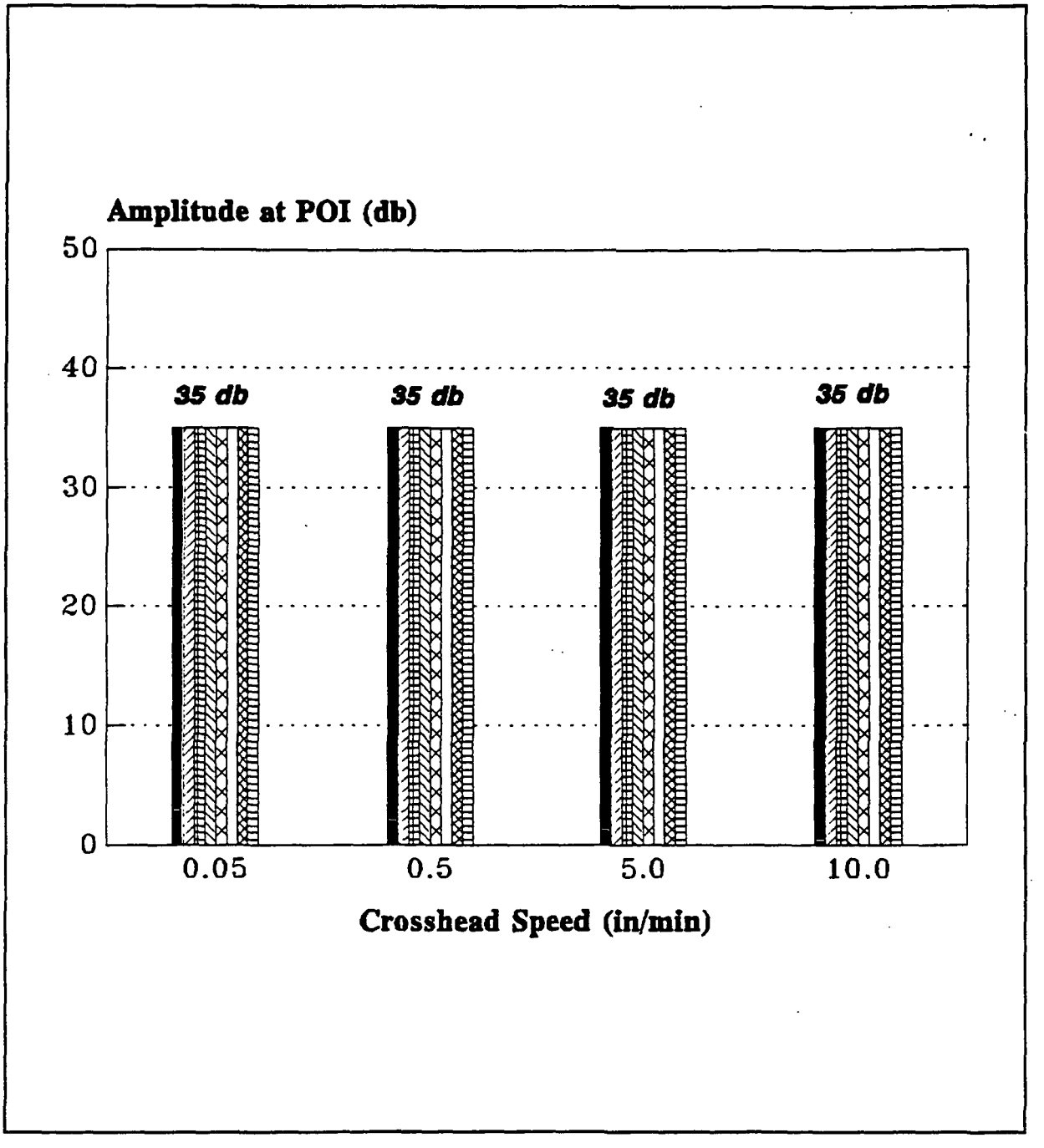

Fig. 16 Amplitude at the point of inflection of the cumulative hit distribution curves for green liquor corrugating paper conditioned at 50% RH, and tested in MD under uniaxial tensile loading at various crosshead speeds.

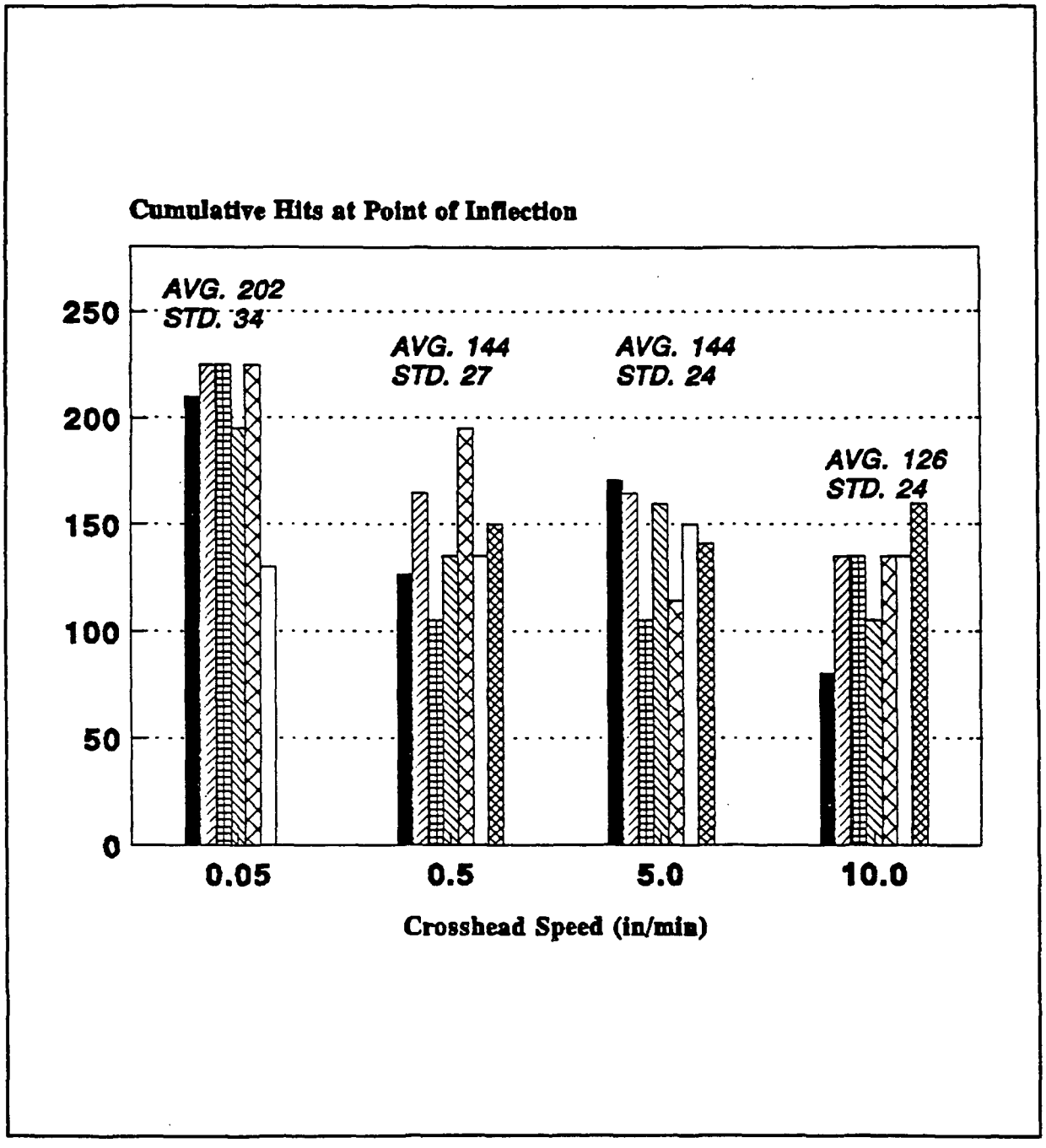

Fig. 17 Ordinate at the point of inflection of the cumulative hit distribution curves for green liquor corrugating paper conditioned at 50% RH, and tested in MD under uniaxial tensile loading at various crosshead speeds.

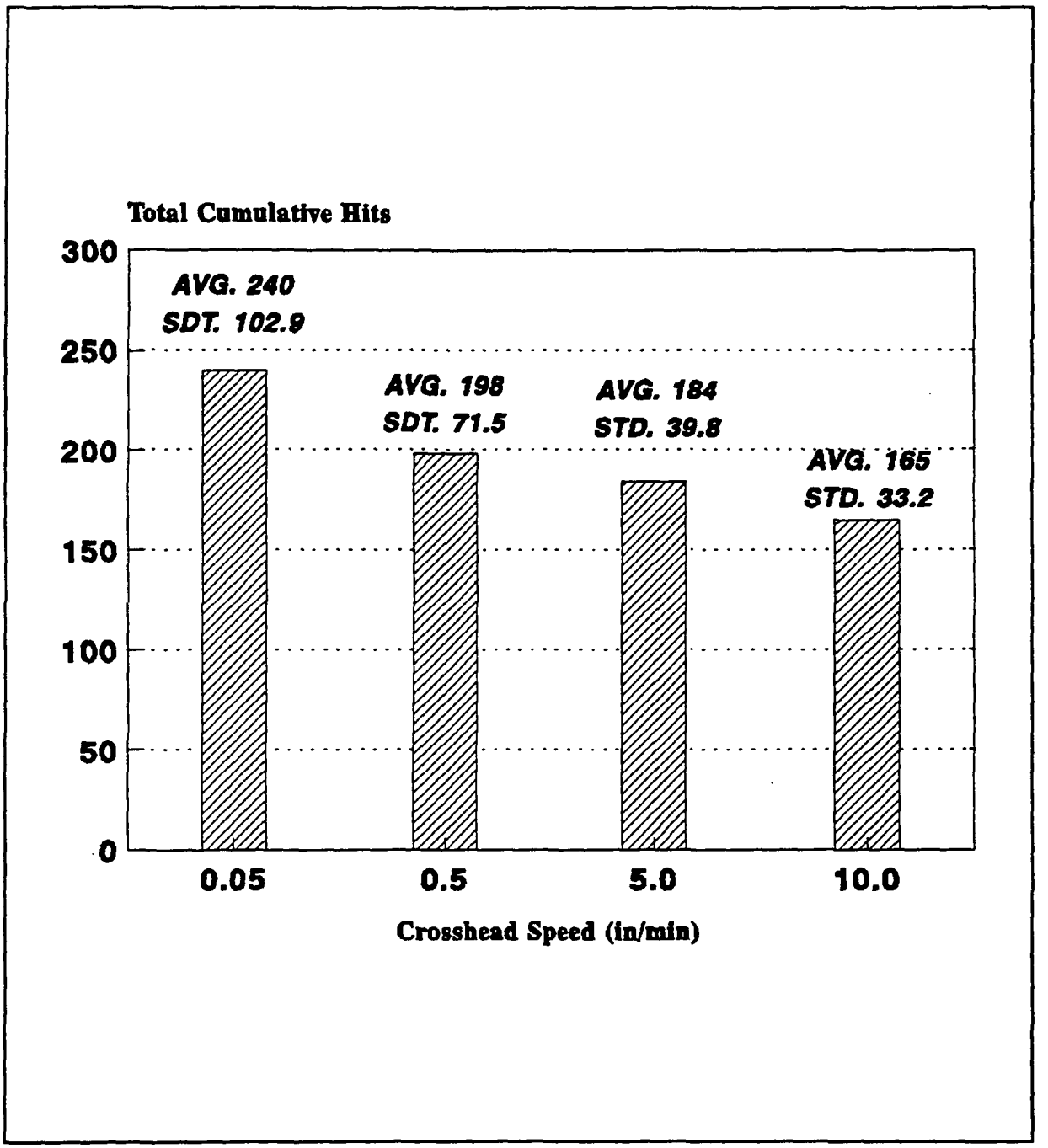

Fig. 18 The effect of crosshead speed on total cumulative hits for green liquor corrugating paper conditioned at 50% RH, and tested in MD under uniaxial tensile loading.

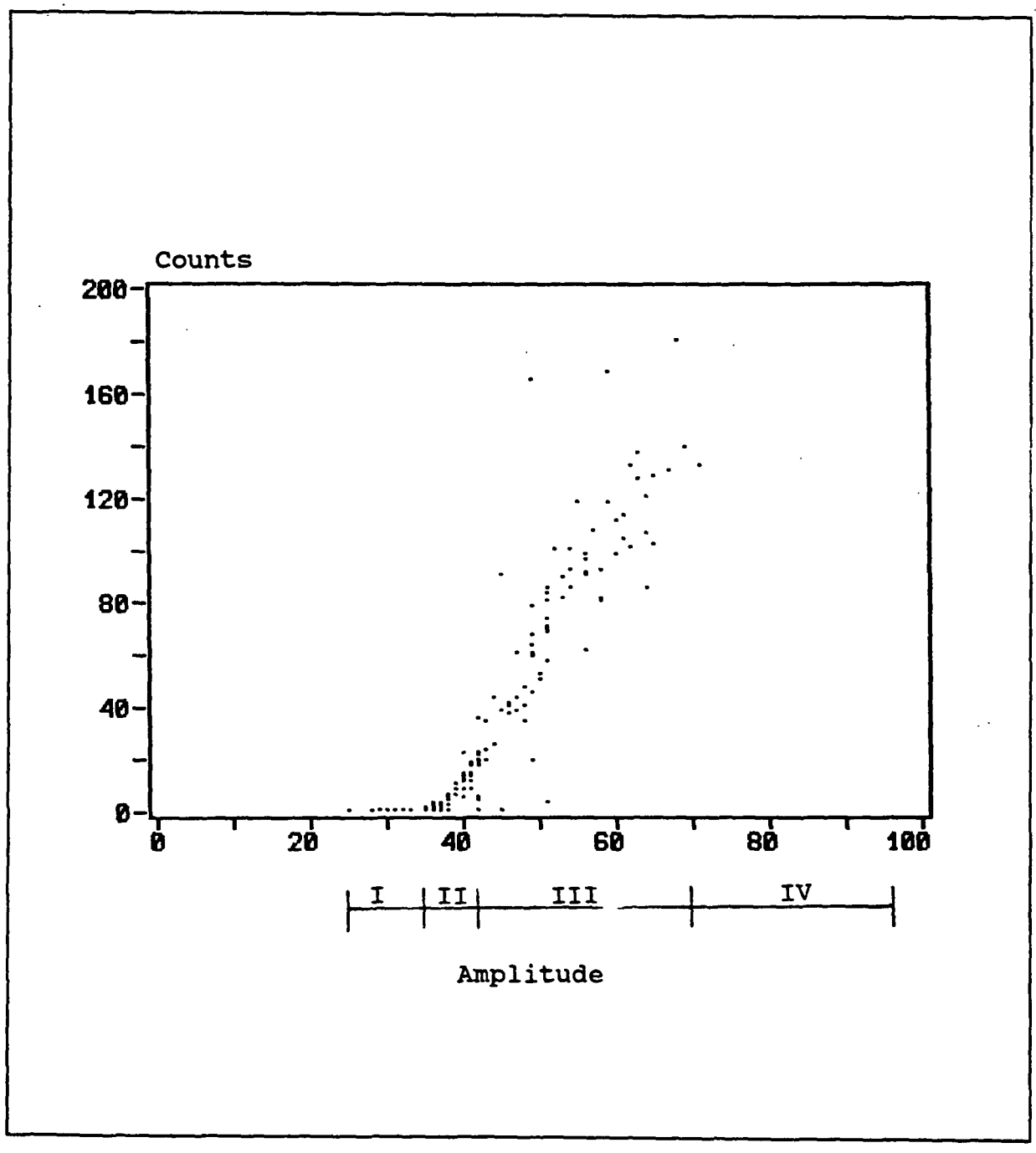

Fig 19 A typical point plot of count versus amplitude for green liquor corrugating paper conditioned at 50% RH, and tested in MD under uniaxial tensile loading at crosshead speed of 0.05 in/min.

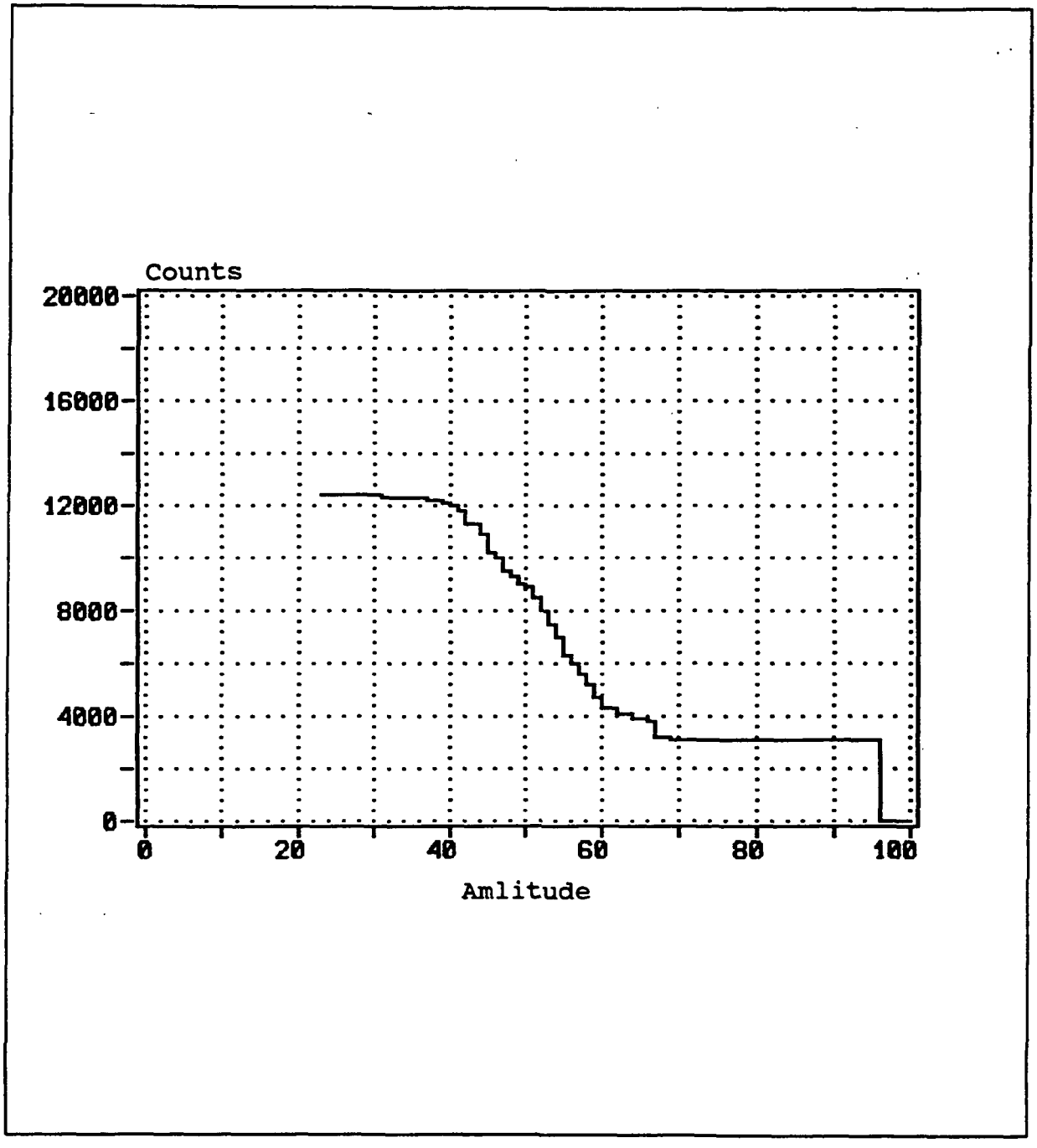

Fig. 20 A typical cumulative distribution plot of counts versus amplitude for green liquor corrugating paper conditioned at 50% RH, and tested in MD under uniaxial tensile loading at crosshead speed of 0.05 in/min.

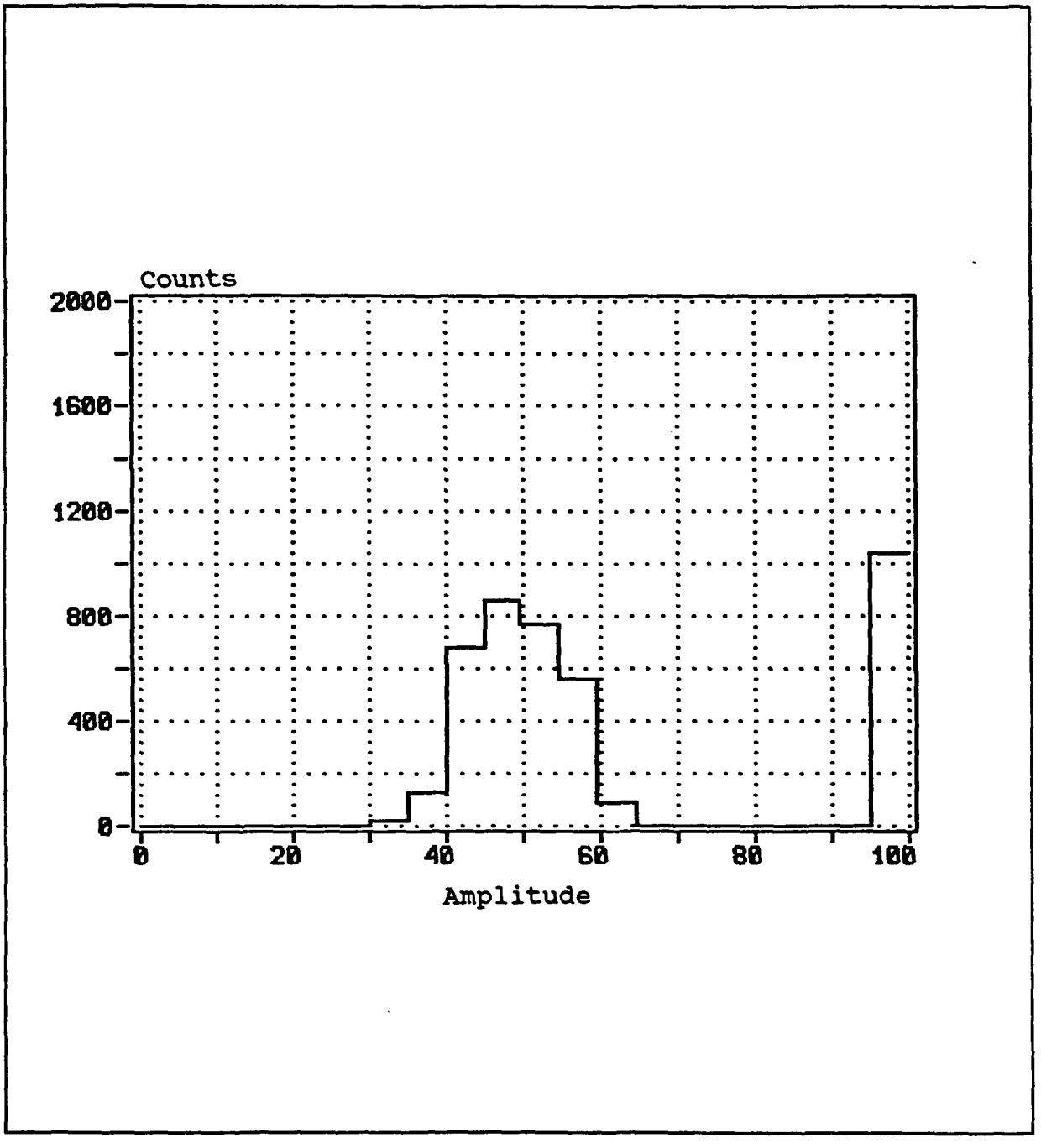

Fig. 21 A typical differential distribution plot of counts versus amplitude for green liquor corrugating paper conditioned at 50% RH, and tested in MD under uniaxial tensile loading at crosshead speed of 0.05 in/min.

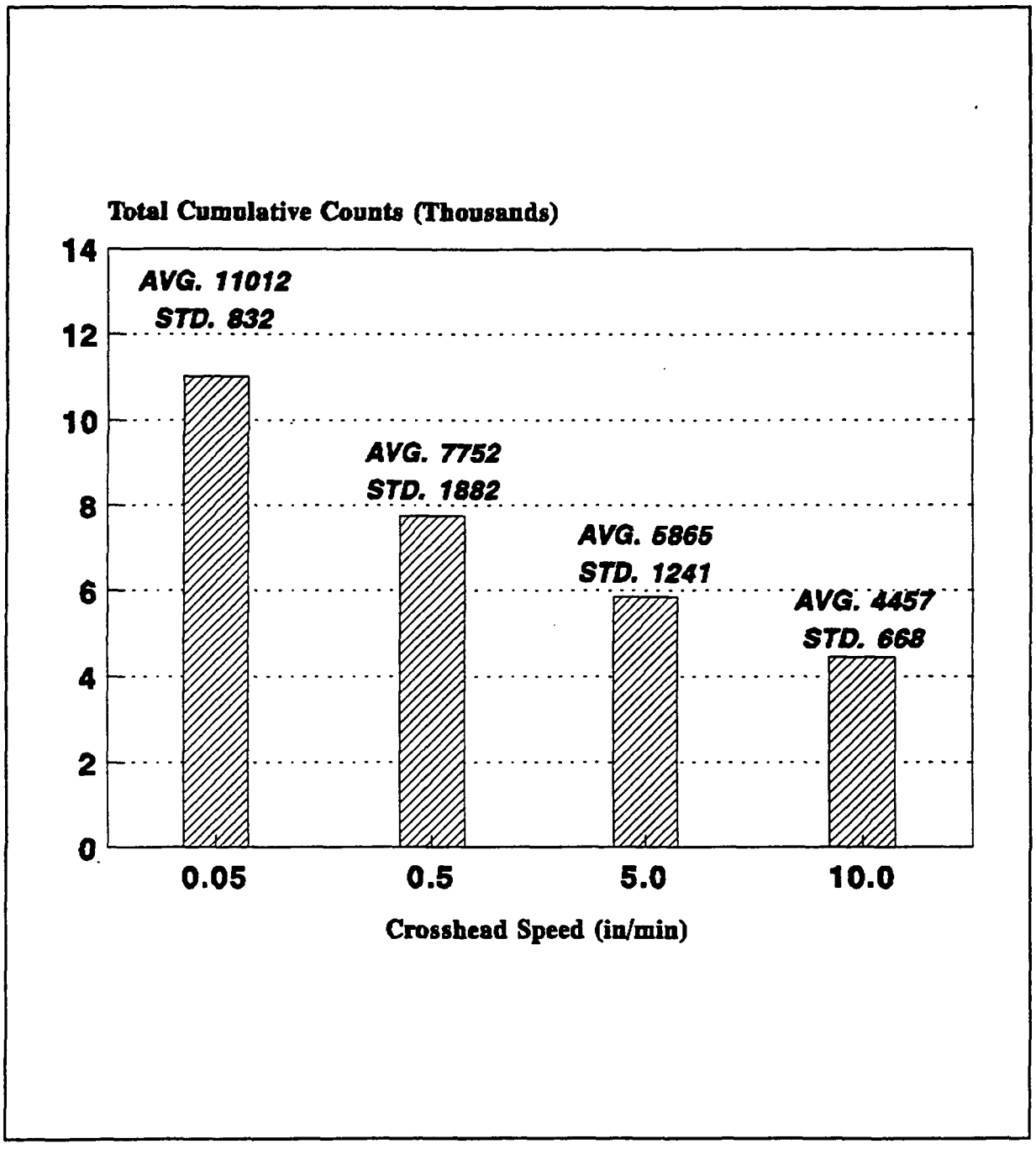

Fig. 22 The effect of crosshead speed on total cumulative counts for green liquor corrugating paper conditioned at 50% RH, and tested in MD under uniaxial tensile loading.

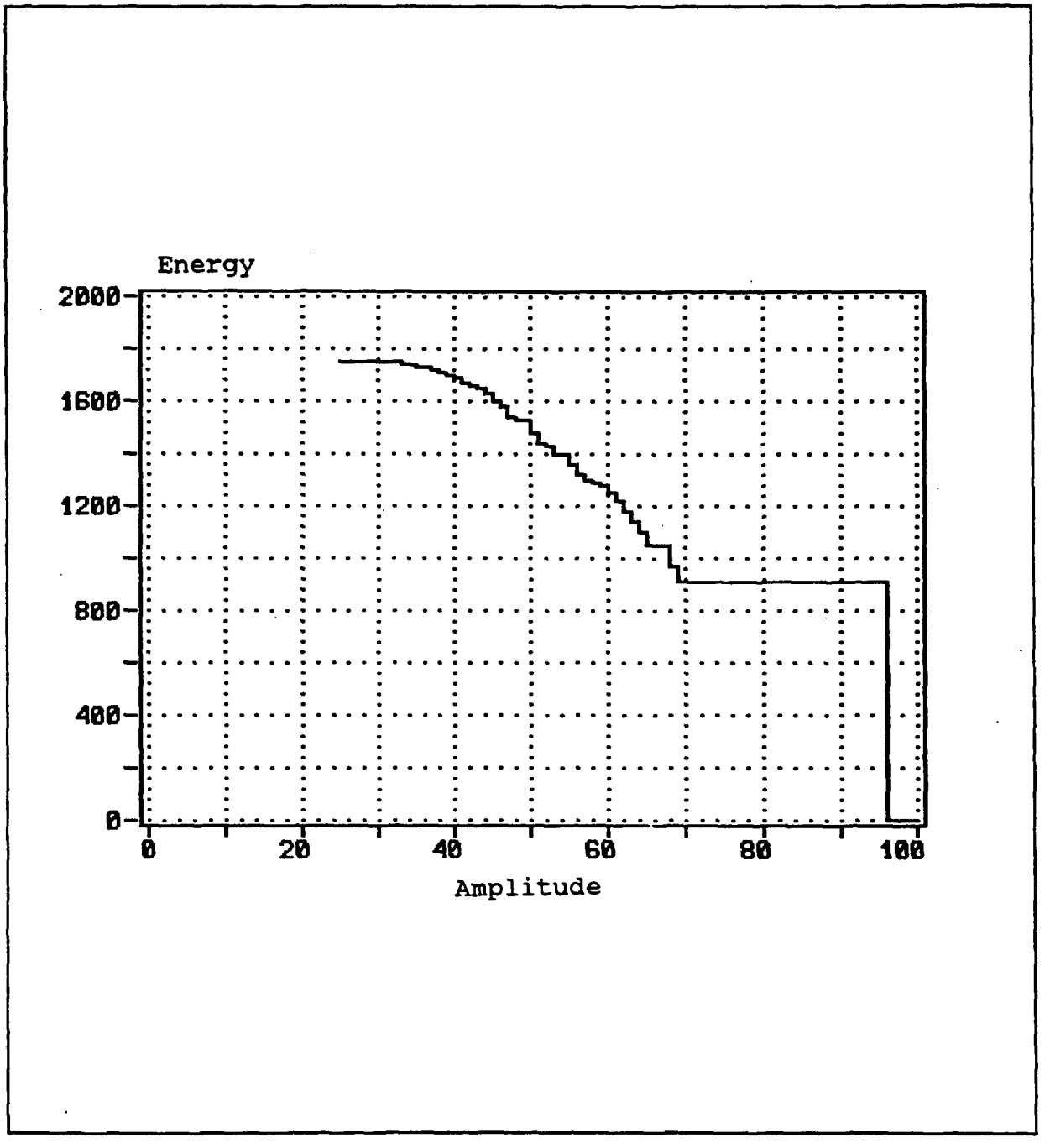

Fig. 23 A typical cumulative distribution plot of energy versus amplitude for green liquor corrugating paper conditioned at 50% RH, and tested in MD under uniaxial tensile loading at crosshead speed of 0.05 in/min.

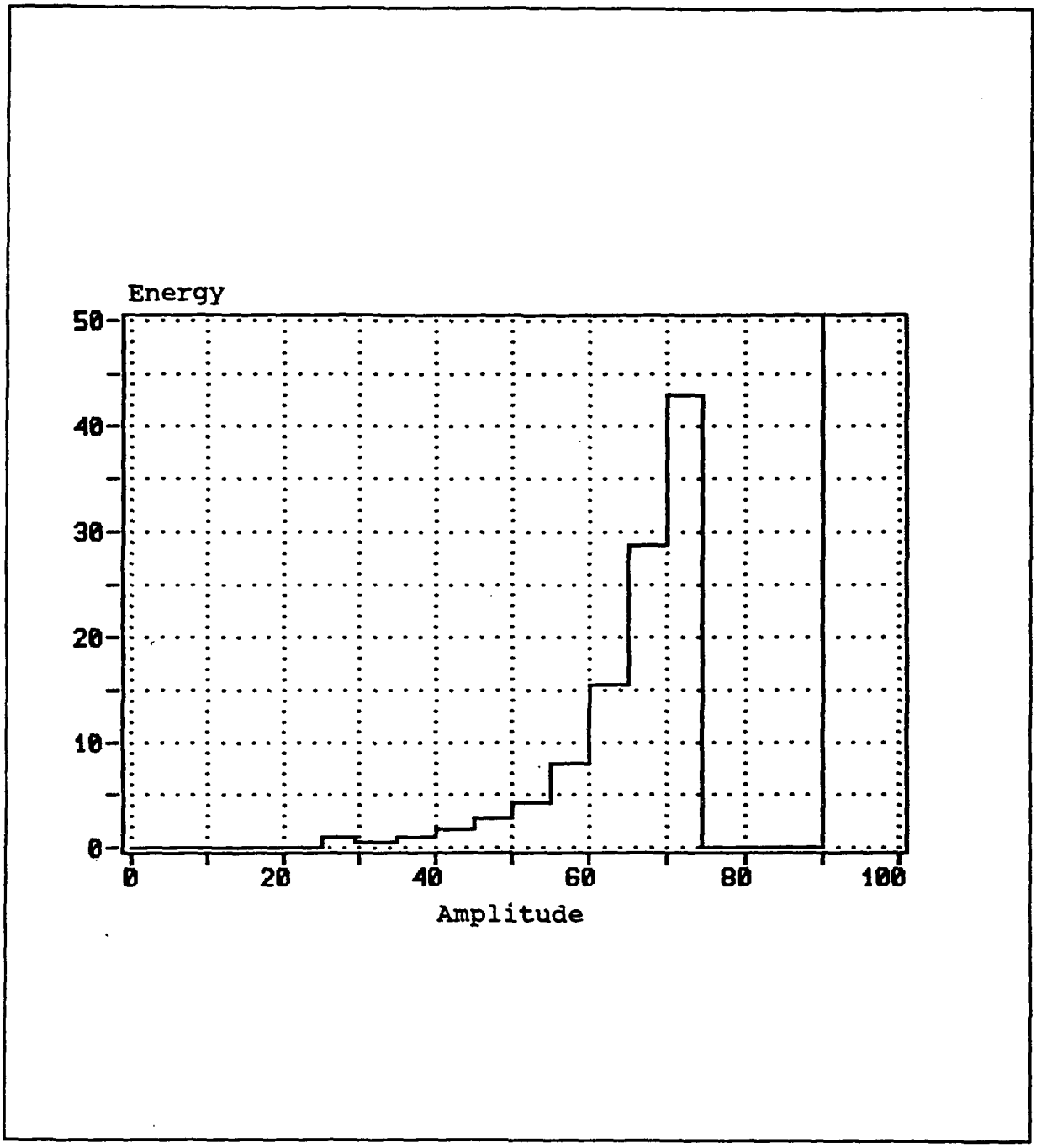

Fig. 24 A typical histogram plot of energy versus amplitude for green liquor corrugating paper conditioned at 50% RH, and tested in MD under uniaxial tensile loading at crosshead speed of 0.05 in/min.

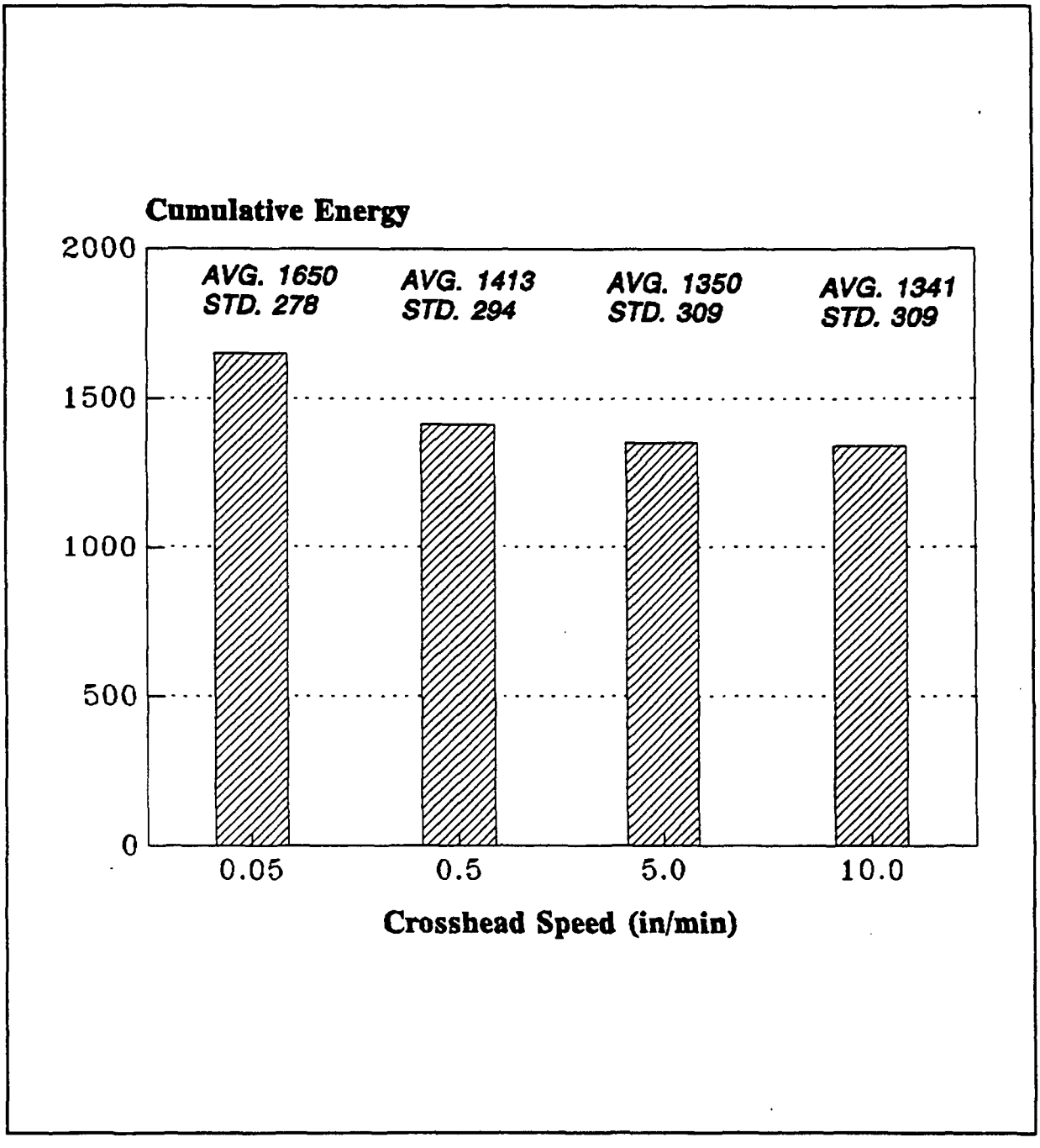

Fig. 25 The effect of crosshead speed on total cumulative energy for green liquor corrugating paper conditioned at 50% RH, and tested in MD under uniaxial tensile loading.

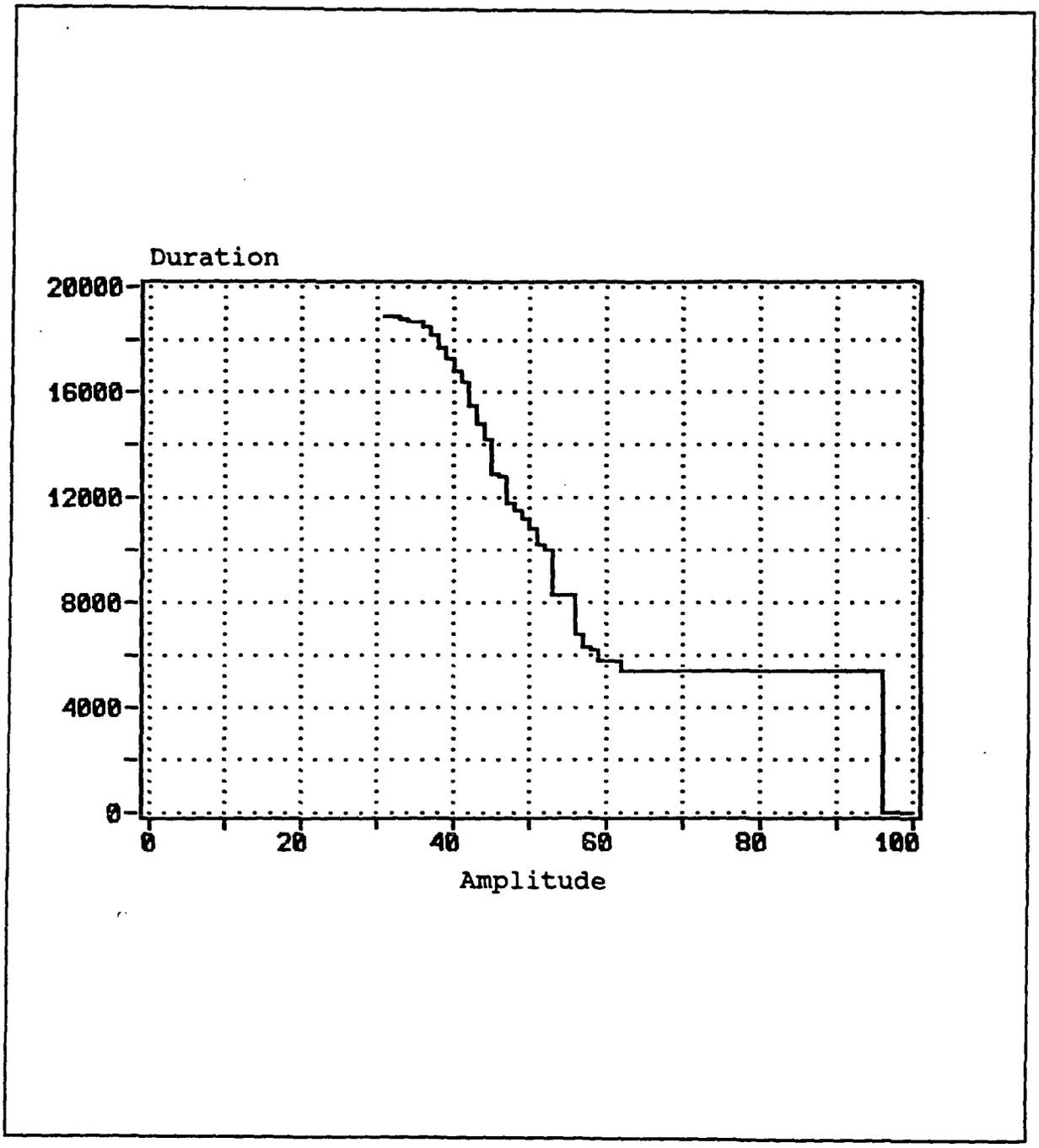

Fig. 26 A typical cumulative distribution plot of duration versus amplitude for green liquor corrugating paper conditioned at 50% RH, and tested in MD under uniaxial tensile loading at crosshead speed of 0.05 in/min.

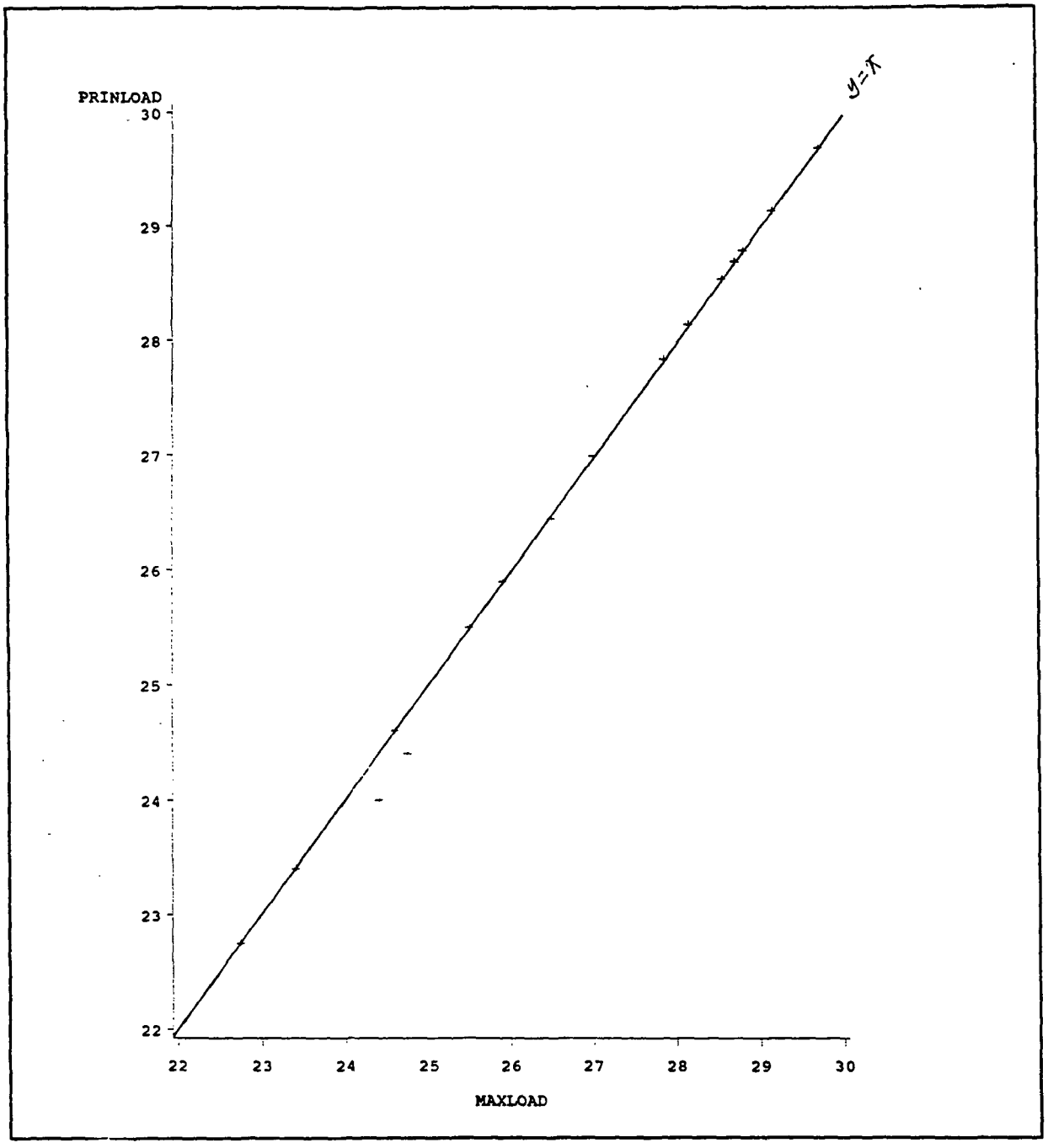

Fig. 27 Correlation between the principal hit load and the maximum failure load. Experiments conducted on green liquor corrugating paper conditioned at 50% RH, and tested in MD under uniaxial tensile loading at crosshead speed of 0.05 in/min.

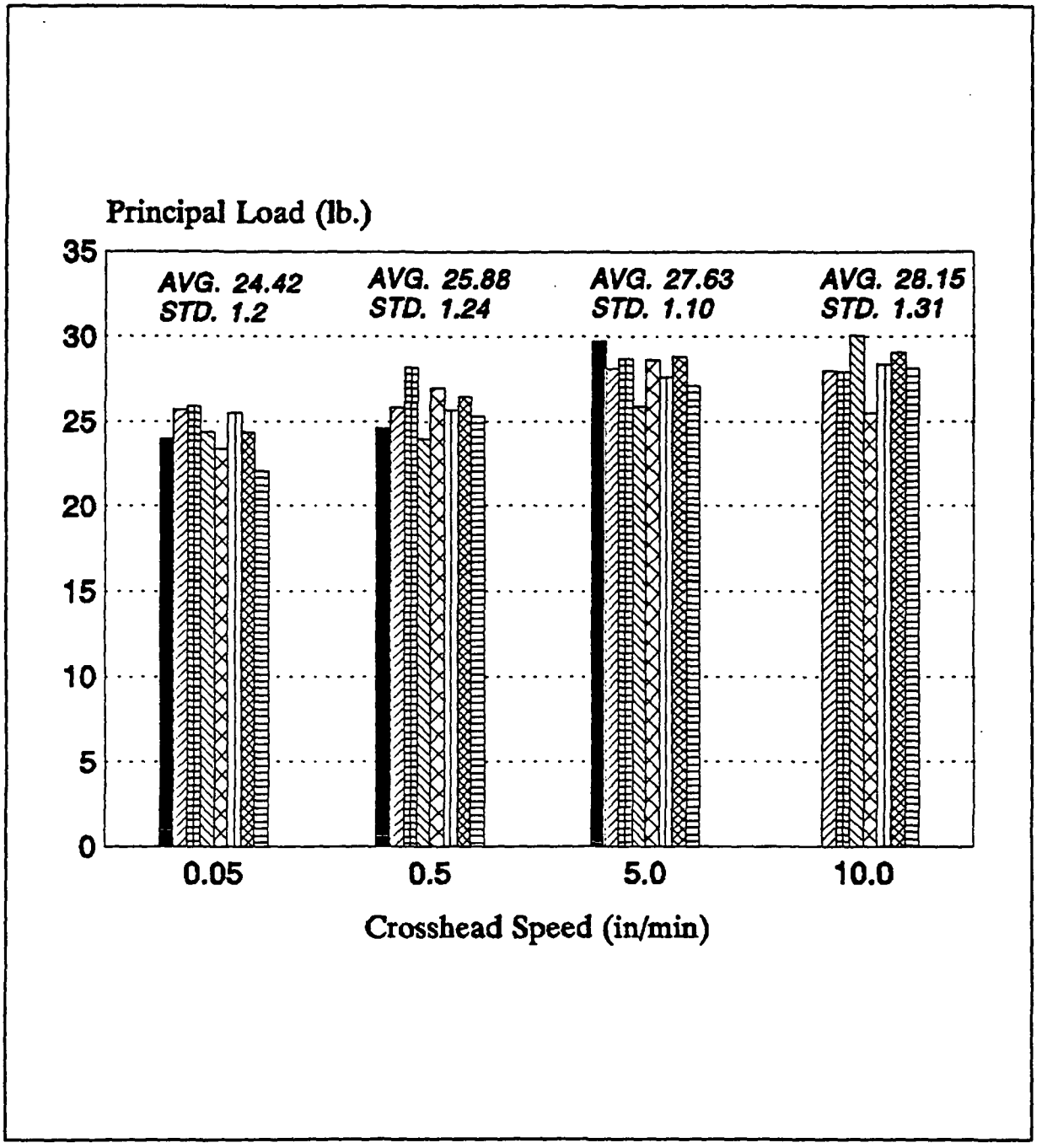

Fig. 28 The effect of crosshead speed on the principal hit load for green liquor corrugating paper conditioned at 50% RH, and tested in MD under uniaxial tensile loading.

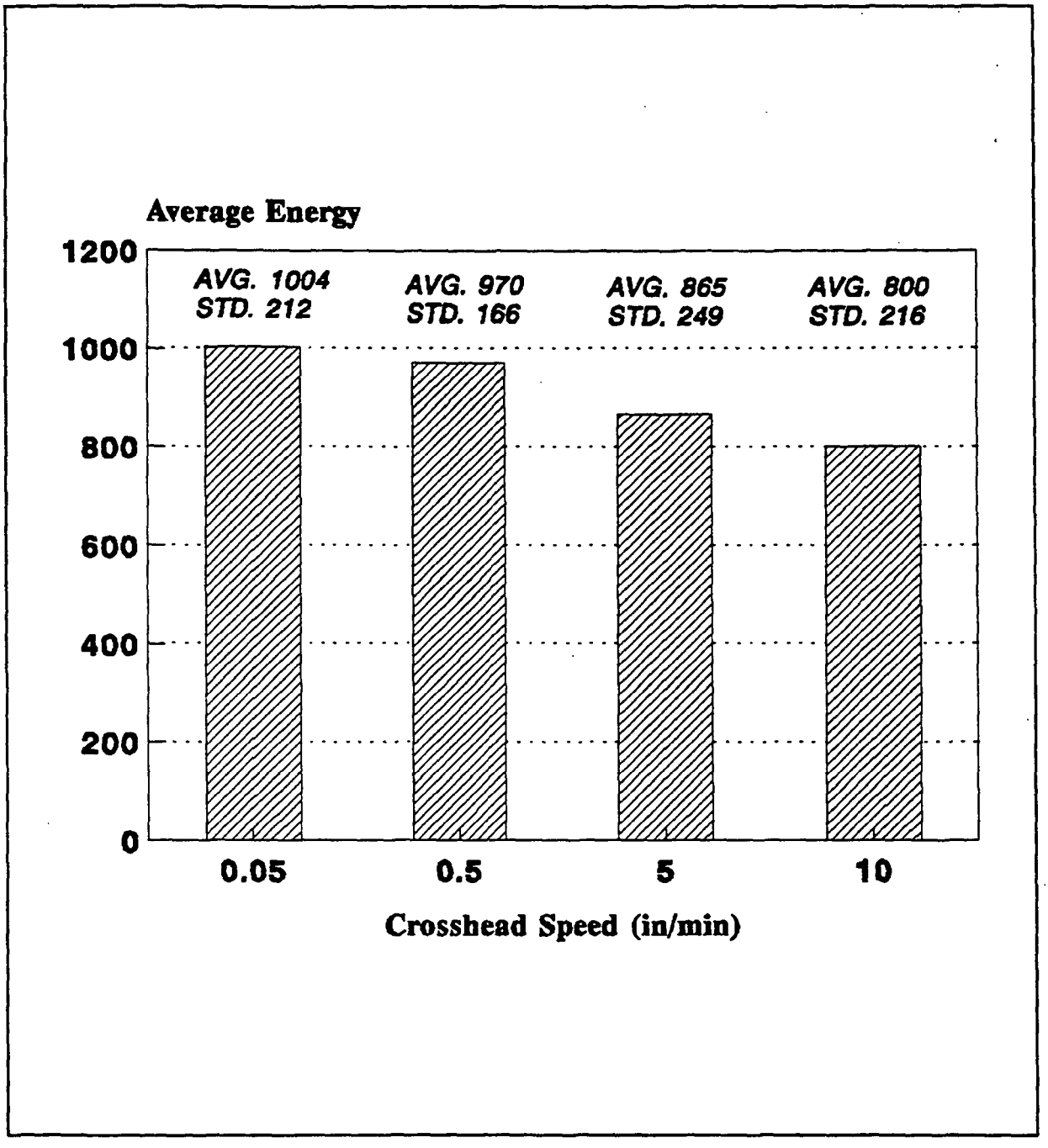

Fig. 29 The effect of crosshead speed on the principal energy for green liquor corrugating paper conditioned at 50% RH, and tested in MD under uniaxial tensile loading.

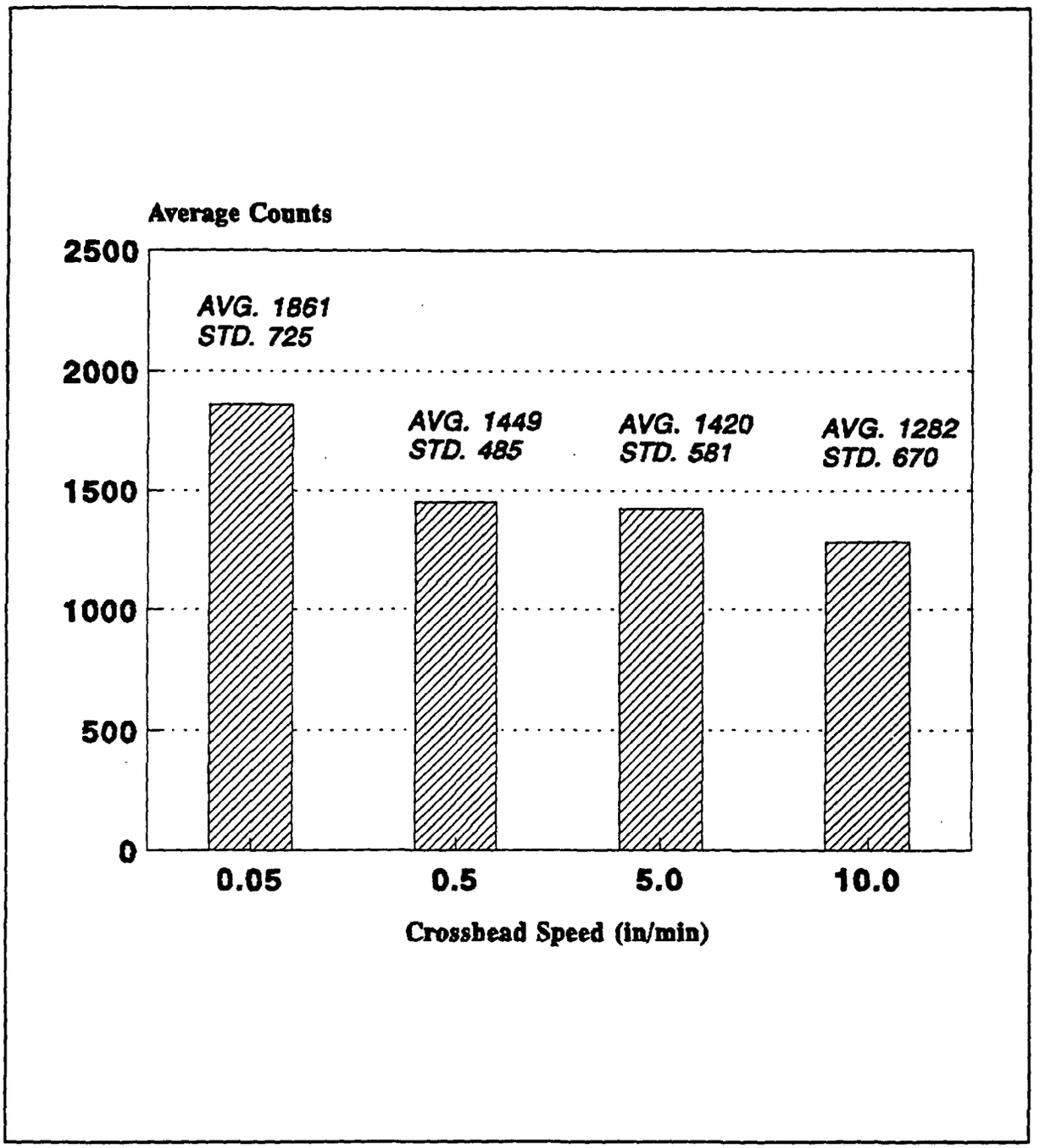

Fig. 30 The effect of crosshead speed on the principal counts for green liquor corrugating paper conditioned at 50% RH, and tested in MD under uniaxial tensile loading.

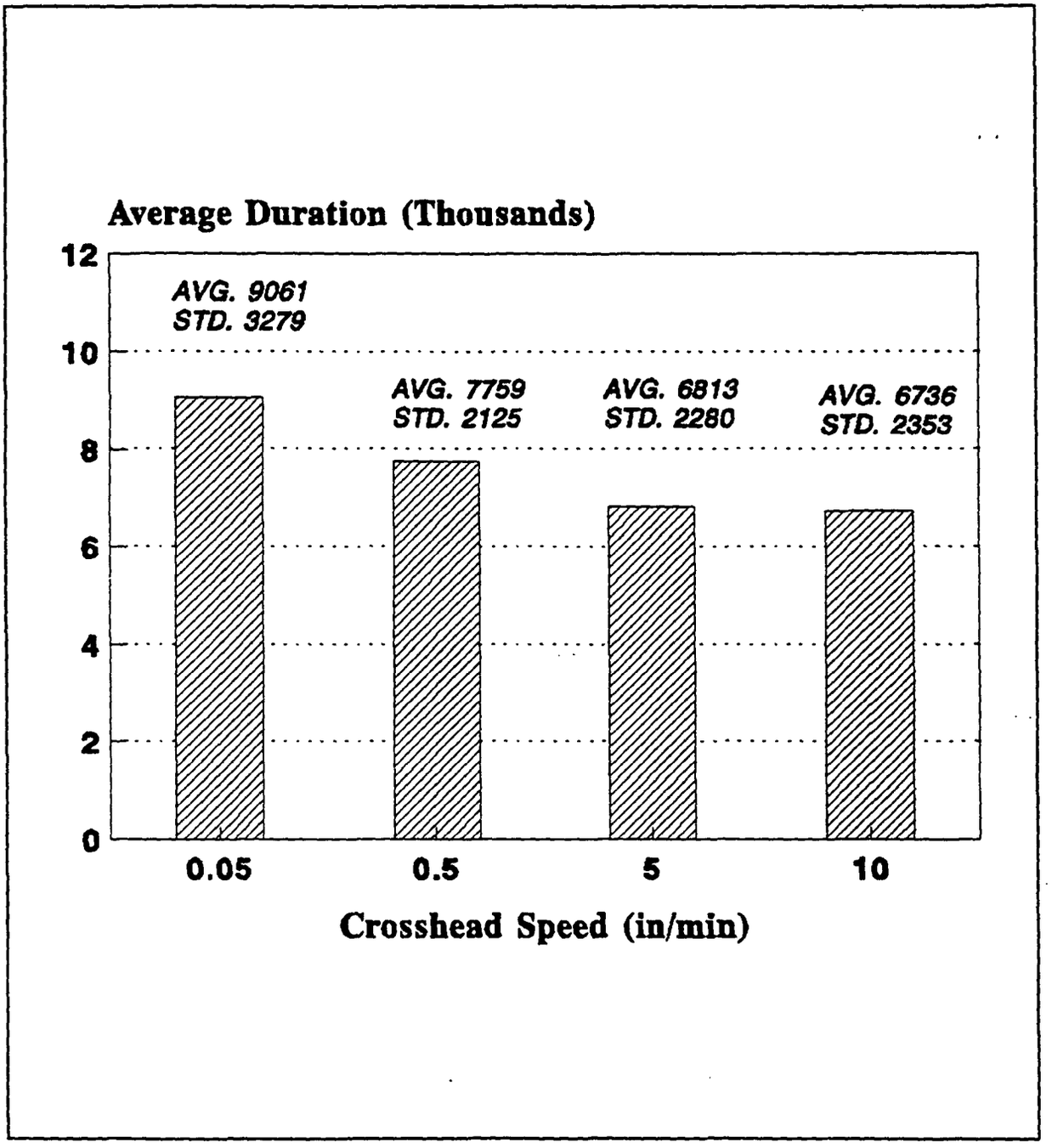

Fig. 31 The effect of crosshead speed on the principal duration for green liquor corrugating paper conditioned at 50% RH, and tested in MD under uniaxial tensile loading.

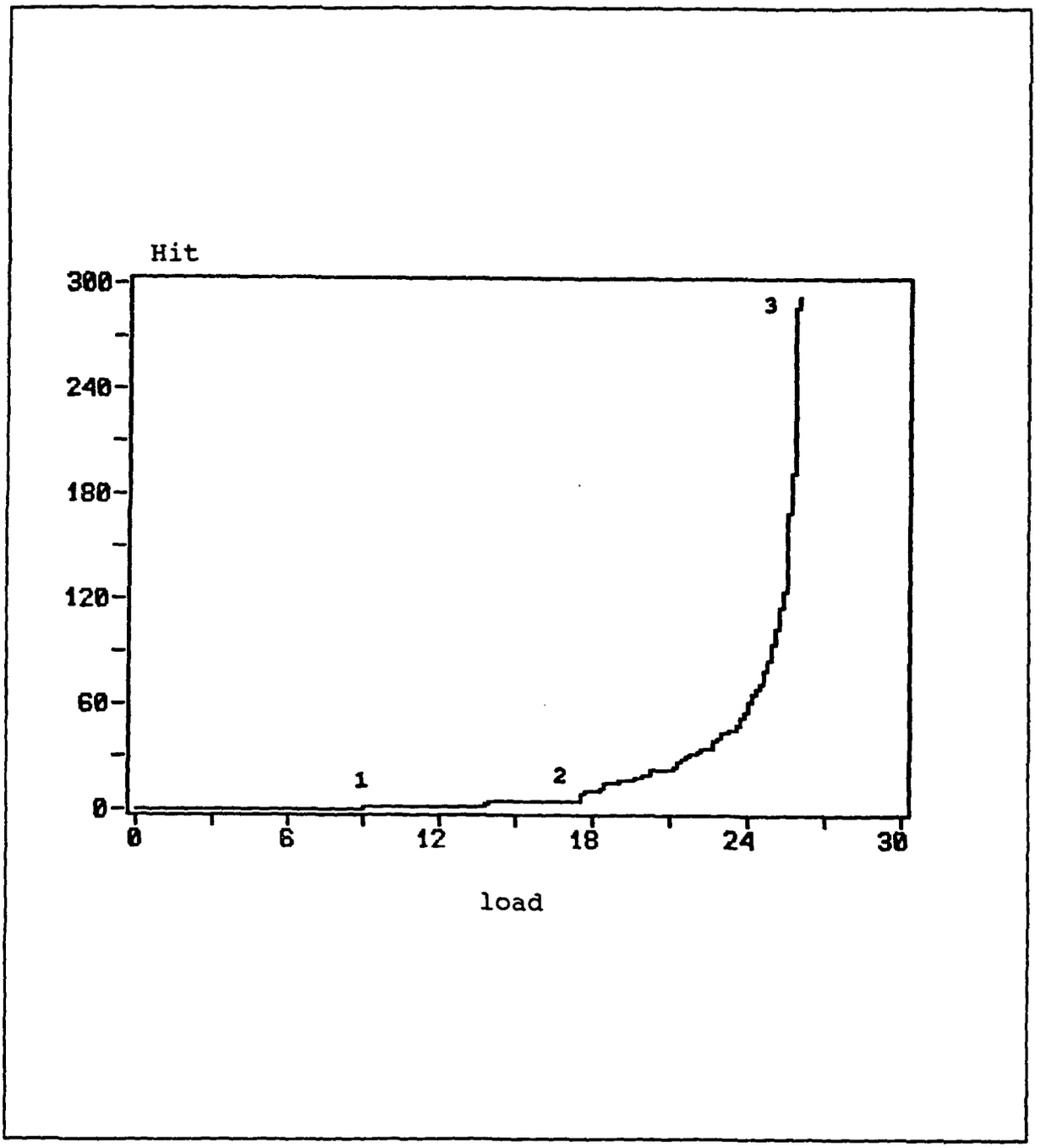

Fig. 32 A typical min-max cumulative load history plot of hit for green liquor corrugating paper conditioned at 50% RH, and tested in MD under uniaxial tensile loading at crosshead speed of 0.05 in/min. 2/3 of the samples exhibited this behavior.

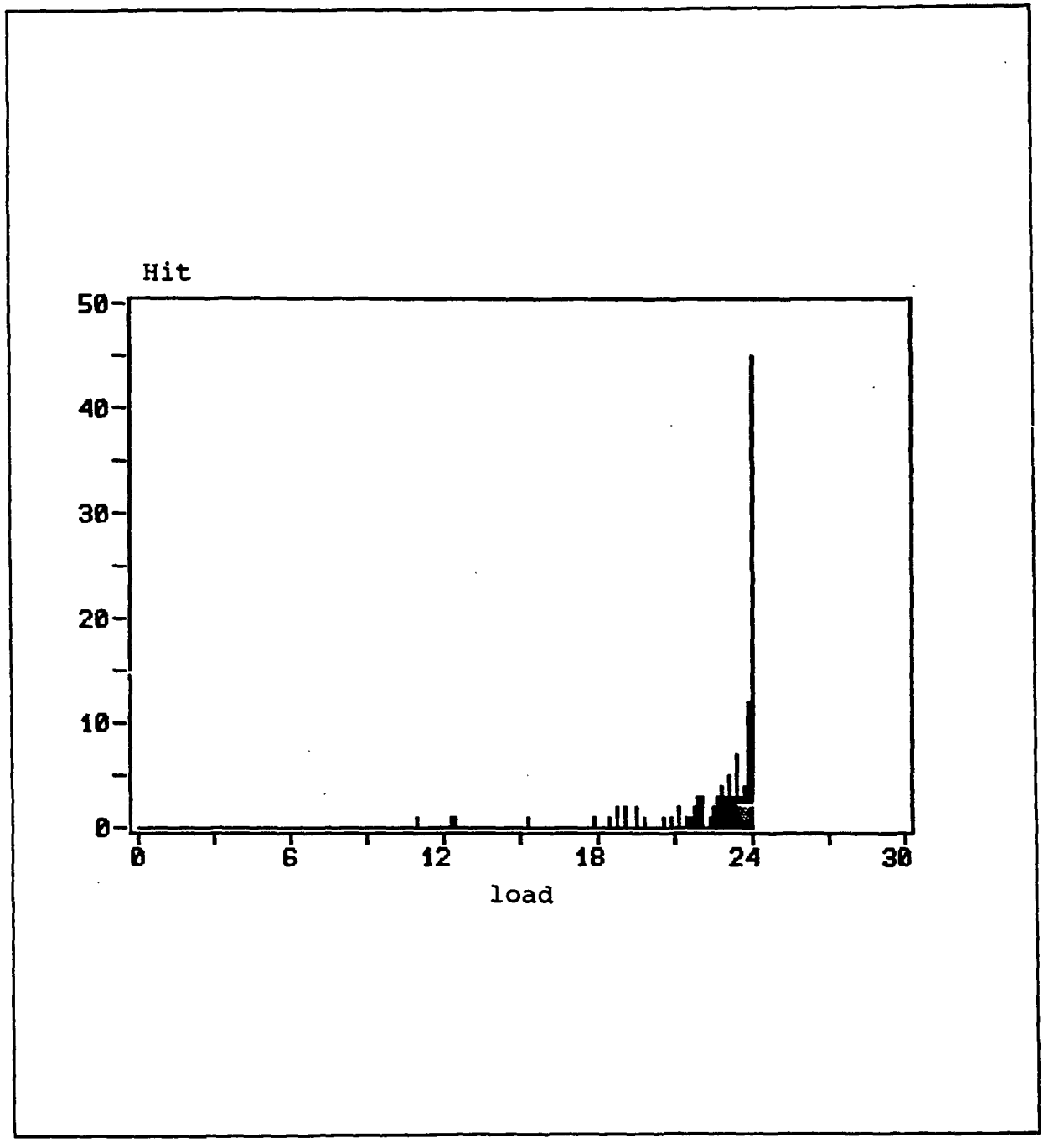

Fig. 33 A typical differential load history plot of hit for green liquor corrugating paper conditioned at 50% RH, and tested in MD under uniaxial tensile loading at crosshead speed of 0.05 in/min.

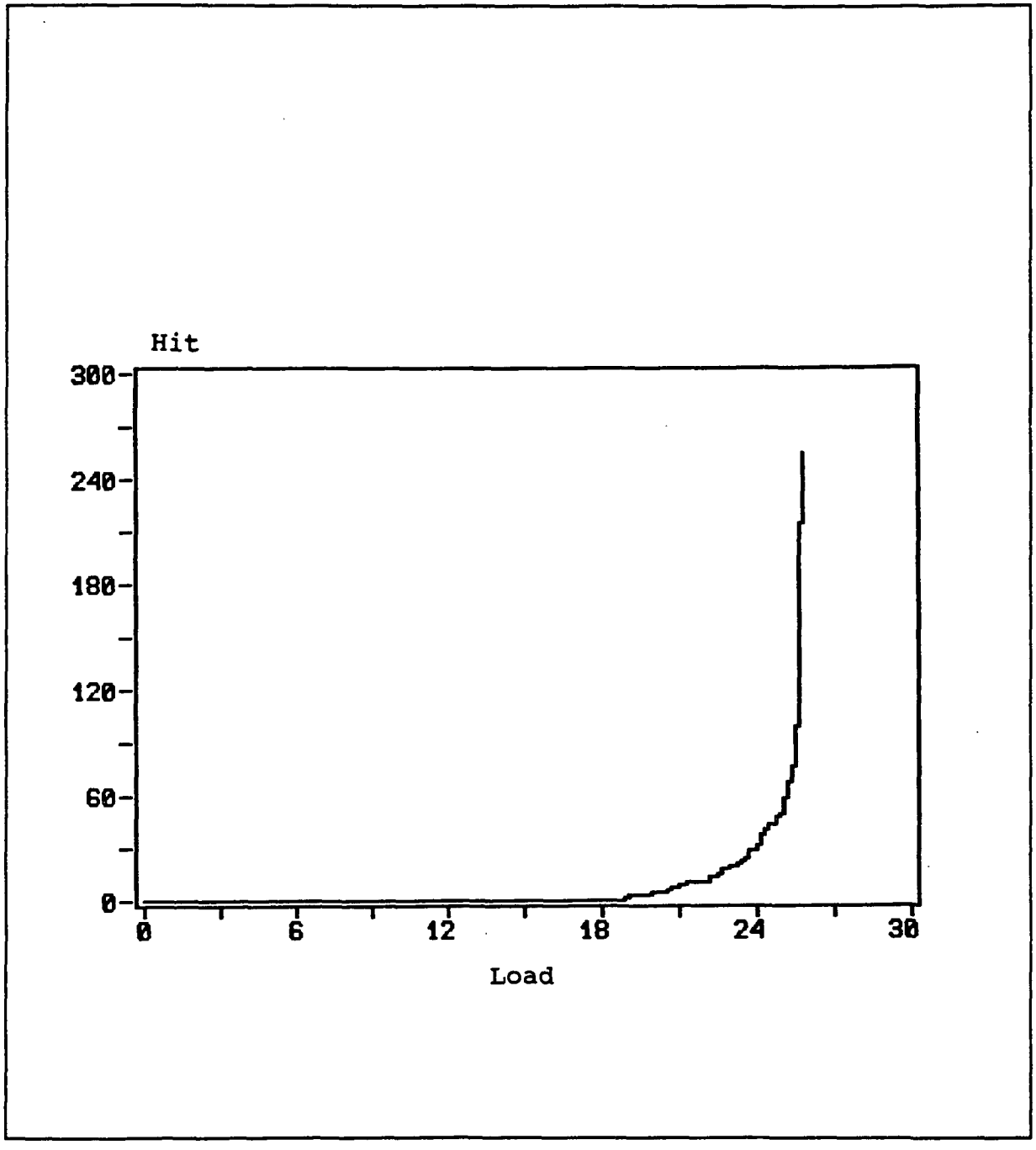

Fig. 34 A typical min-max cumulative load history plot of hit for green liquor corrugating paper conditioned at 50% RH, and tested in MD under uniaxial tensile loading at crosshead speed of 0.05 in/min. 1/3 of the samples exhibited this behavior.

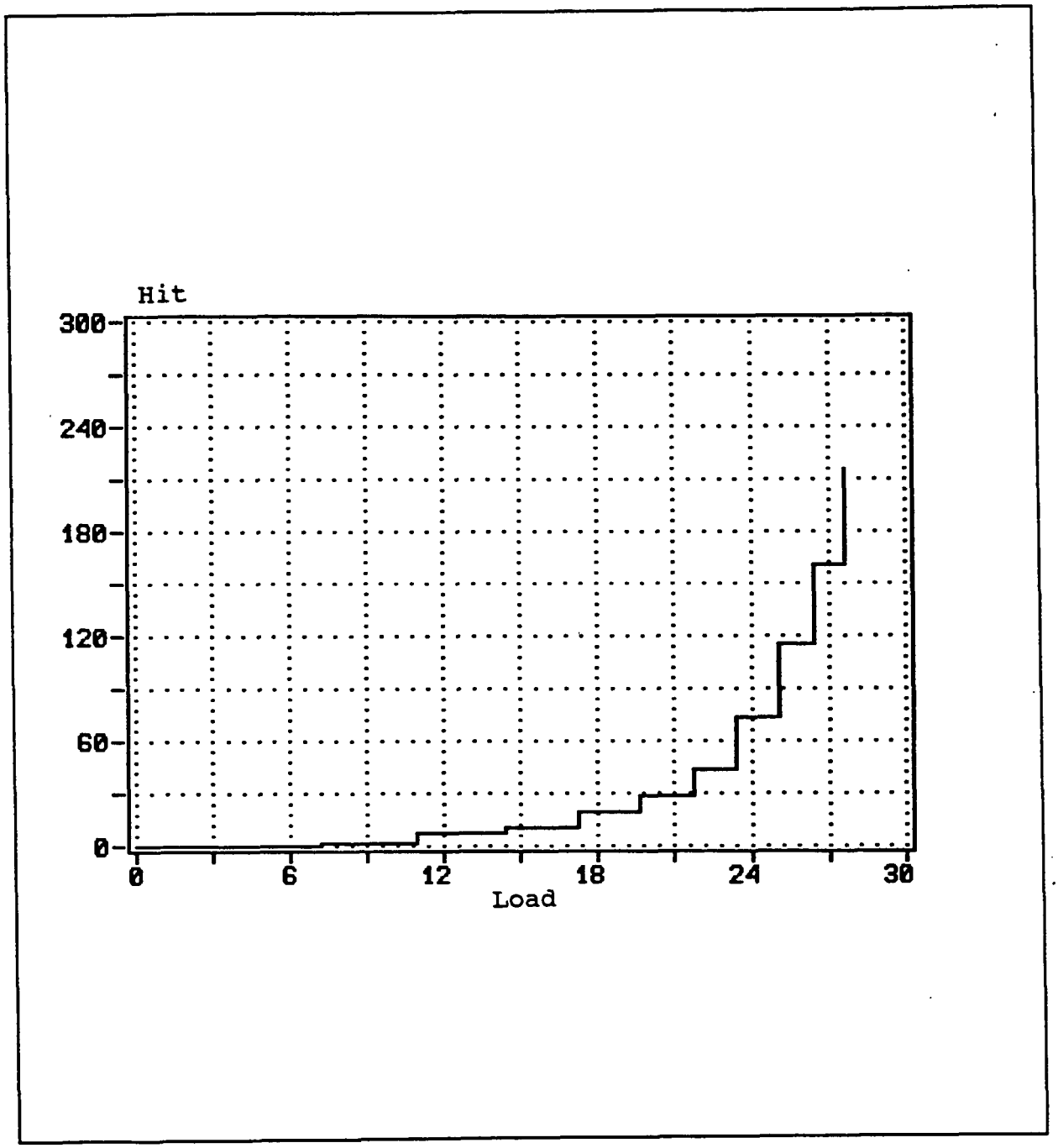

Fig. 35 A typical min-max cumulative load history plot of hit for green liquor corrugating paper conditioned at 50% RH, and tested in MD under uniaxial tensile loading at crosshead speed of 5.0 in/min.

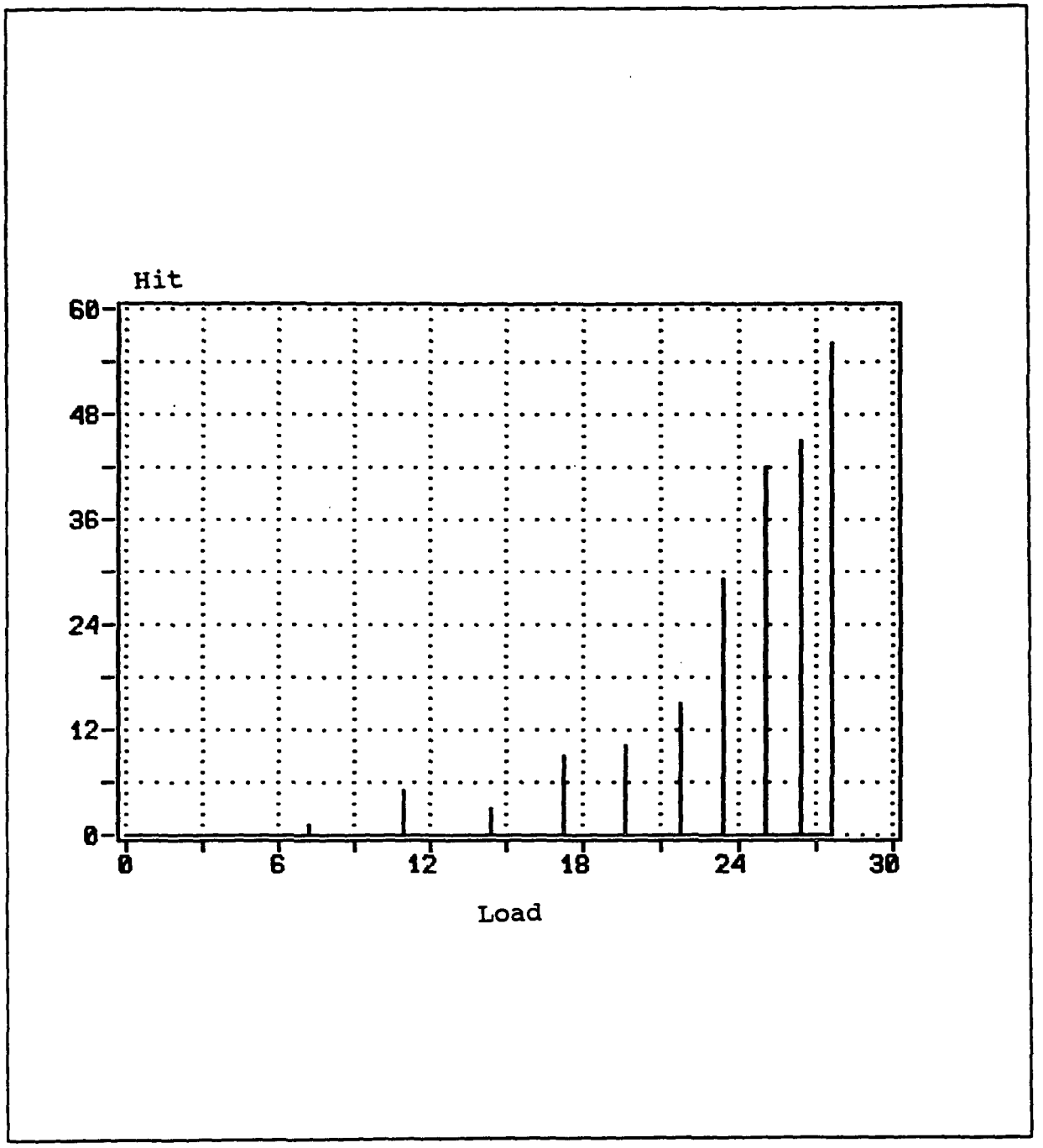

Fig. 36 A typical differential load history plot of hit for green liquor corrugating paper conditioned at 50% RH, and tested in MD under uniaxial tensile loading at crosshead speed of 5.0 in/min.

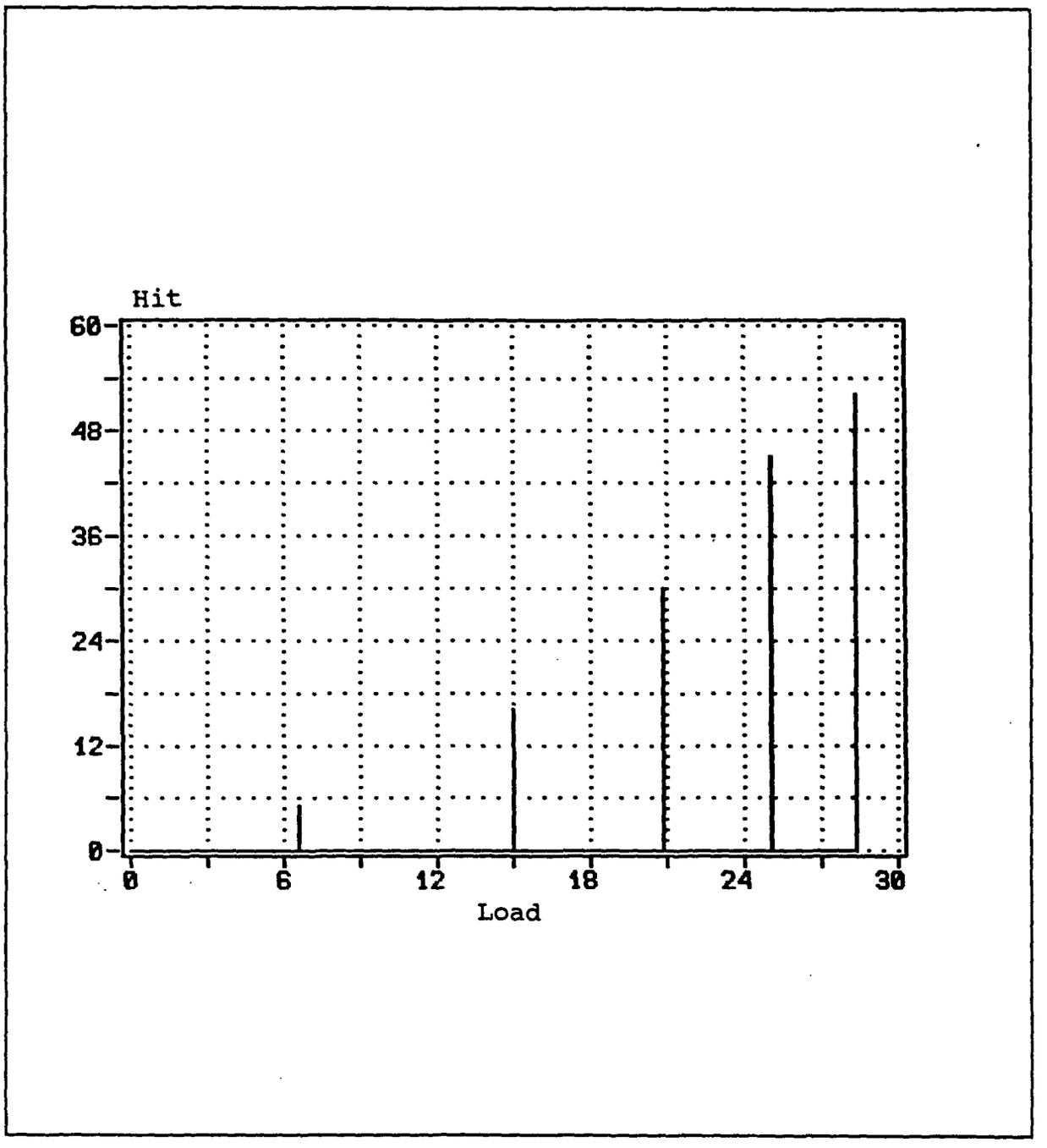

Fig. 37 A typical differential load history plot of hit for green liquor corrugating paper conditioned at 50% RH, and tested in MD under uniaxial tensile loading at crosshead speed of 10.0 in/min.

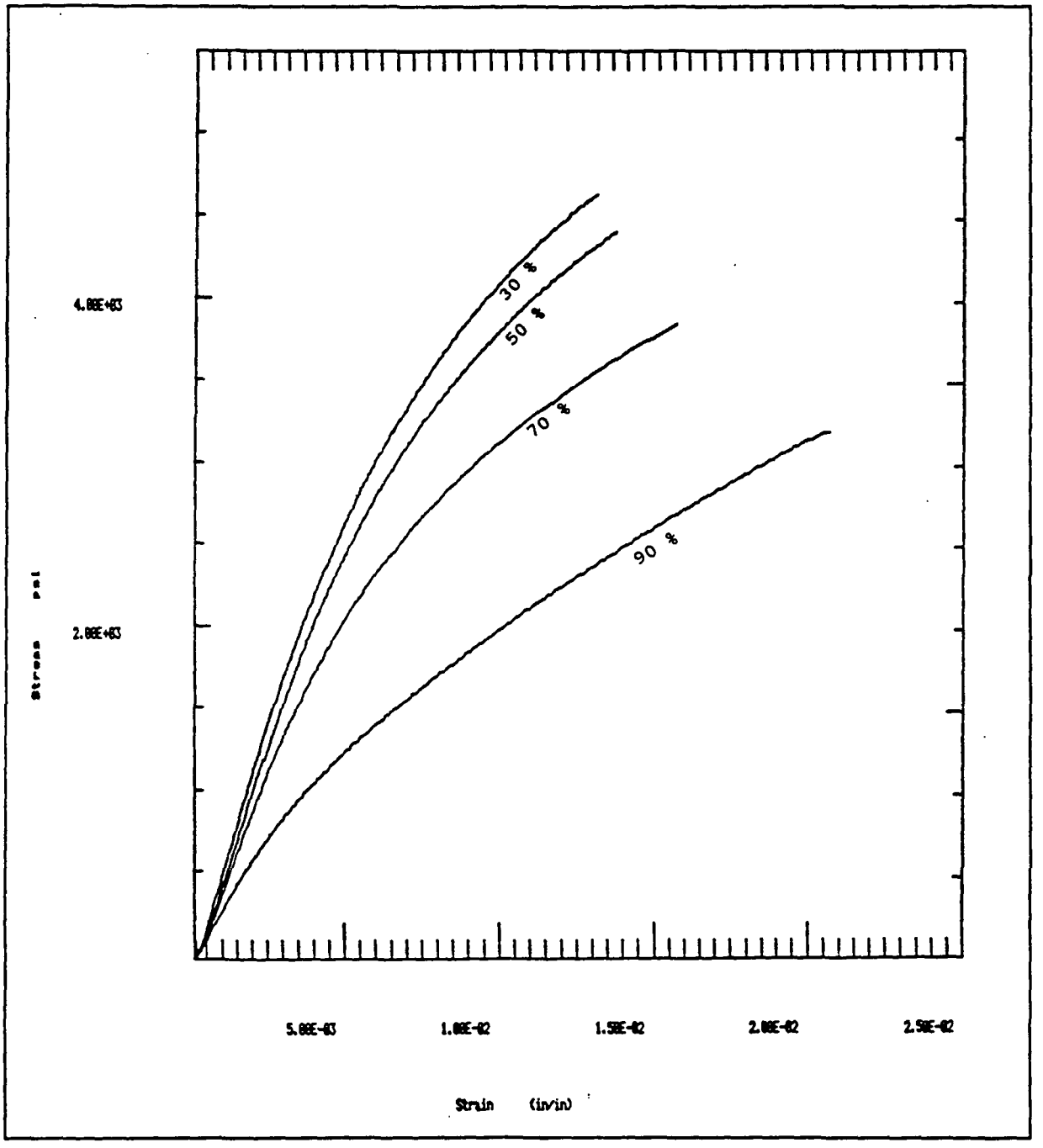

Fig. 38 Constitutive curves for green liquor corrugating paper conditioned at various RH, and tested in MD under uniaxial tensile loading at crosshead speed of 0.5 in/min.

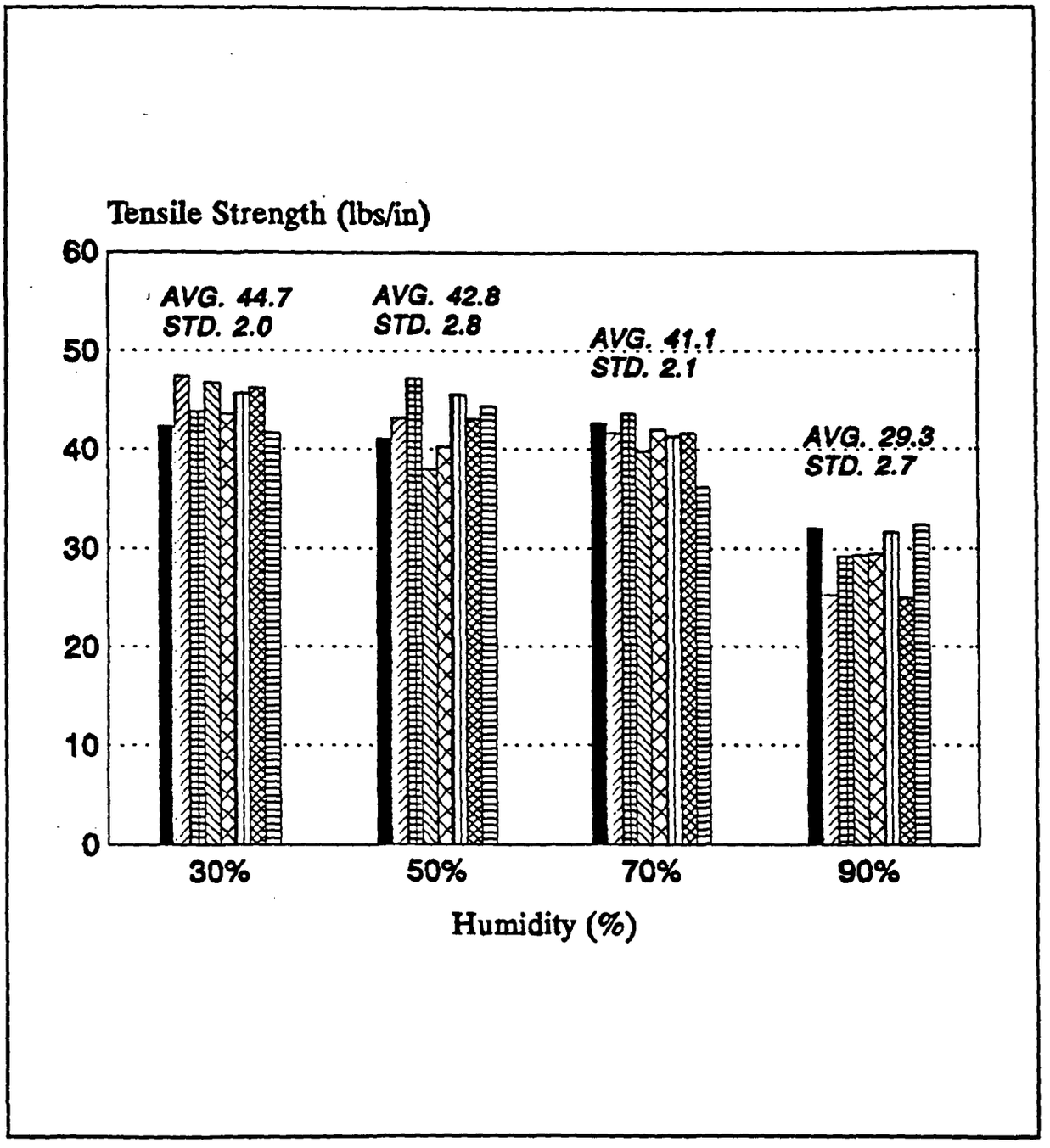

Fig. 39 The effect of relative humidity on tensile strength for green liquor corrugating paper tested in MD, under uniaxial tensile loading, and at acrosshead speed of 0.5 in/min.

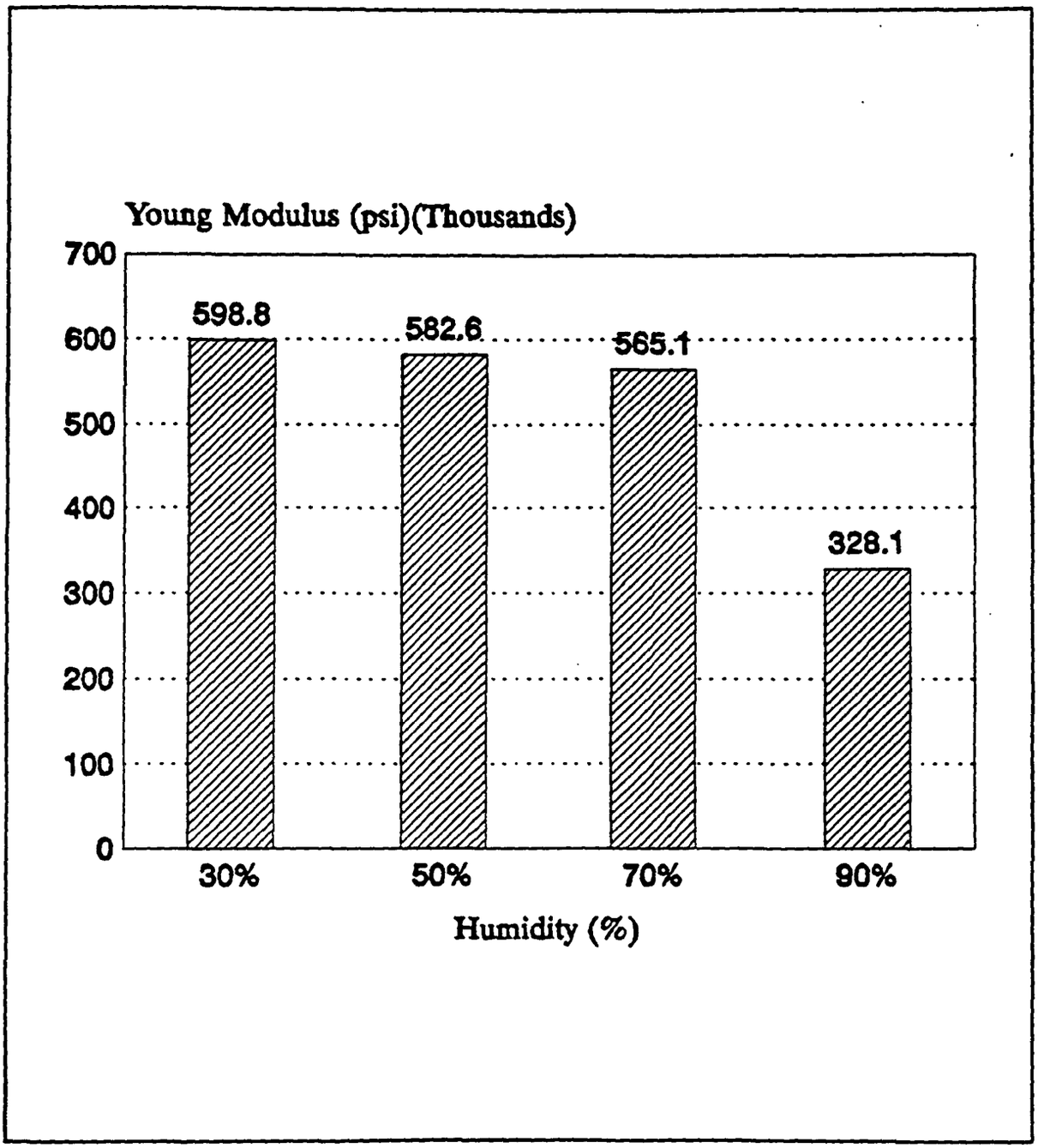

Fig. 40 The effect of relative humidity on elastic modulus for green liquor corrugating paper tested in MD, under uniaxial tensile loading, and at a crosshead speed of 0.5 in/min.

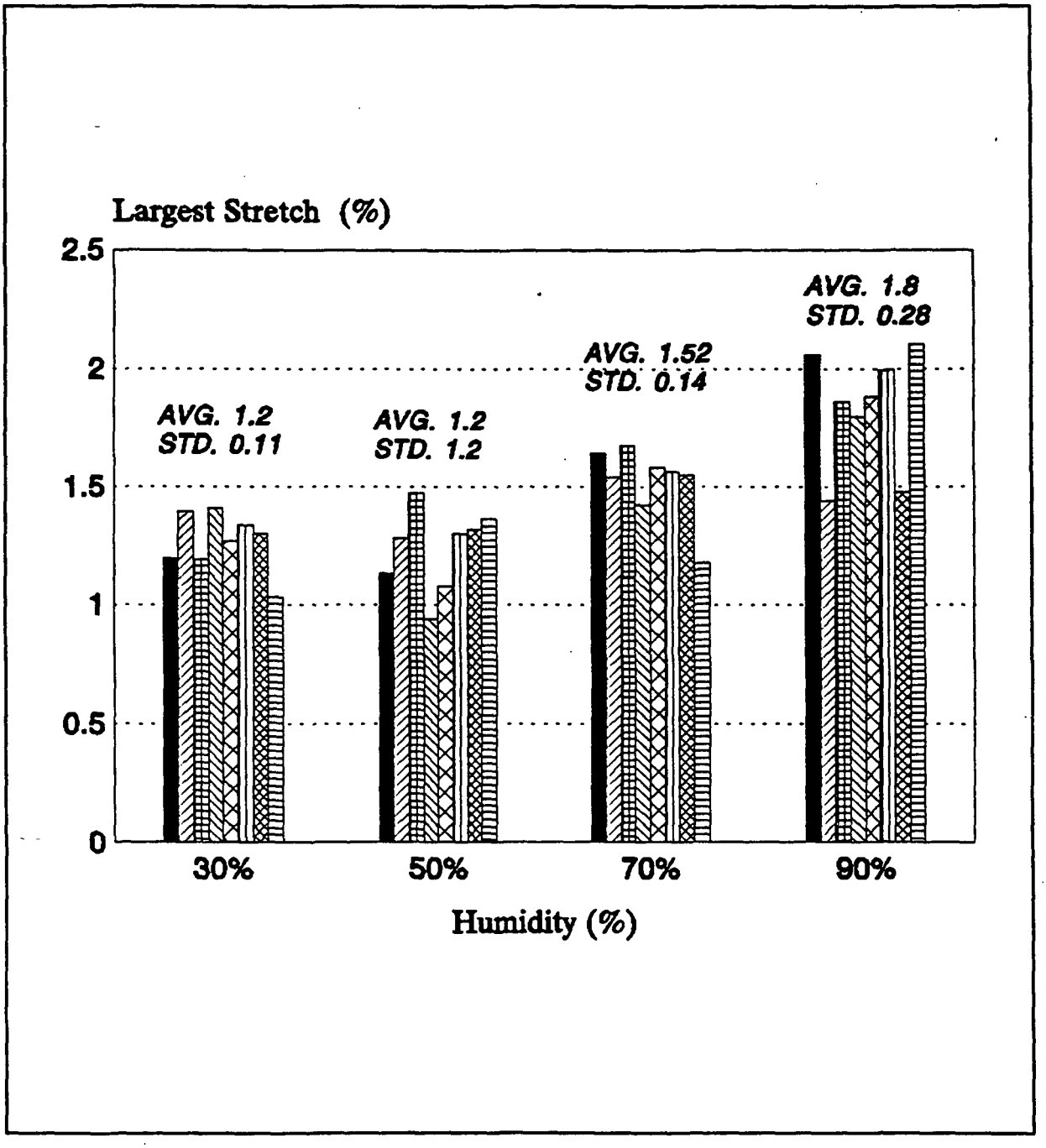

Fig. 41 The effect of relative humidity on stretch for green liquor corrugating paper tested in MD, under uniaxial tensile loading, and at a crosshead speed of 0.5 in/min.

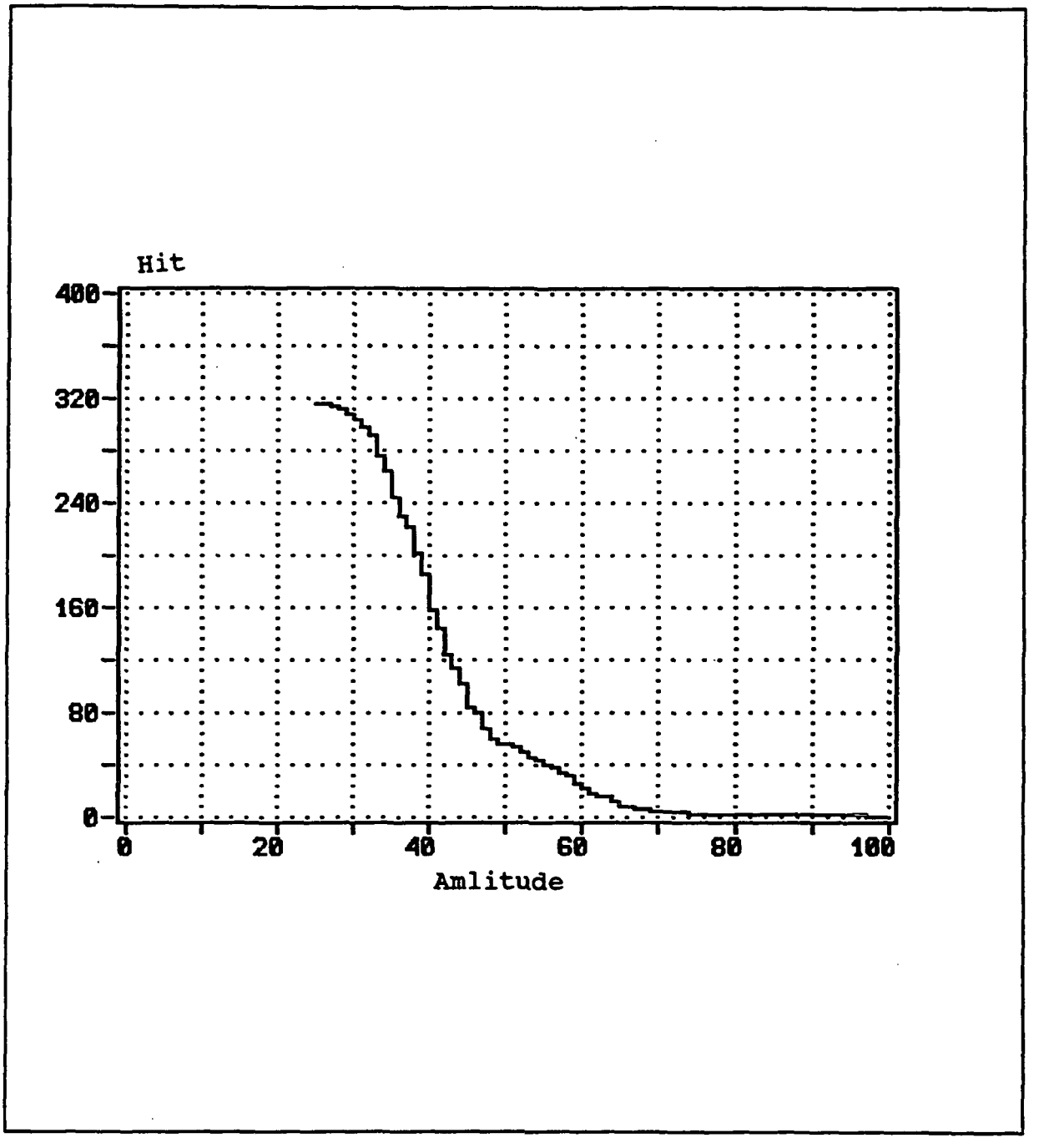

Fig. 42 A typical cumulative distribution plot of hit versus amplitude for green liquor corrugating paper conditioned at 30% RH, and tested in MD under uniaxial tensile loading at crosshead speed of 0.5 in/min.

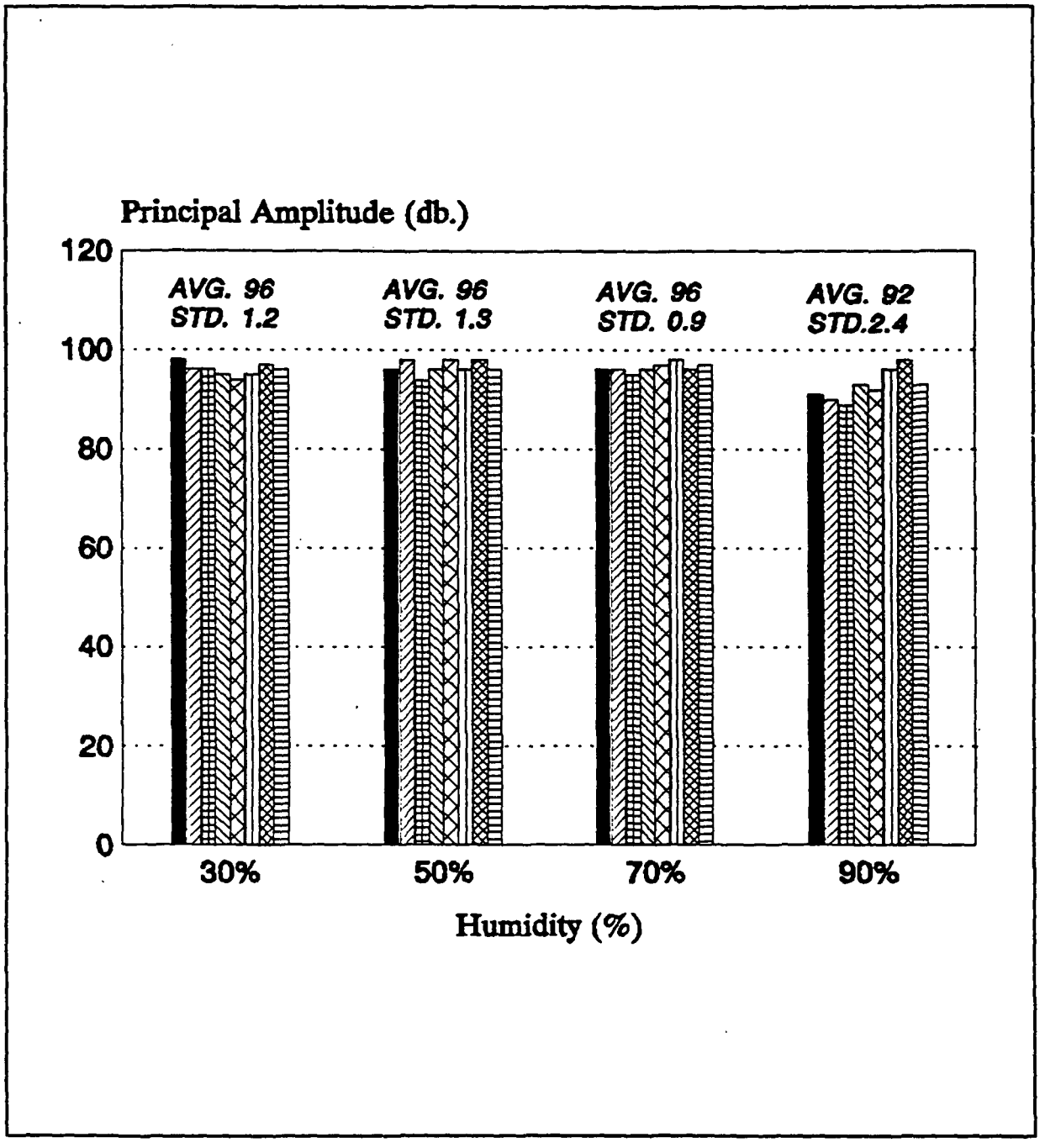

Fig. 43 The effect of relative humidity on principal amplitude for green liquor corrugating paper tested in MD, under uniaxial tensile loading, and at a crosshead speed of 0.5 in/min.

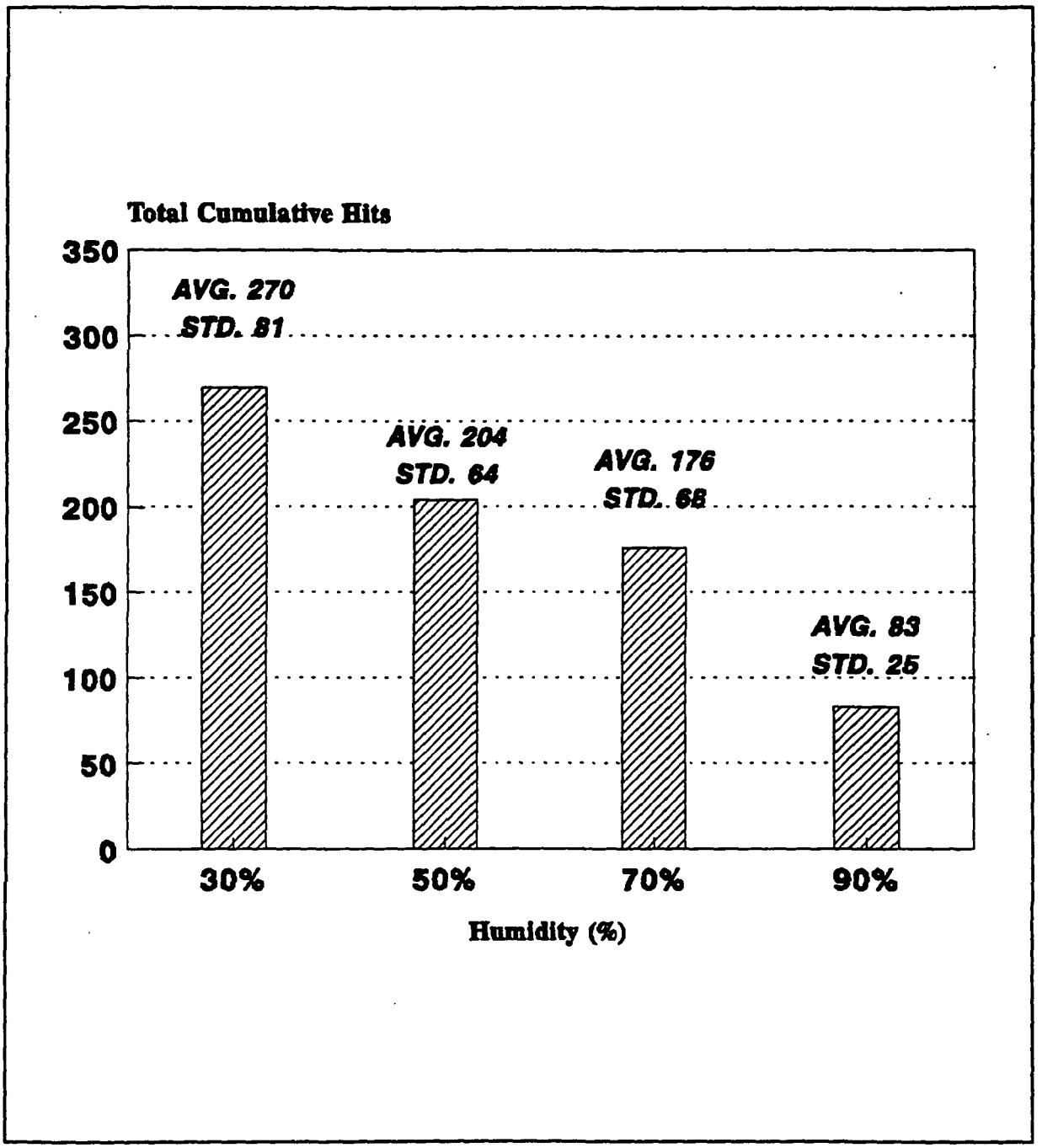

Fig. 44 The effect of relative humidity on total cumulative hits for green liquor corrugating paper tested in MD, under uniaxial tensile loading, and at a crosshead speed of 0.5 in/min.

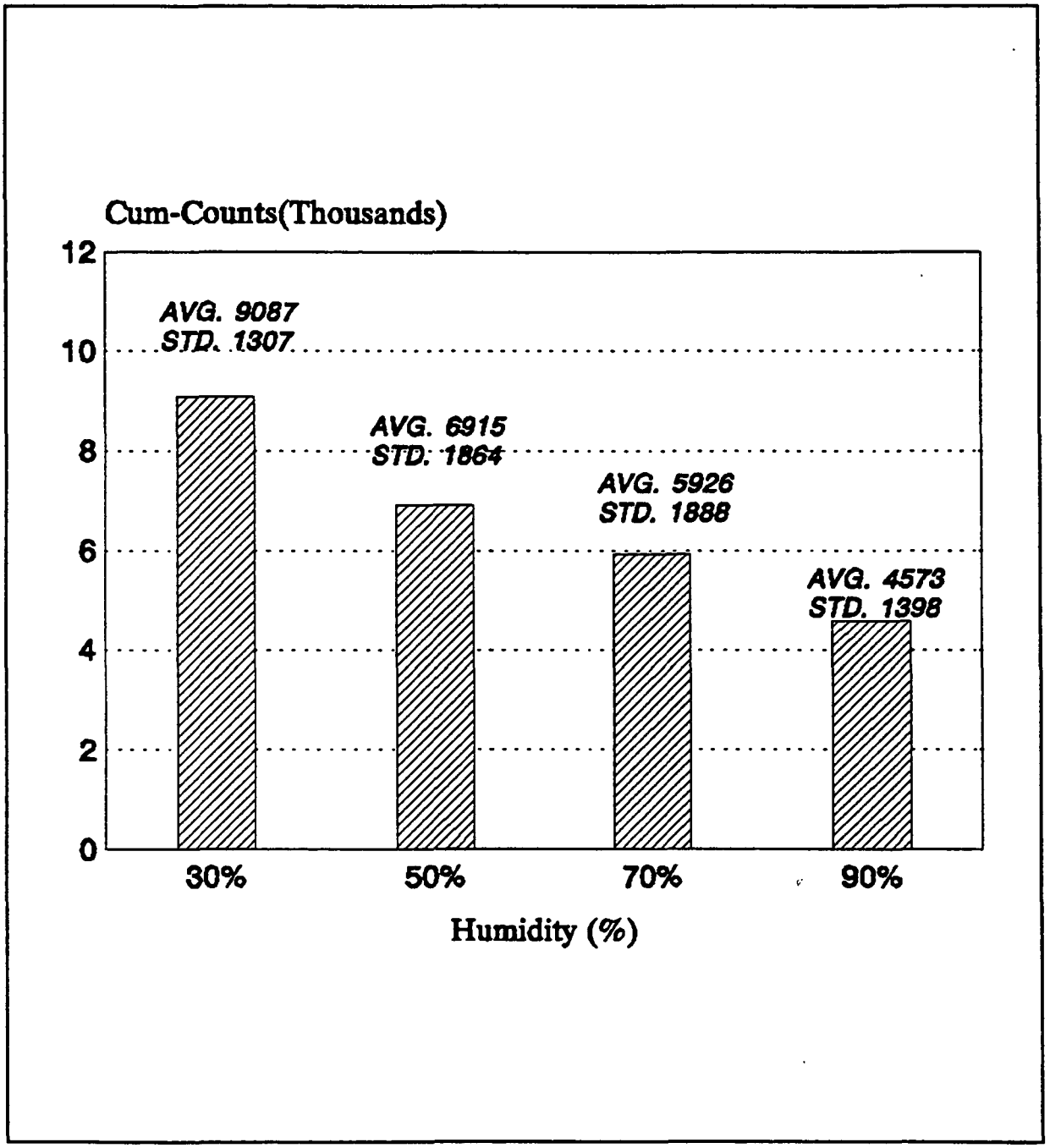

Fig. 45 The effect of relative humidity on total cumulative counts for green liquor corrugating paper tested in MD, under uniaxial tensile loading, and at a crosshead speed of 0.5 in/min.

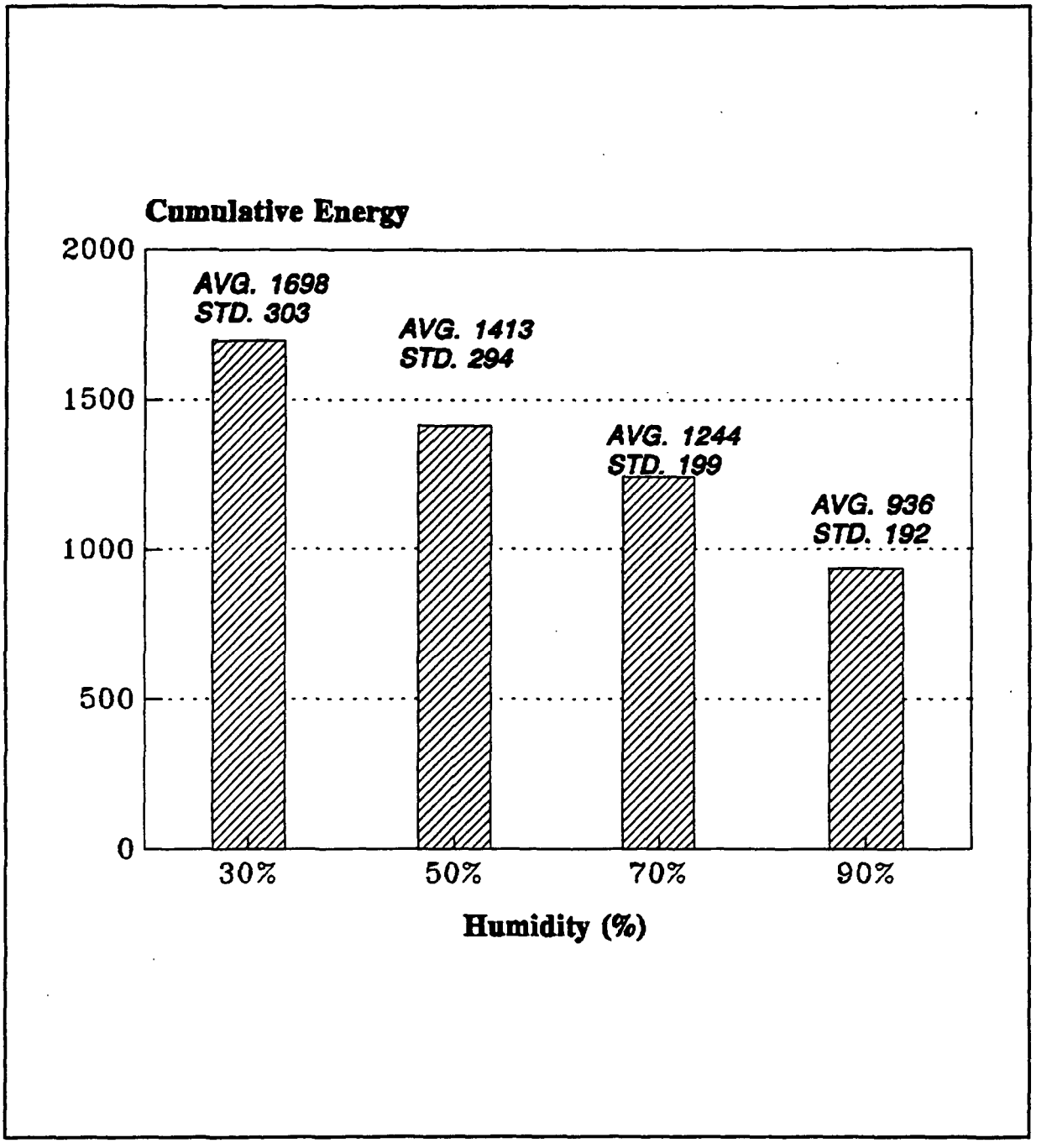

Fig. 46 The effect of relative humidity on total cumulative energy for green liquor corrugating paper tested in MD, under uniaxial tensile loading, and at a crosshead speed of 0.5 in/min.

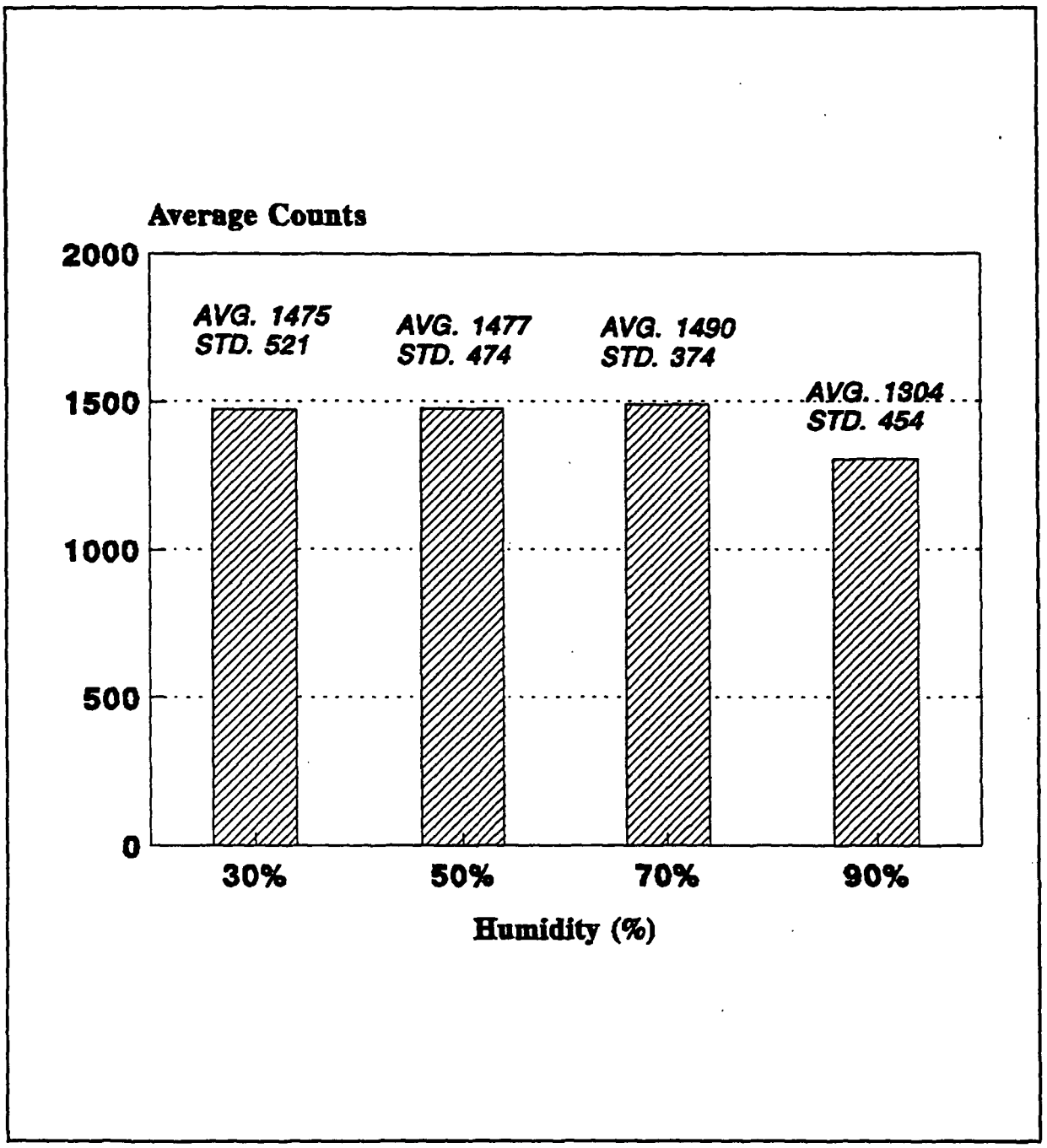

Fig. 47 The effect of relative humidity on principal counts for green liquor corrugating paper tested in MD, under uniaxial tensile loading, and at a crosshead speed of 0.5 in/min.

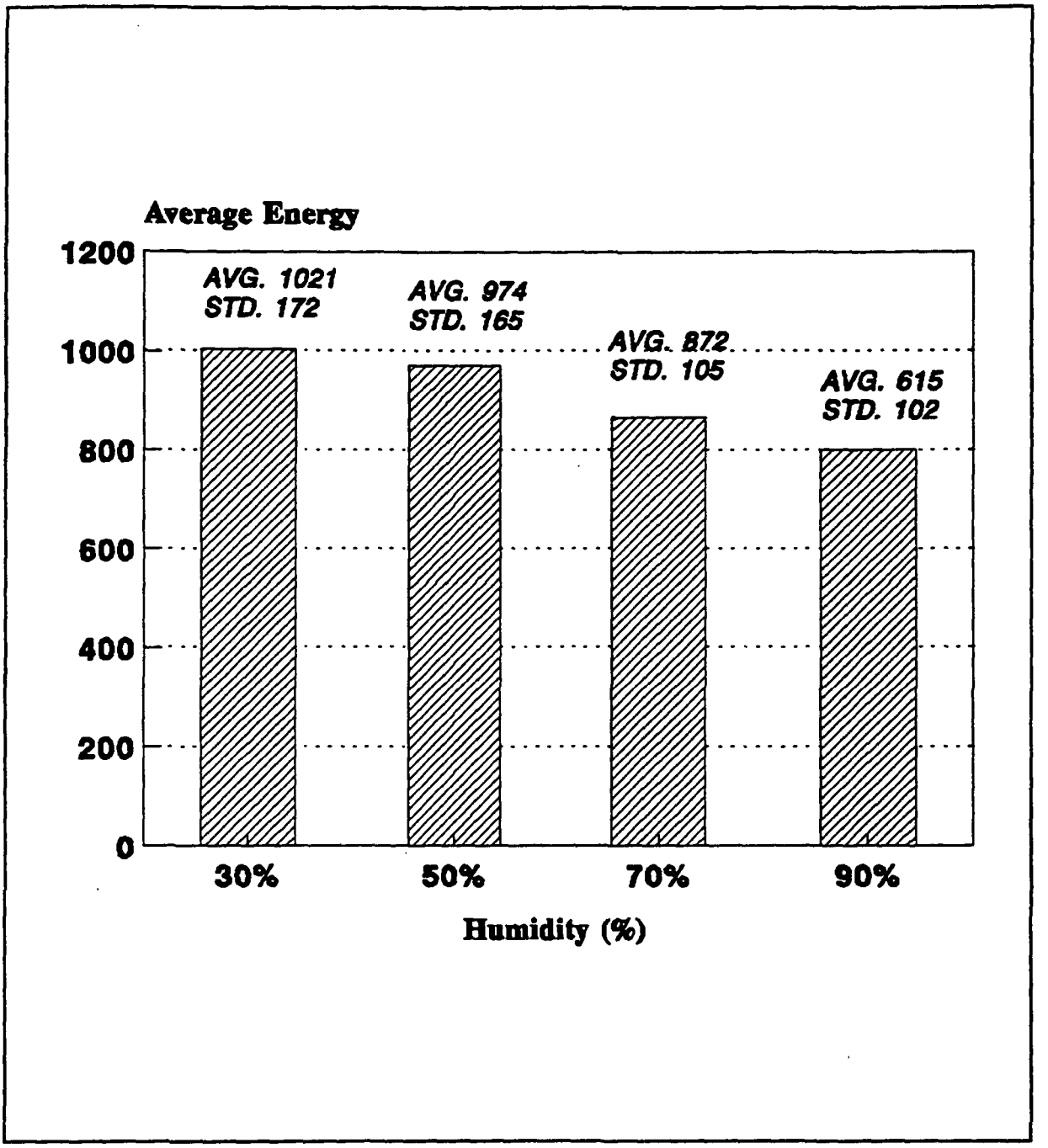

Fig. 48 The effect of relative humidity on principal energy for green liquor corrugating paper tested in MD, under uniaxial tensile loading, and at a crosshead speed of 0.5 in/min.

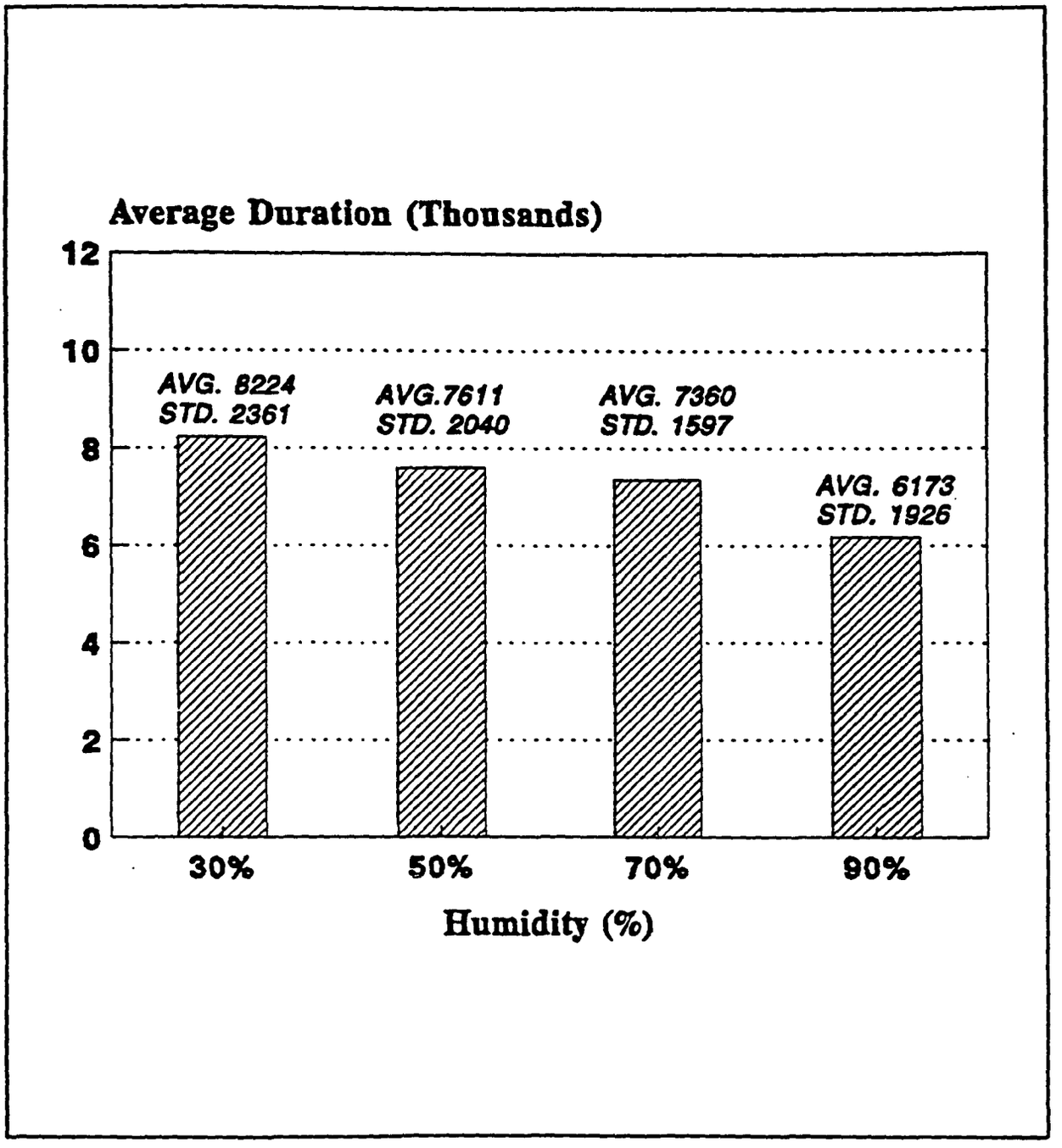

Fig. 49 The effect of relative humidity on principal duration for green liquor corrugating paper tested in MD, under uniaxial tensile loading, and at a crosshead speed of 0.5 in/min.

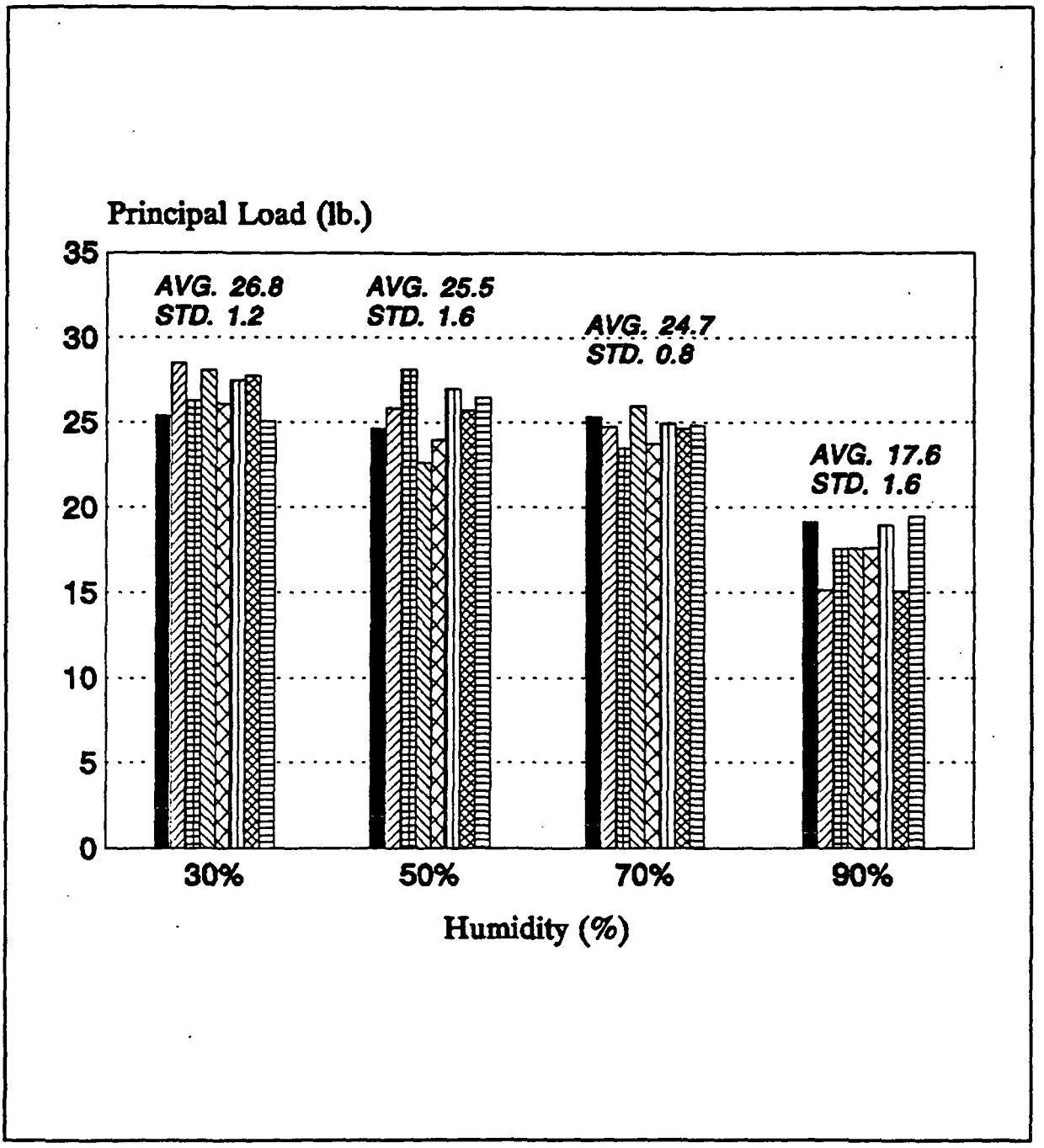

Fig. 50 The effect of relative humidity on principal load for green liquor corrugating paper tested in MD, under uniaxial tensile loading, and at a crosshead speed of 0.5 in/min.

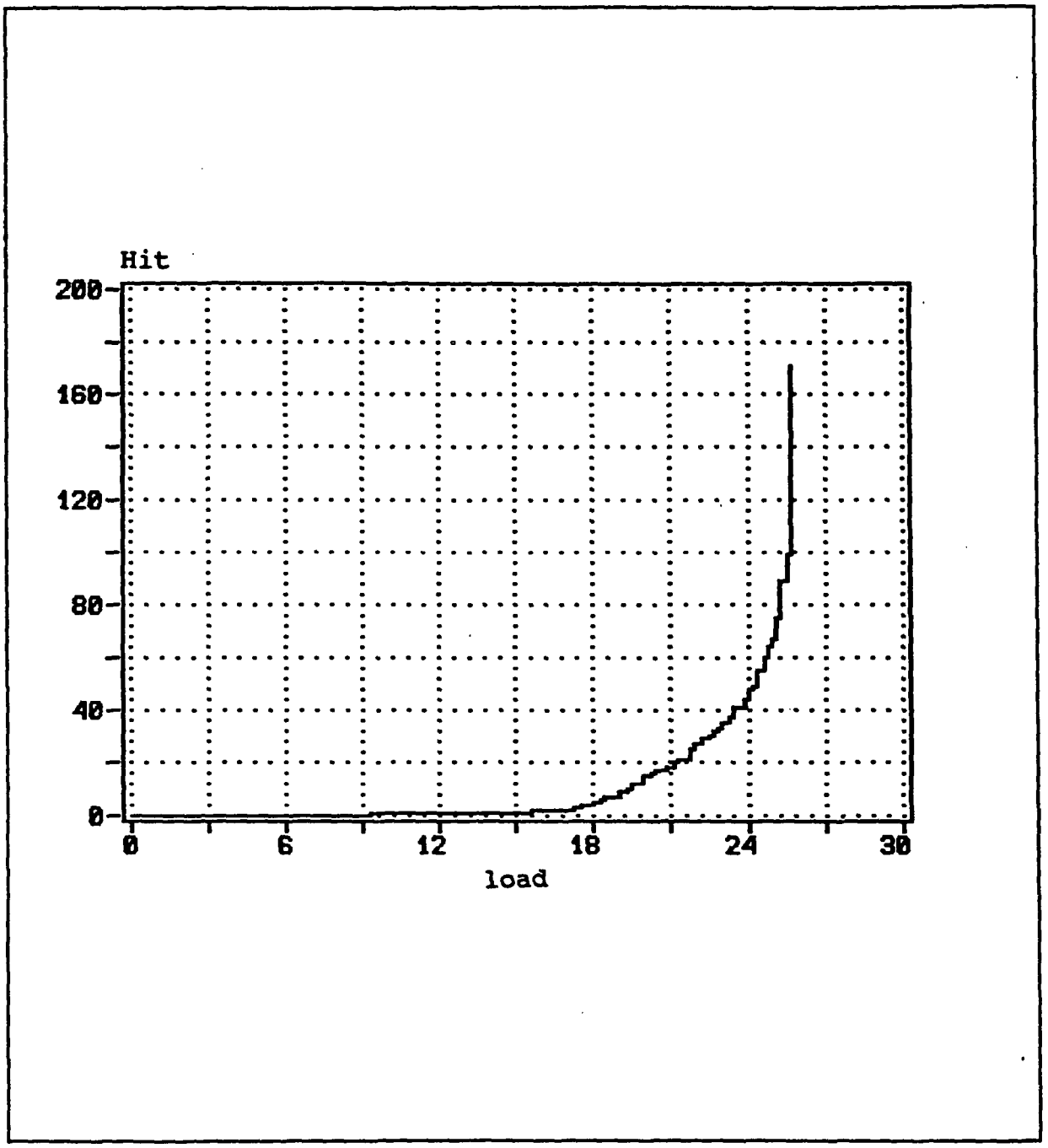

Fig. 51 A typical min-max cumulative load history plot of hit for green liquor corrugating paper conditioned at 30% RH, and tested in MD under uniaxial tensile loading at crosshead speed of 0.5 in/min.

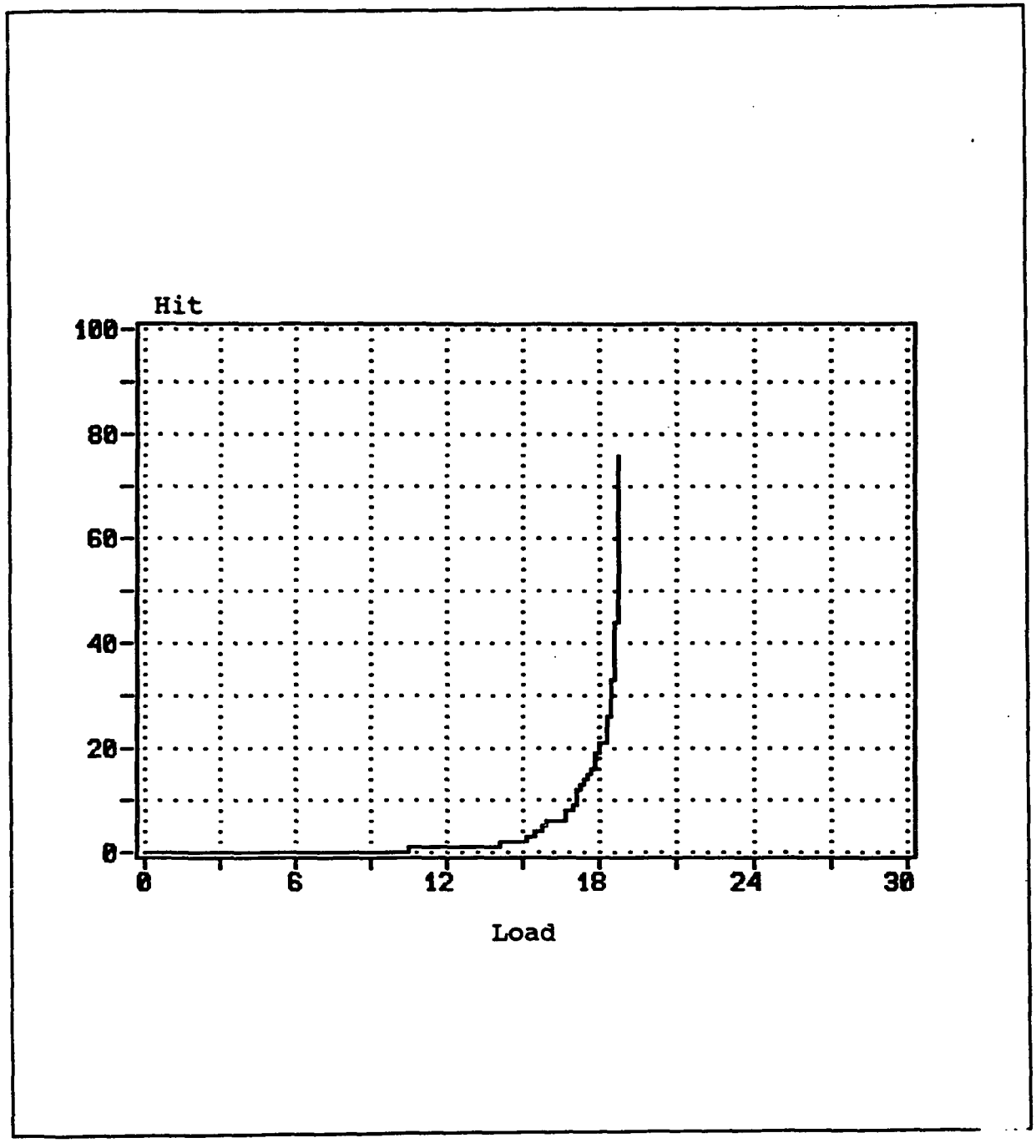

Fig. 52 A typical min-max cumulative load history plot of hit for green liquor corrugating paper conditioned at 90% RH, and tested in MD under uniaxial tensile loading at crosshead speed of 0.5 in/min.

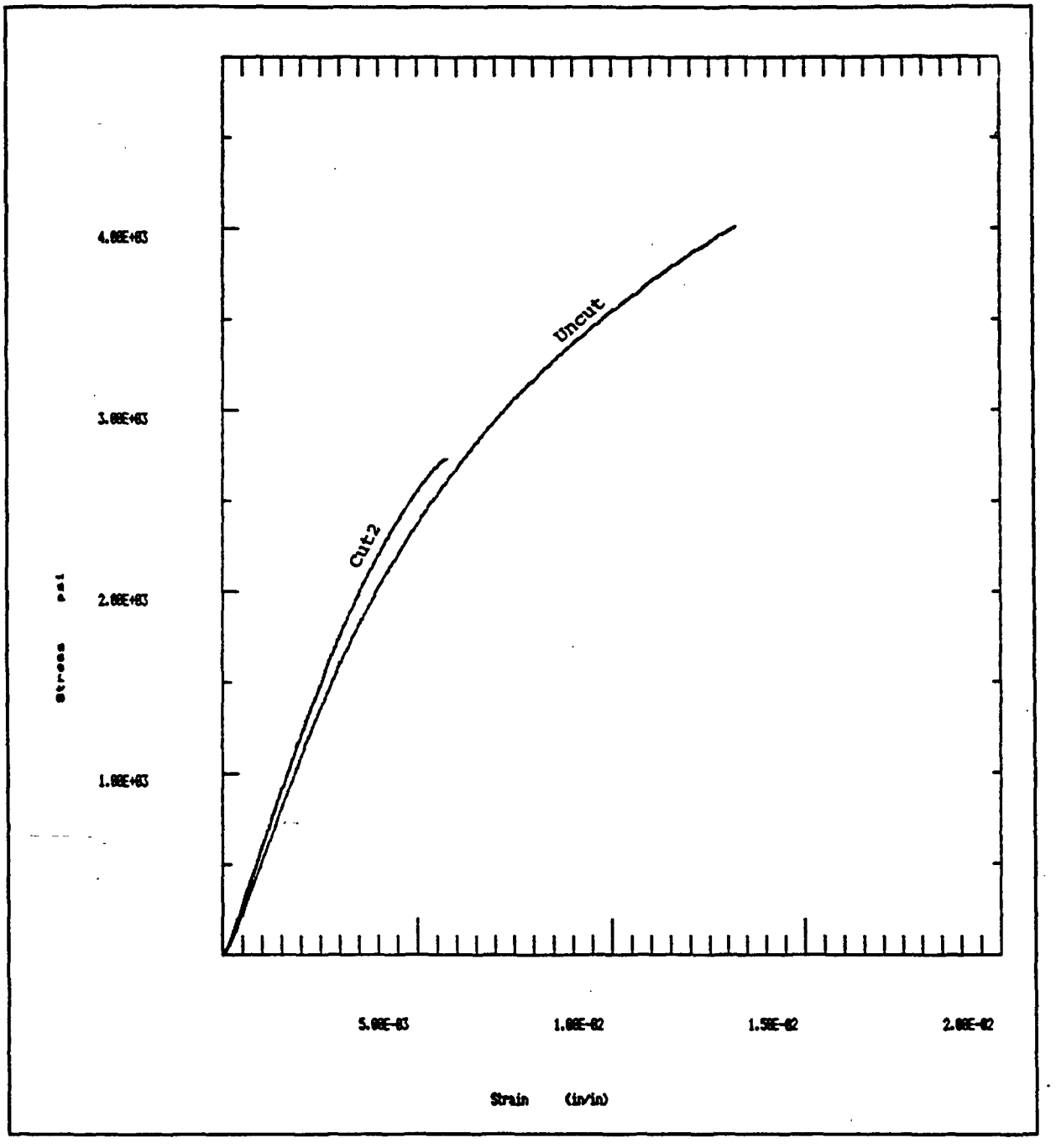

Fig. 53 Constitutive curves for CUT2 and uncut specimens of green liquor corrugating paper conditioned at 50% RH, and tested in MD under uniaxial tensile loading at crosshead speed of 0.05 in/min.

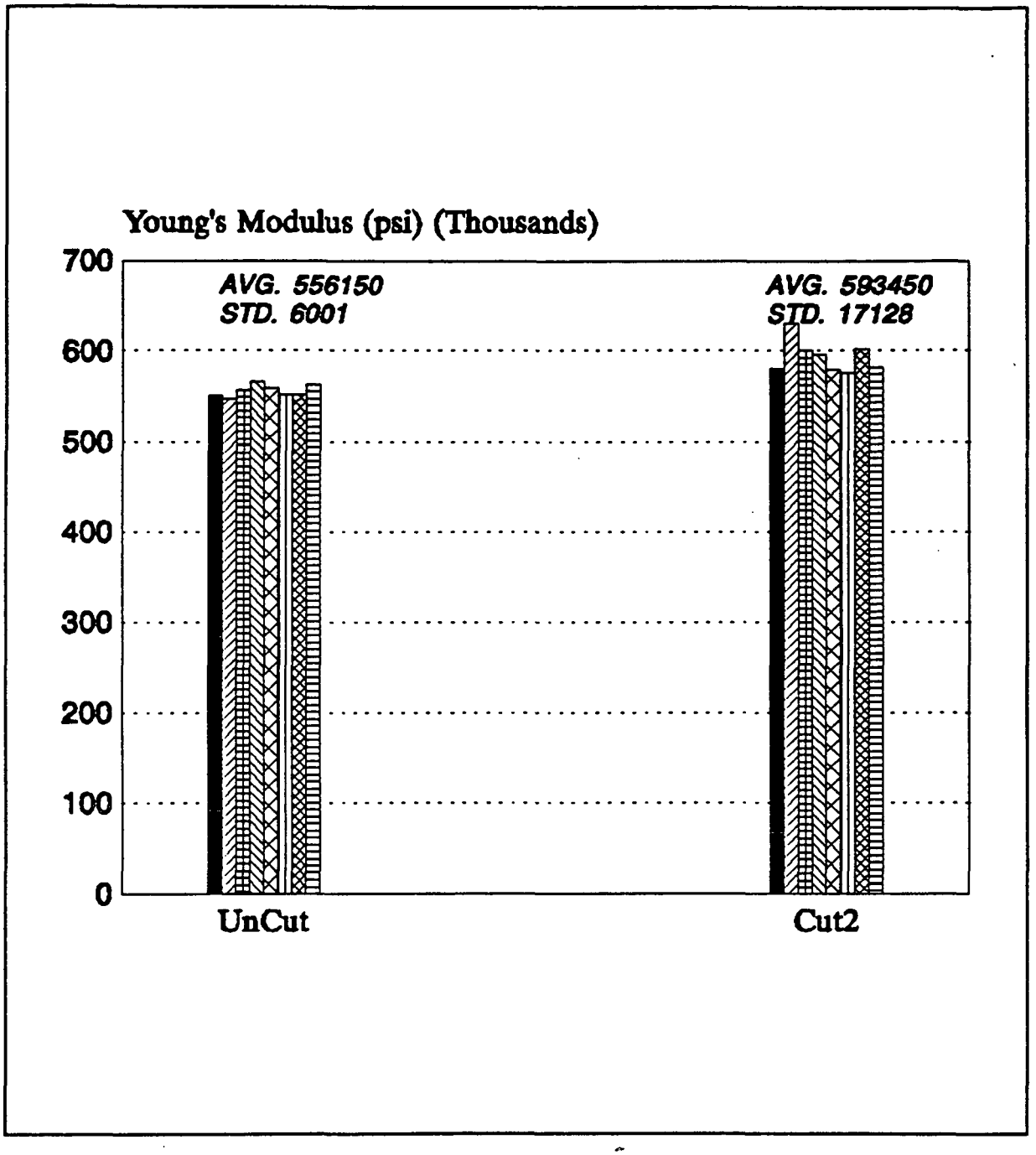

Fig. 54 Comparison of the elastic moduli for CUT2 and uncut specimens of green liquor corrugating paper conditioned at 50% RH, and tested in MD under uniaxial tensile loading at a crosshead speed of 0.05 in/min.

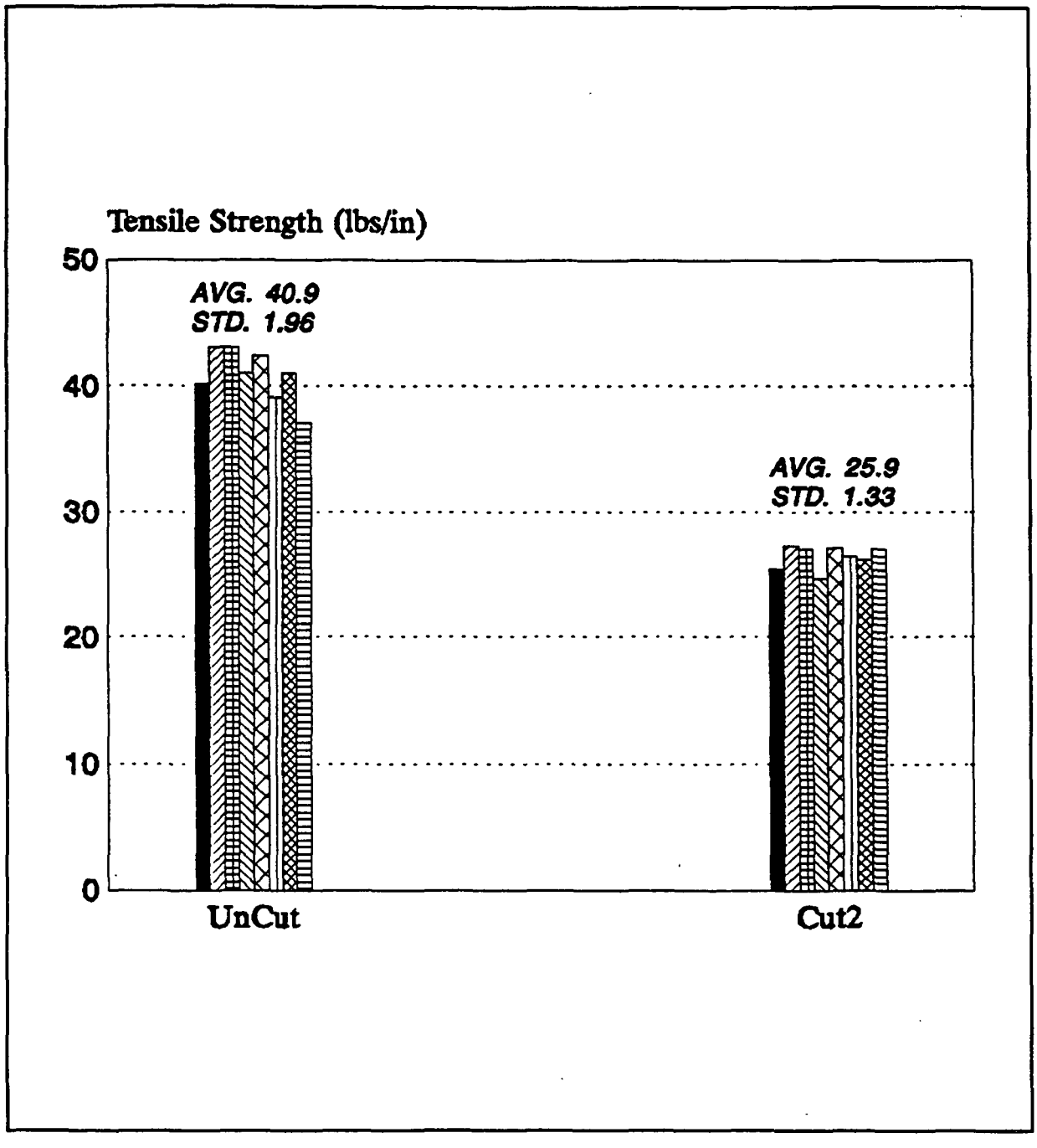

Fig. 55 Comparison of the tensile strengths for CUT2 and uncut specimens of green liquor corrugating paper conditioned at 50% RH, and tested in MD under uniaxial tensile loading at a crosshead speed of 0.05 in/min.

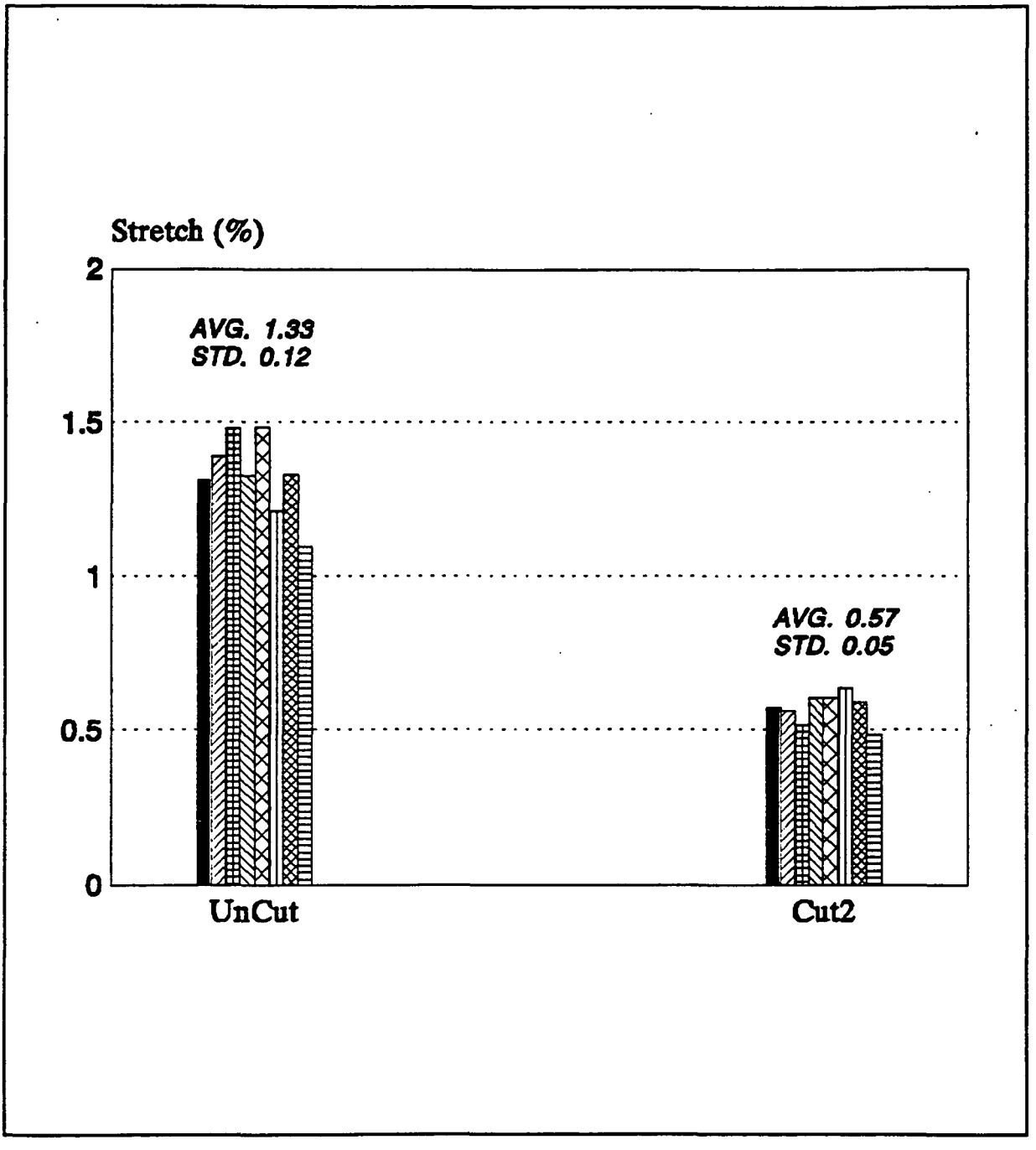

Fig. 56 Comparison of the values of stretch for CUT2 and uncut specimens of green liquor corrugating paper conditioned at 50% RH, and tested in MD under uniaxial tensile loading at a crosshead speed of 0.05 in/min.

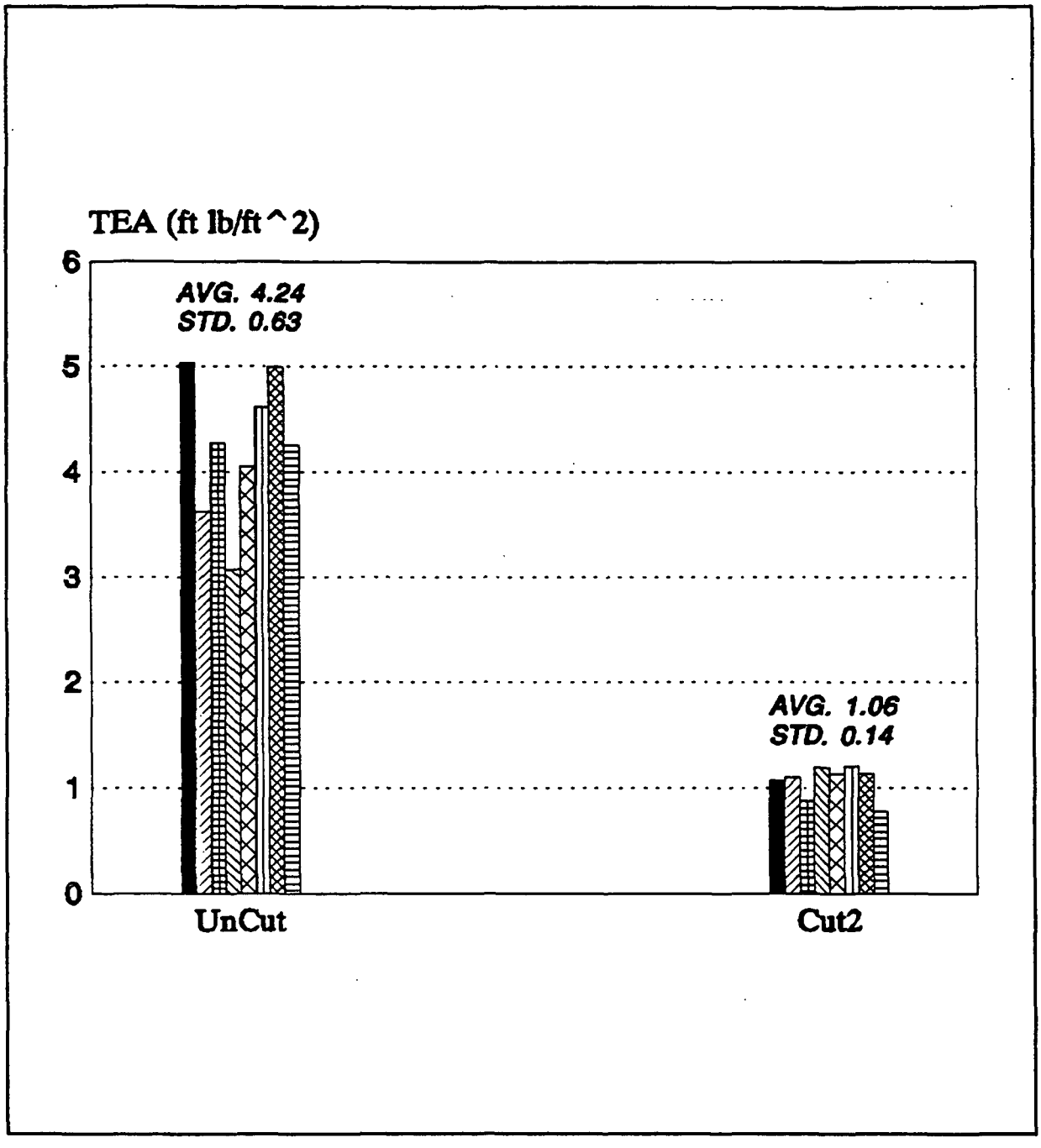

Fig. 57 Comparison of the values of TEA for CUT2 and uncut specimens of green liquor corrugating paper conditioned at 50% RH, and tested in MD under uniaxial tensile loading at a crosshead speed of 0.05 in/min.

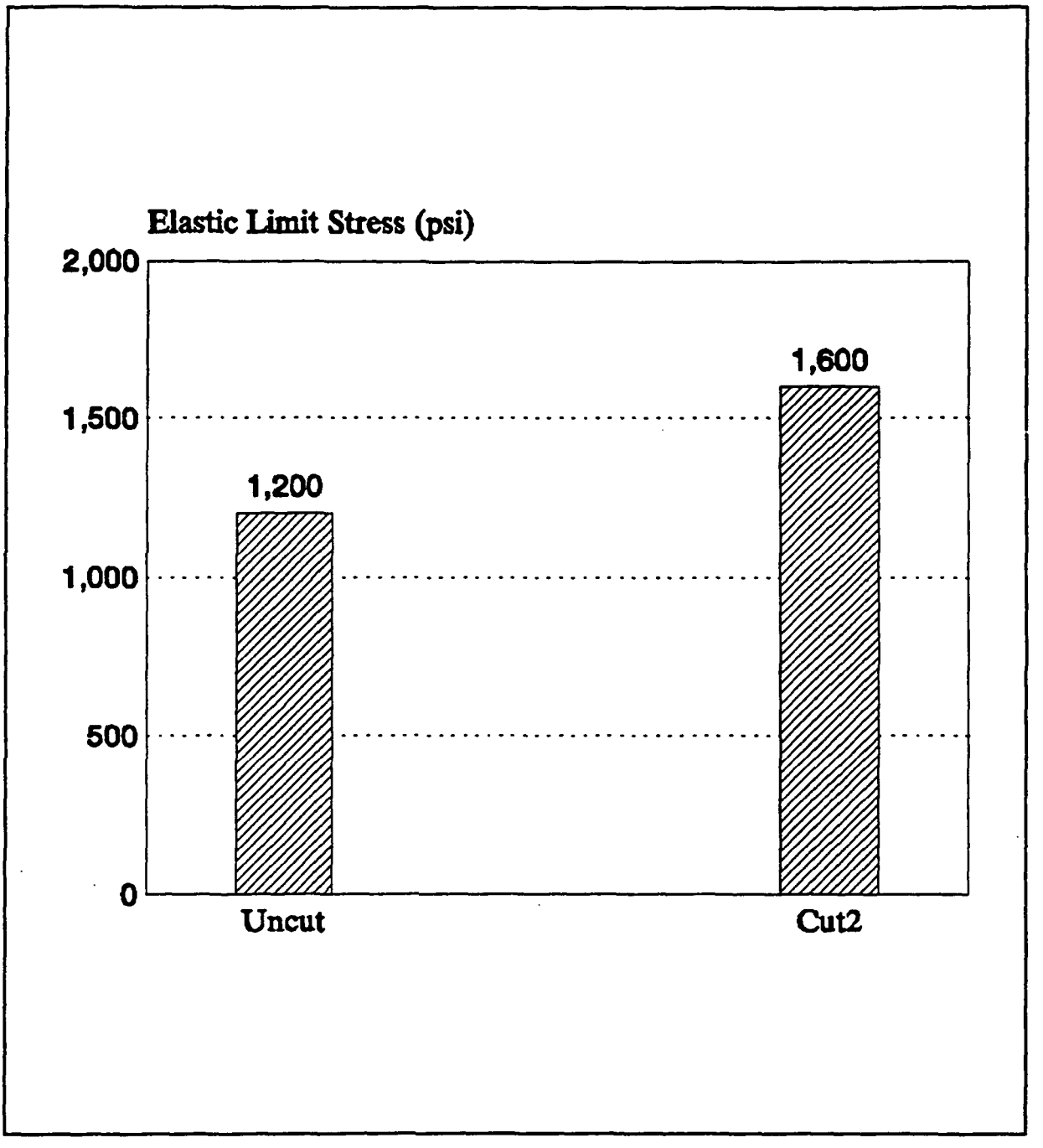

Fig. 58 Comparison of the values of elastic limit for CUT2 and uncut specimens of green liquor corrugating paper conditioned at 50% RH, and tested in MD under uniaxial tensile loading at a crosshead speed of 0.05 in/min.

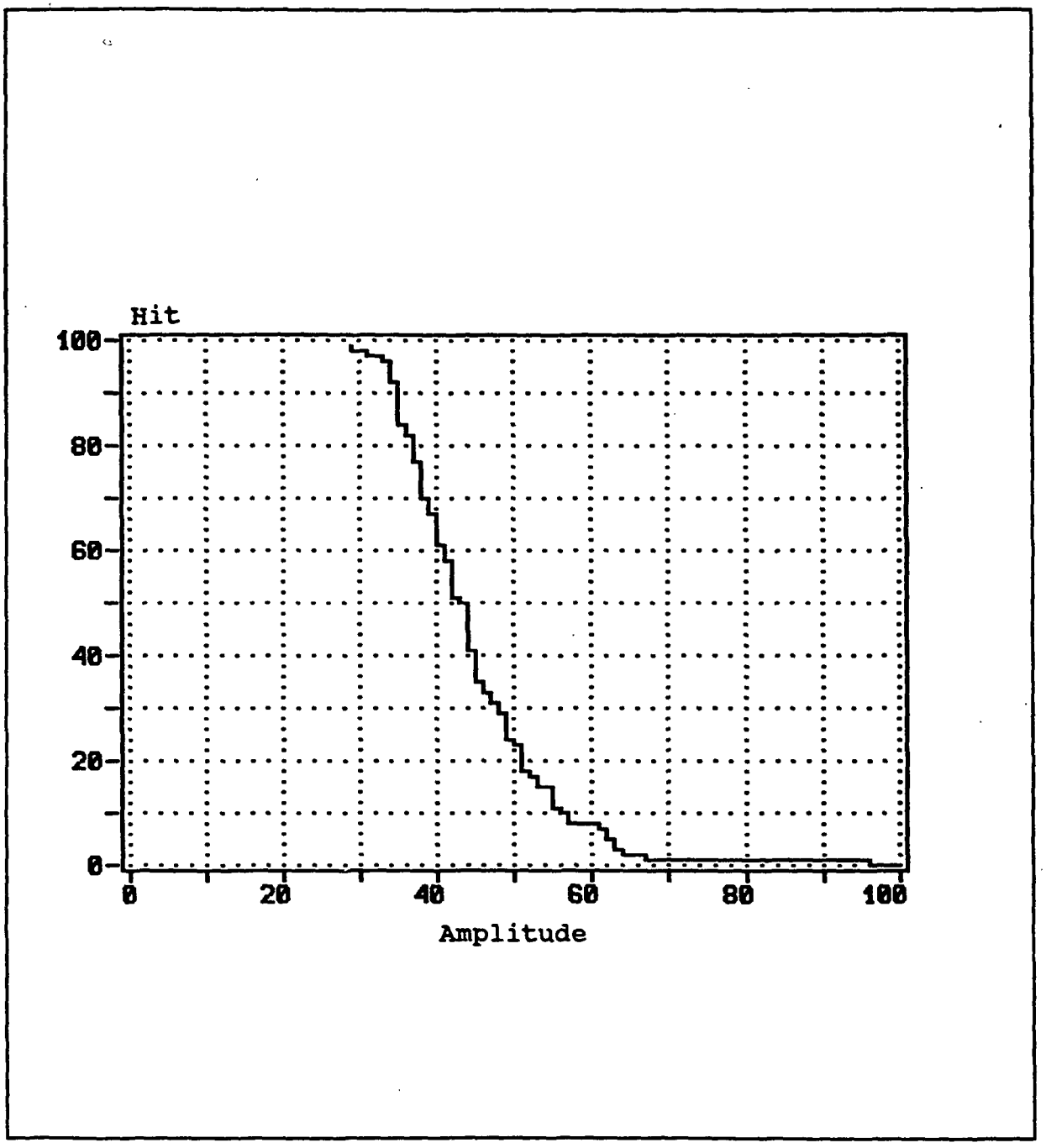

Fig. 59 A typical cumulative distribution plot of hit versus amplitude for CUT2 specimens of green liquor corrugating paper conditioned at 50% RH, and tested in MD under uniaxial tensile loading at crosshead speed of 0.05 in/min.

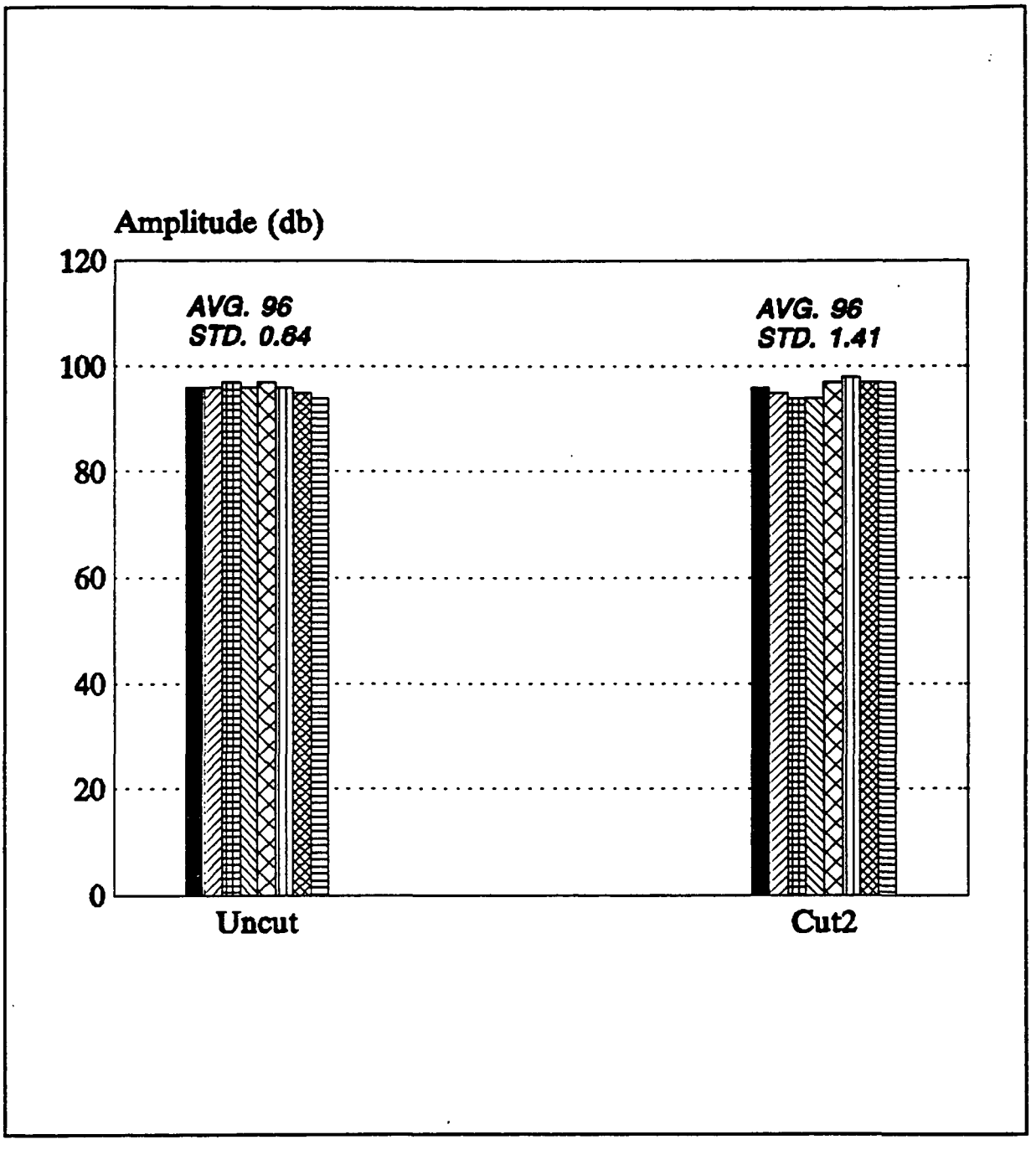

Fig. 60 Comparison of the principal amplitudes for CUT2 and uncut specimens of green liquor corrugating paper conditioned at 50% RH, and tested in MD under uniaxial tensile loading at a crosshead speed of 0.05 in/min.

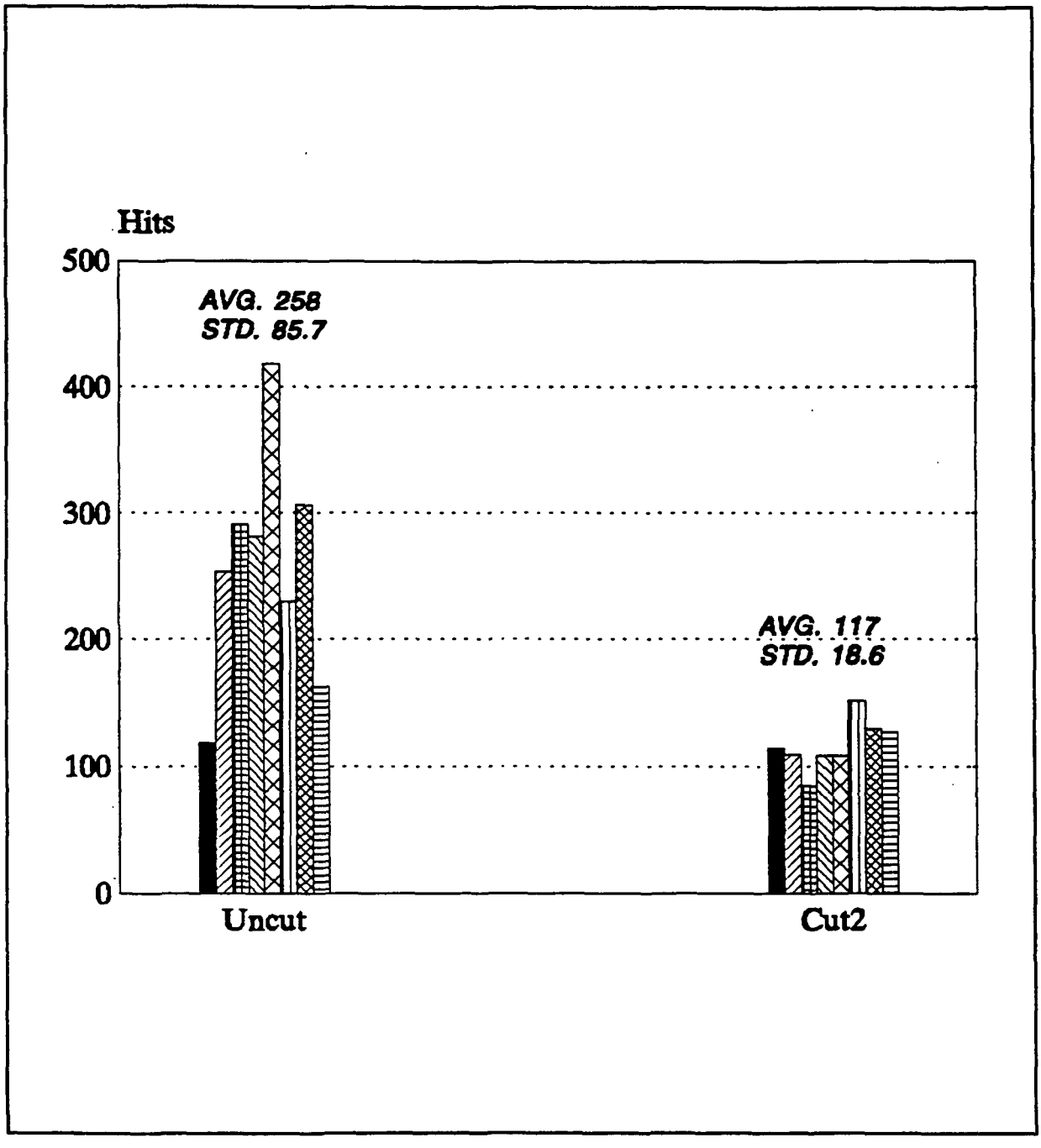

Fig. 61 Comparison of the cumulative hits for CUT2 and uncut specimens of green liquor corrugating paper conditioned at 50% RH, and tested in MD under uniaxial tensile loading at a crosshead speed of 0.05 in/min.

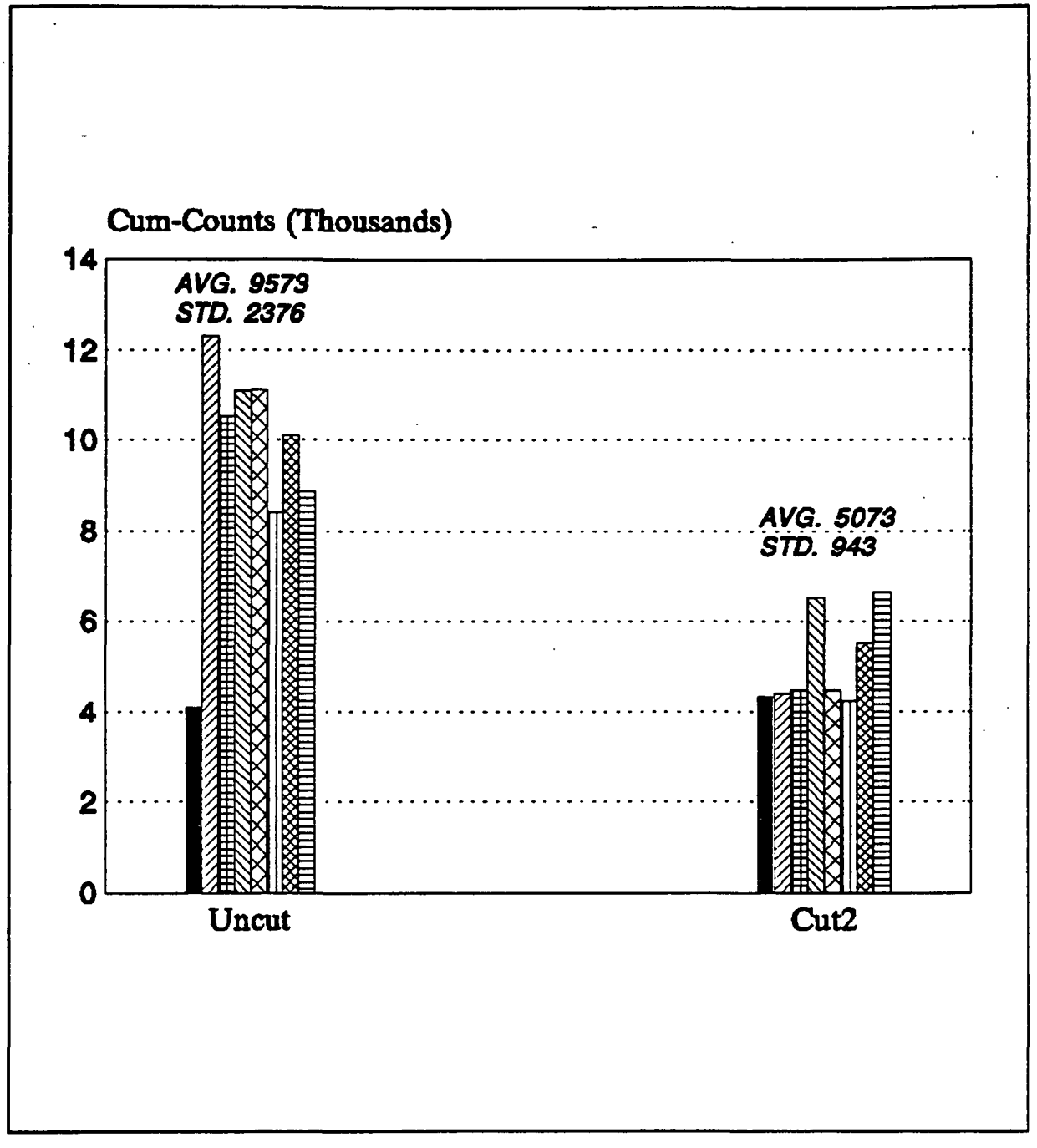

Fig. 62 Comparison of the cumulative counts for CUT2 and uncut specimens of green liquor corrugating paper conditioned at 50% RH, and tested in MD under uniaxial tensile loading at a crosshead speed of 0.05 in/min.

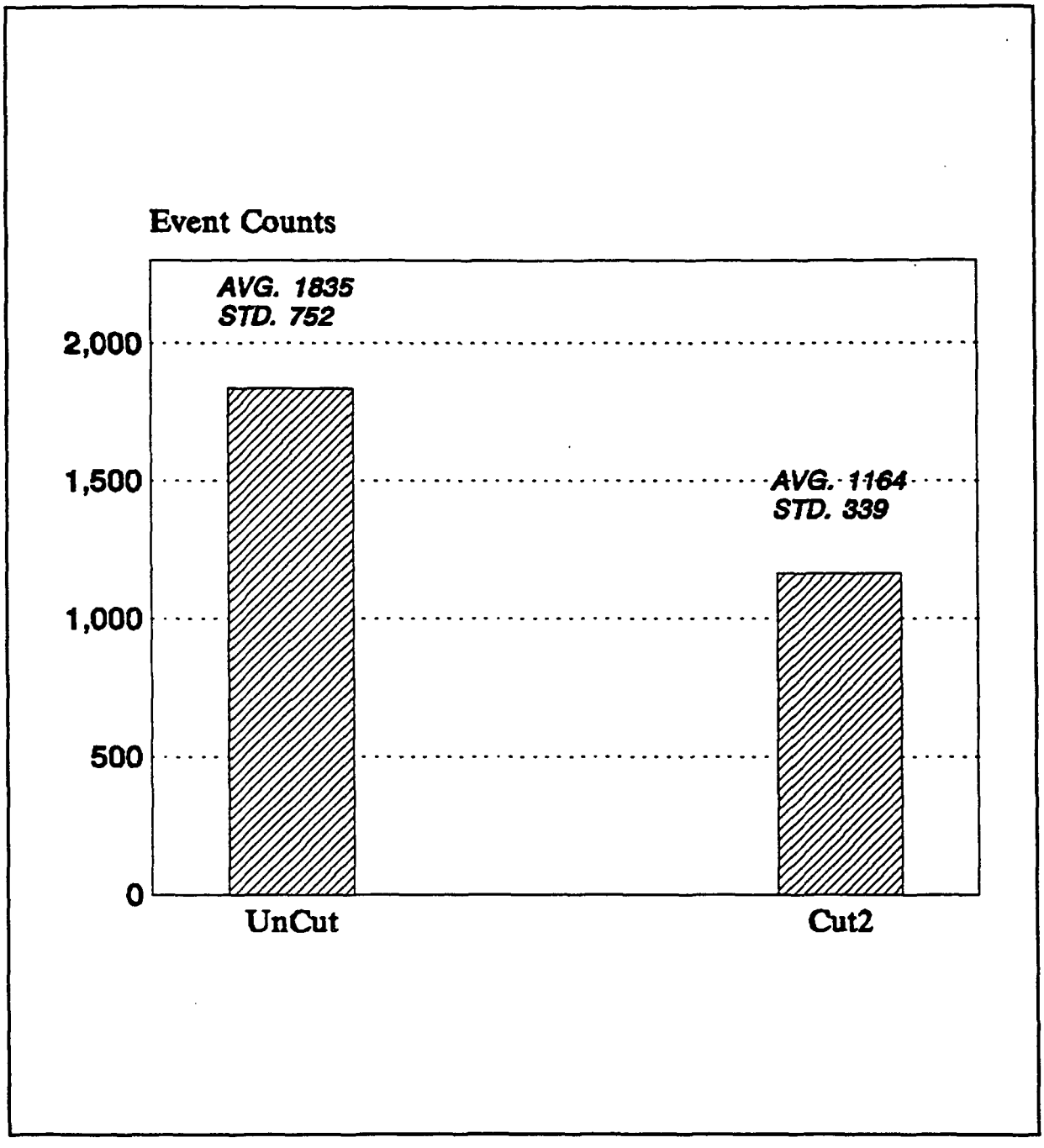

Fig. 63 Comparison of the principal counts for CUT2 and uncut specimens of green liquor corrugating paper conditioned at 50% RH, and tested in MD under uniaxial tensile loading at a crosshead speed of 0.05 in/min.

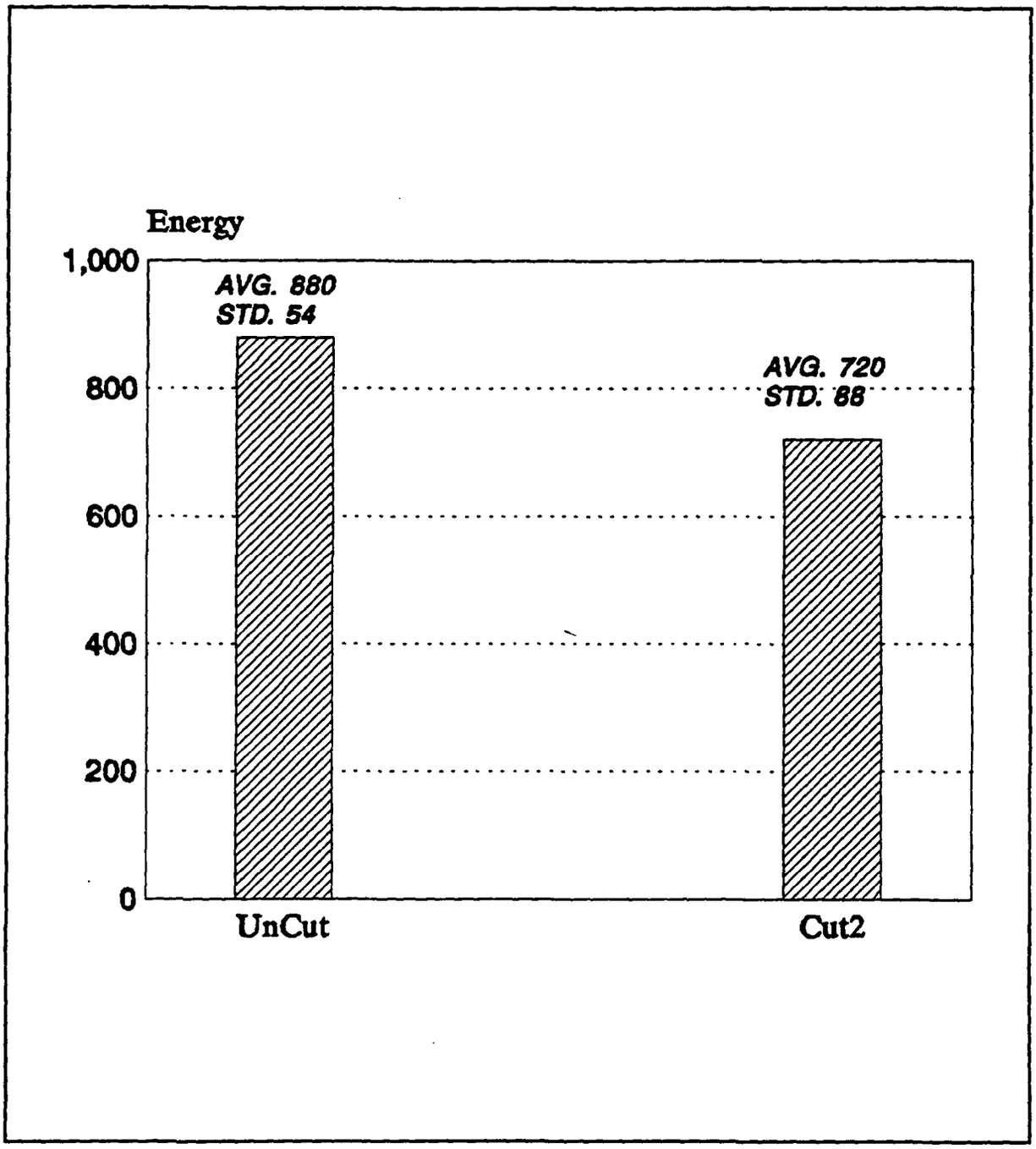

Fig. 64 Comparison of the principal eneregies for CUT2 and uncut specimens of green liquor corrugating paper conditioned at 50% RH, and tested in MD under uniaxial tensile loading at a crosshead speed of 0.05 in/min.

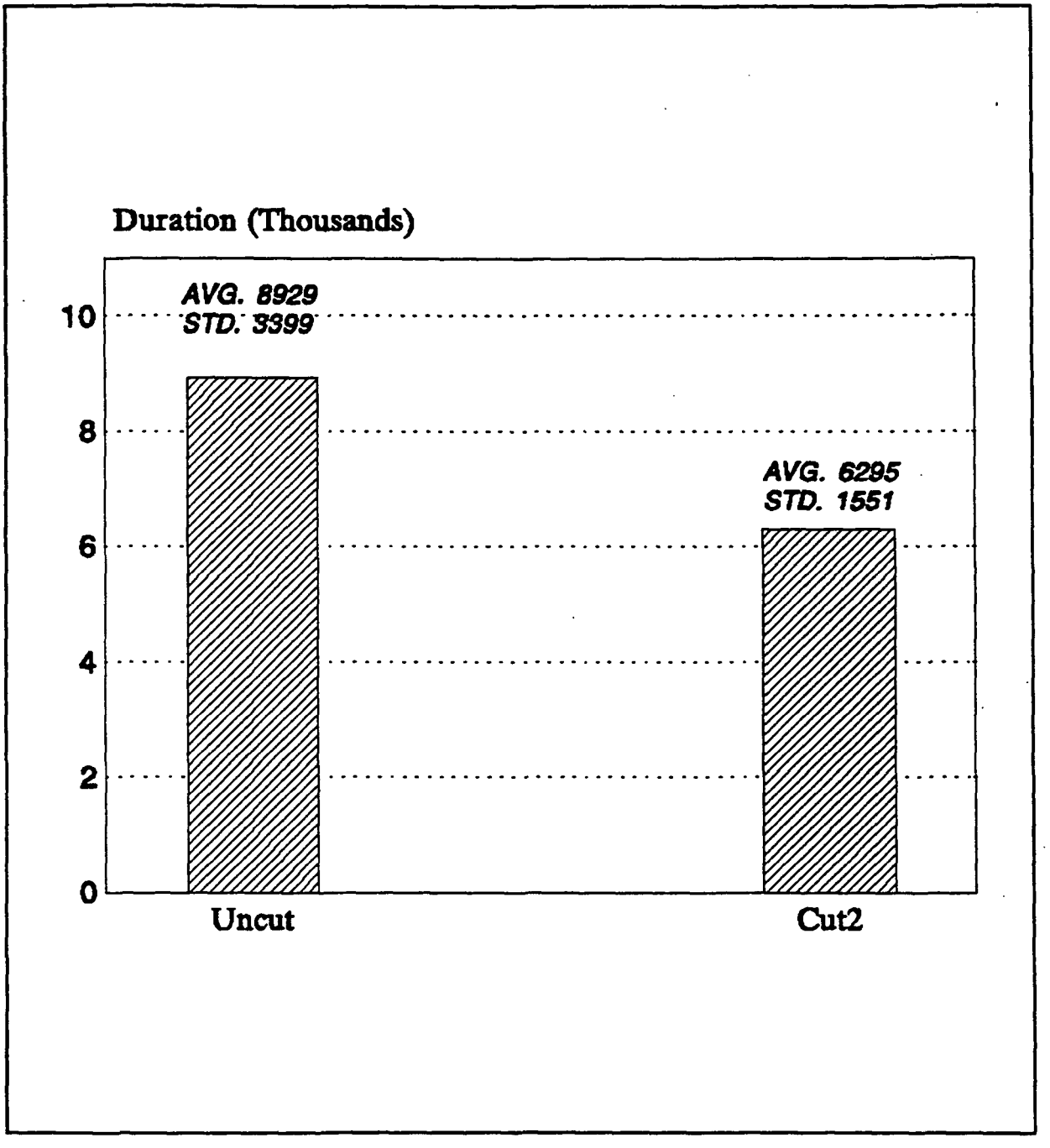

Fig. 65 Comparison of the principal durations for CUT2 and uncut specimens of green liquor corrugating paper conditioned at 50% RH, and tested in MD under uniaxial tensile loading at a crosshead speed of 0.05 in/min.

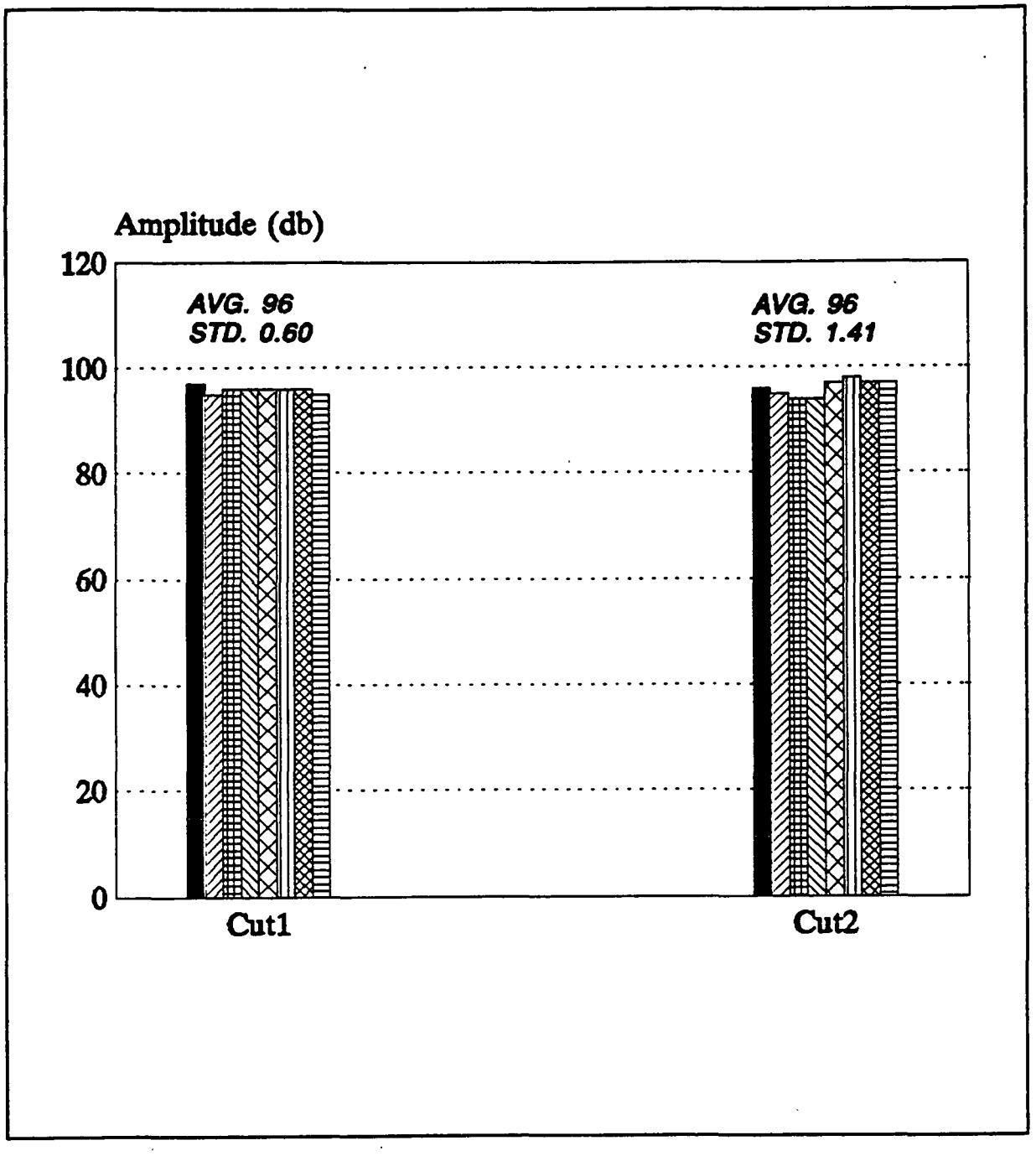

Fig. 66 Comparison of the principal amplitudes for CUT1 and CUT2 specimens of green liquor corrugating paper conditioned at 50% RH, and tested in MD under uniaxial tensile loading at a crosshead speed of 0.05 in/min.

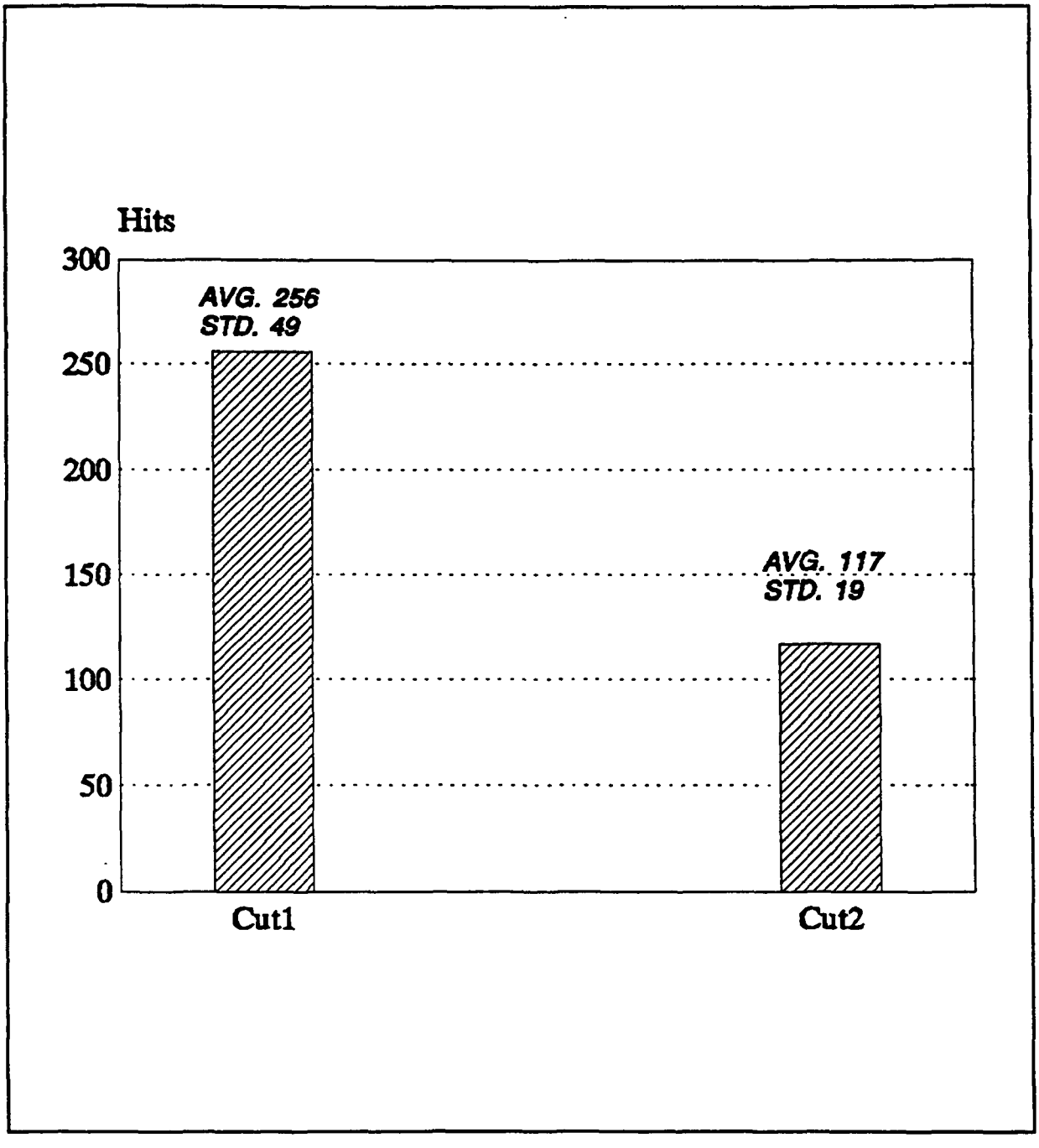

Fig. 67 Comparison of the cumulative hits for CUT1 and CUT2 specimens of green liquor corrugating paper conditioned at 50% RH, and tested in MD under uniaxial tensile loading at a crosshead speed of 0.05 in/min.

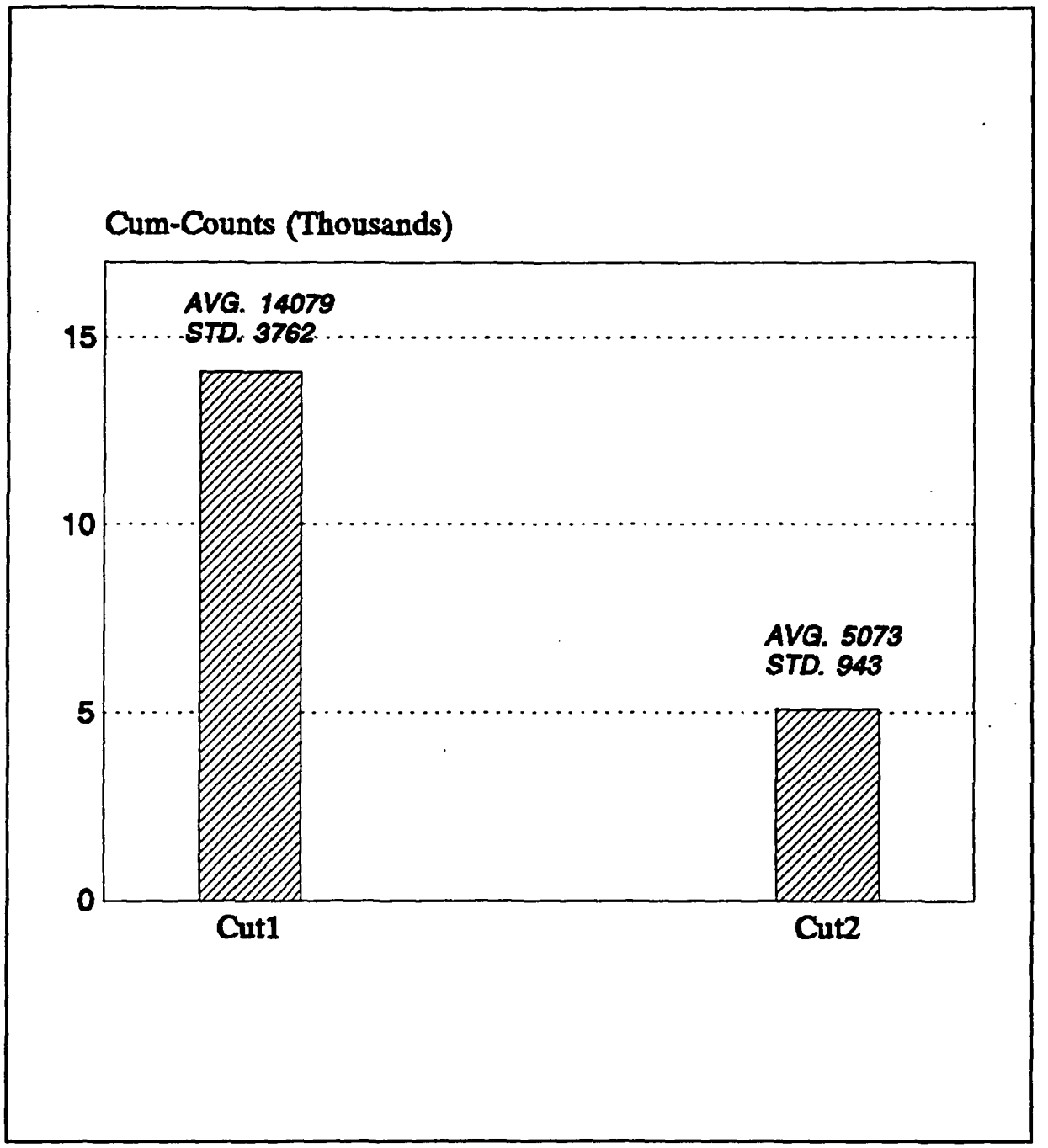

Fig. 68 Comparison of the cumulative counts for CUT1 and CUT2 specimens of green liquor corrugating paper conditioned at 50% RH, and tested in MD under uniaxial tensile loading at a crosshead speed of 0.05 in/min..

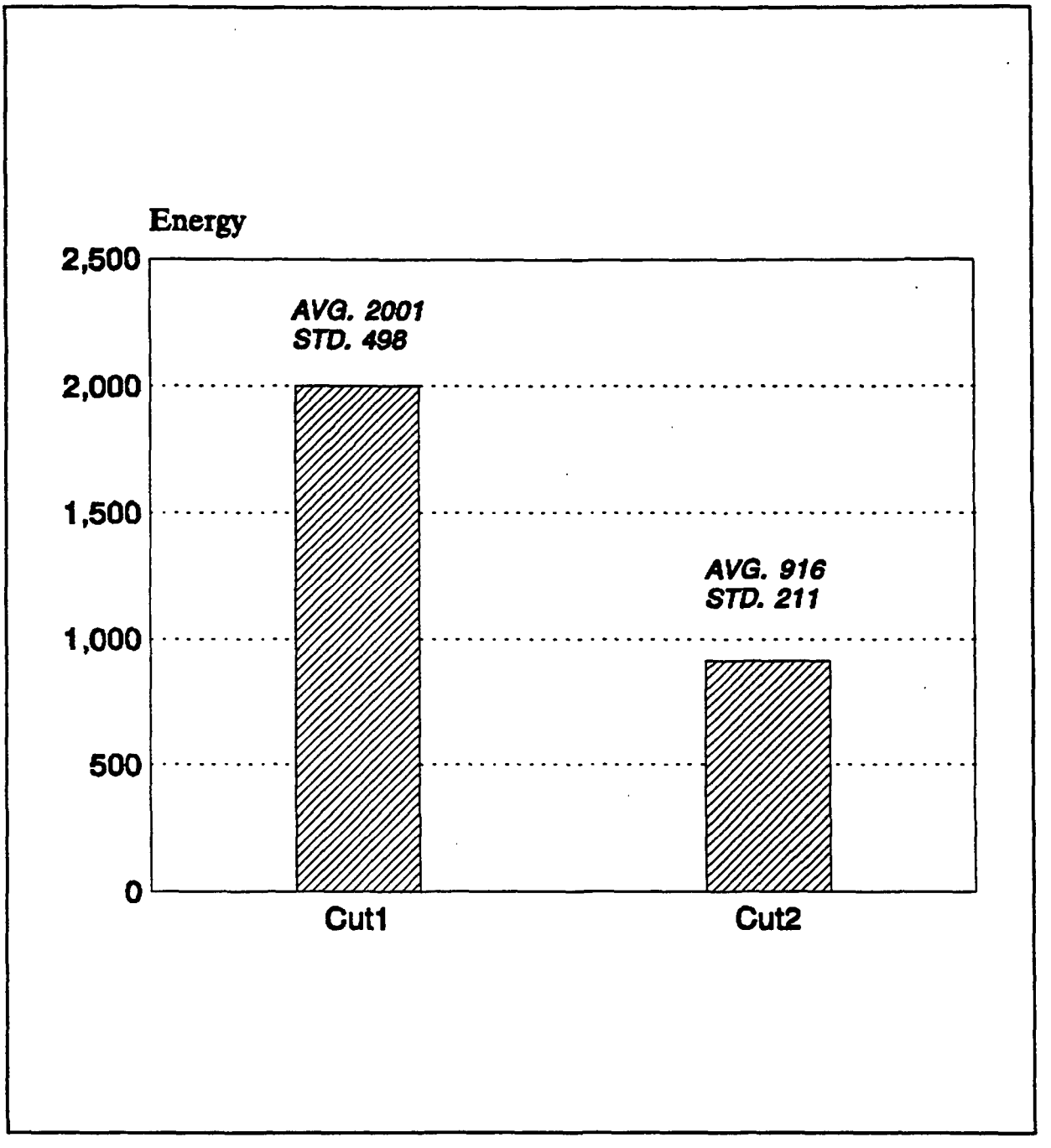

Fig. 69 Comparison of the principal energy for CUT1 and CUT2 specimens of green liquor corrugating paper conditioned at 50% RH, and tested in MD under uniaxial tensile loading at a crosshead speed of 0.05 in/min.

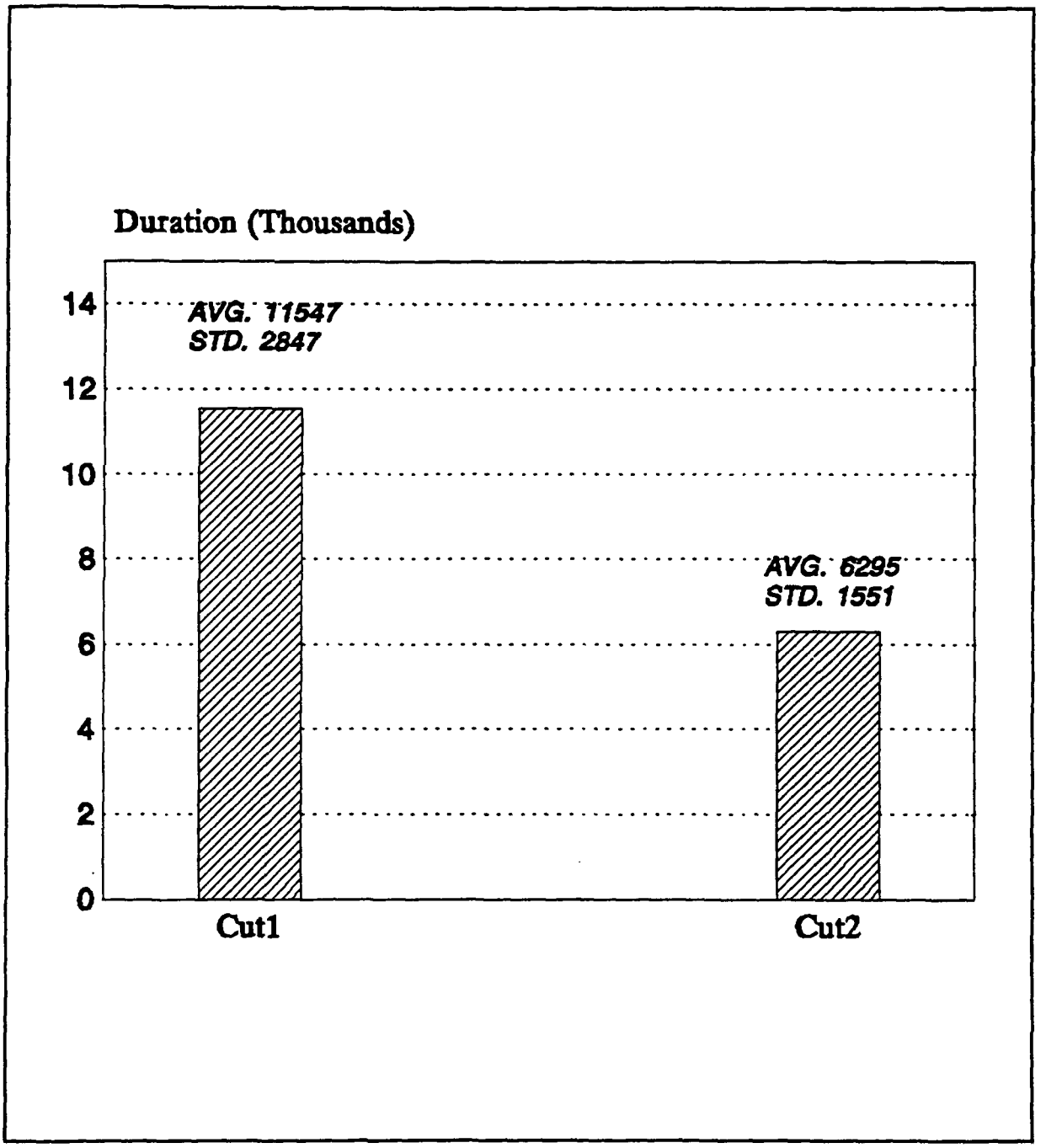

Fig. 70 Comparison of the principal durations for CUT1 and CUT2 specimens of green liquor corrugating paper conditioned at 50% RH, and tested in MD under uniaxial tensile loading at a crosshead speed of 0.05 in/min.

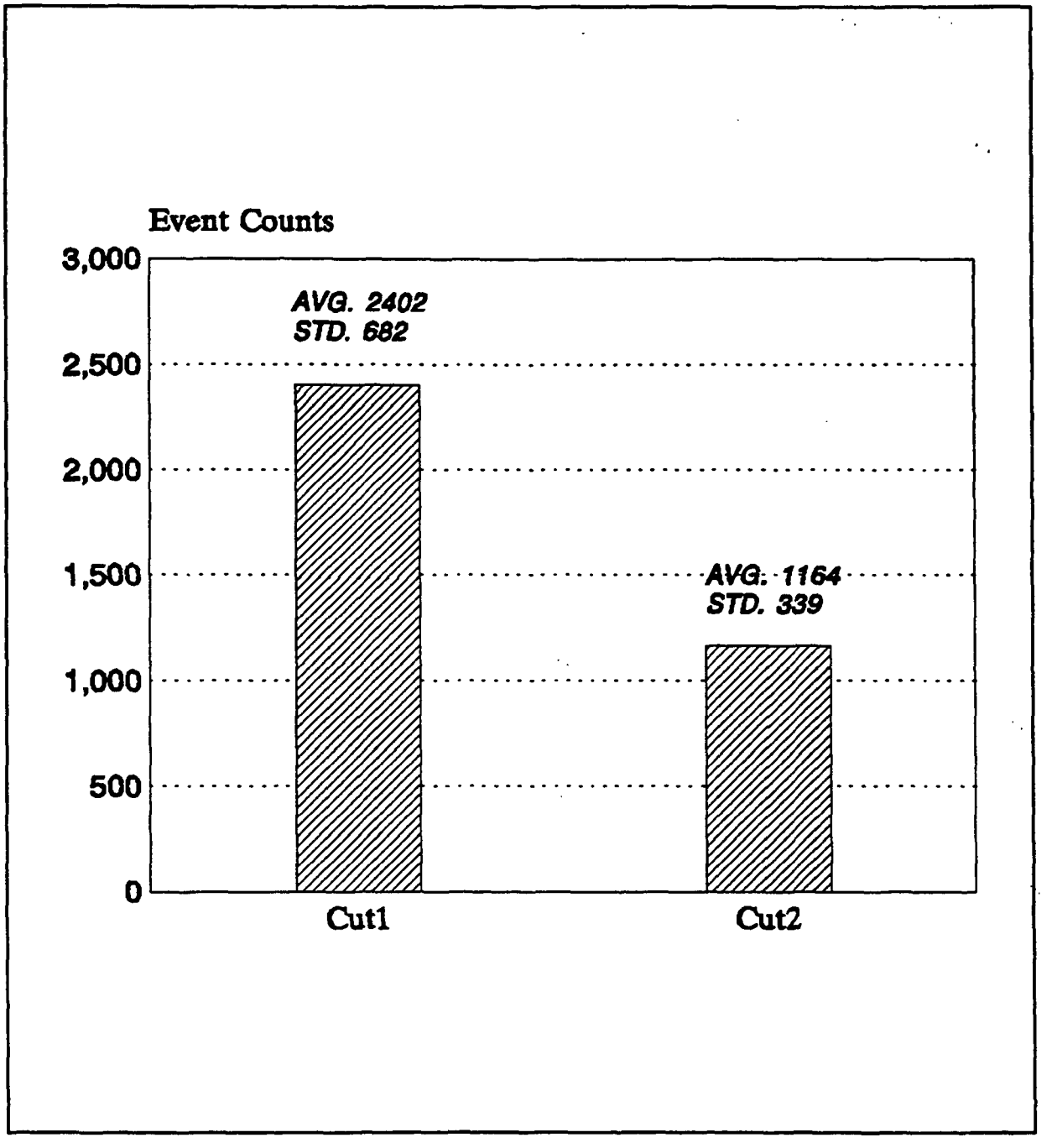

Fig. 71 Comparison of the principal counts for CUT1 and CUT2 specimens of green liquor corrugating paper conditioned at 50% RH, and tested in MD under uniaxial tensile loading at a crosshead speed of 0.05 in/min.